SCHOOL OF CIVIL AND
ENVIRONMENTAL ENGINEERING
OKLAHOMA STATE UNIVERSITY

FATIGUE ASSESSMENT OF BRIDGE MEMBERS
BASED ON IN-SERVICE STRESSES

By

Farrel J. Zwerneman
Paul G. Poynter
Michael D. Abbas
Abdul Rauf
Jie Yang

Report No. FHWA\OK-95(07)

August, 1996

INTERIM REPORT
NO. 1:
FIELD TESTS, ANALYSES,
AND LABORATORY TESTS

1. REPORT NO. FHWA\OK-95(07)	2. GOVERNMENT ACCESSION NO.	3. RECIPIENT'S CATALOG NO.	
4. TITLE AND SUBTITLE Fatigue Assessment Of Bridge Members Based on In-Service Stresses—Interim Report No. 1: Field Tests, Analyses, and Laboratory Tests		**5. REPORT DATE** AUGUST1996	
		6. PERFORMING ORGANIZATION CODE	
7. AUTHOR(S) Farrel J. Zwerneman, Paul G. Poynter , Michael D. Abbas, Abdul Rauf, Jie Yang		**8. PERFORMING ORGANIZATION REPORT** 95-07	
		10. WORK UNIT NO.	
9. PERFORMING ORGANIZATION AND ADDRESS School of Civil and Environmental Engineering Oklahoma State University Stillwater, OK 74078		**11. CONTRACT OR GRANT NO.** 2196	
12. SPONSORING AGENCY NAME AND ADDRESS Oklahoma Department of Transportation Research and Development 200 NE 21st Street Oklahoma City, OK 73105		**13. TYPE OF REPORT AND PERIOD COVERED** Interim Report: Dec 1993-Aug 1995	
		14. SPONSORING AGENCY CODE Item 2196	

15. SUPPLEMENTARY NOTES

Conducted in cooperation with U.S. Department of Transportation, Federal Highway Administration

16. ABSTRACT

Construction problems involving poor welding practice occurred during widening of the U.S. 69 bridge over the South Canadian River. As a result of these problems, concerns developed regarding the remaining fatigue life of the bridge. A research project was initiated to address these concerns

The first portion of the project involved instrumenting the bridge and recording strains under both known loads and normal traffic. These measured strains were used to calibrate an analytical model prepared as a second part of the project. The analytical model was then used to determine the critical location for fatigue. A third part of the project involved conducting laboratory fatigue tests on beam specimens with a welded detail similar to the detail of concern on the bridge. The results of the fatigue tests were used to construct an S-N curve for the detail. Based on the developed S-N curve and stress ranges from computations and measurements, the remaining fatigue life of the bridge is estimated. The estimate indicates that the remaining fatigue life of the bridge is infinite.

The reader is cautioned against using the results of this research as justification for poor welding practice. The laboratory tests show that poor welding significantly reduces the fatigue life of a beam. The long remaining life which is estimated for this particular bridge is a result of the low stress ranges in the bridge, which compensate for the inferior quality of the welds. The same result should not be expected in every case.

17. KEY WORDS Bridge, Plate Girder, Fatigue, Weld, Repair, Testing, Finite Element		**18. DISTRIBUTION ST ATEMENT** No Restrictions	
19. SECURITY CLASSIF. (OF THIS REPORT) None	**20. SECURITY CLASSIF. (OF THIS PAGE)** None	**21. NO. OF PAGES** 139	**22. PRICE**

SI (METRIC) CONVERSION FACTORS

	Approximate Conversions to SI Units					Approximate Conversions from SI Units			
Symbol	When You Know	Multiply by	To Find	Symbol	Symbol	When You Know	Multiply by	To Find	Symbol
		Length					**Length**		
in.	inches	25.40	millimeters	mm	mm	millimeters	0.0394	inches	in.
ft	feet	0.3048	meters	m	m	meters	3.281	feet	ft
yd	yards	0.9144	meters	m	m	meters	1.094	yards	yd
mi	miles	1.609	kilometers	km	km	kilometers	0.6214	miles	mi
		Area					**Area**		
$in.^2$	square inches	645.2	square millimeters	mm^2	mm^2	square millimeters	0.00155	square inches	$in.^2$
ft^2	square feet	0.0929	square meters	m^2	m^2	square meters	10.764	square feet	ft^2
yd^2	square yards	0.8361	square meters	m^2	m^2	square meters	1.196	square yards	yd^2
ac	acres	0.4047	hectares	ha	ha	hectares	2.471	acres	ac
mi^2	square miles	2.590	square kilometers	km^2	km^2	square kilometers	0.3861	square miles	mi^2
		Volume					**Volume**		
fl oz	fluid ounces	29.57	milliliters	mL	mL	milliliters	0.0338	fluid ounces	fl oz
gal	gallons	3.785	liters	L	L	liters	0.2642	gallons	gal
ft^3	cubic feet	0.0283	cubic meters	m^3	m^3	cubic meters	35.315	cubic feet	ft^3
yd^3	cubic yards	0.7645	cubic meters	m^3	m^3	cubic meters	1.308	cubic yards	yd^3
		Mass					**Mass**		
oz	ounces	28.35	grams	g	g	grams	0.0353	ounces	oz
lb	pounds	0.4536	kilograms	kg	kg	kilograms	2.205	pounds	lb
T	short tons (2000 lb)	0.907	megagrams	Mg	Mg	megagrams	1.1023	short tons (2000 lb)	T
		Temperature (exact)					**Temperature (exact)**		
°F	degrees Fahrenheit	(°F-32)/18	degrees Celsius	°C	°C	degrees Celsius	9/5+32	degrees Fahrenheit	°F
		Force and Pressure or Stress					**Force and Pressure or Stress**		
lbf	poundforce	4.448	Newtons	N	N	Newtons	0.2248	poundforce	lbf
$lbf/in.^2$	poundforce per square inch	6.895	kilopascals	kPa	kPa	kilopascals	0.1450	poundforce per square inch	$lbf/in.^2$

FATIGUE ASSESSMENT OF BRIDGE MEMBERS
BASED ON IN-SERVICE STRESSES

State Study No. 2196

Interim Report No. 1:
Field Tests, Analyses, and Laboratory Tests

By

Farrel J. Zwerneman
Paul G. Poynter
Michael D. Abbas
Abdul Rauf
and
Jie Yang

The contents of this report reflect the views of the authors who are responsible for the facts and accuracy of the data presented herein. The contents do not necessarily reflect the official views of the Oklahoma Department of Transportation or the Federal Highway Administration. The report does not constitute a standard, specification, or regulation. While equipment and contractor names are used in this report, it is not intended as an endorsement of any machine, contractor, or product.

EXECUTIVE SUMMARY

Construction problems involving poor welding quality occurred during widening of the U.S. 69 bridge over the South Canadian River. As a result of these problems, concerns developed regarding the remaining fatigue life of the bridge. A research project was initiated to address these concerns.

The first portion of the project included a visual inspection of the bridge welds followed by installation of equipment for recording strains under both known loads and normal traffic. These measured strains were used to calibrate an analytical model prepared as a second part of the project. The analytical model was then used to determine the critical location for fatigue. A third part of the project involved conducting laboratory fatigue tests on beam specimens with a welded detail similar to the detail of concern on the bridge. The results of the fatigue tests were used to construct plots of stress range versus number of cycles to failure (S-N curves) for the detail. Based on the developed S-N curve and stress ranges from computations and measurements, the remaining fatigue life of the bridge is estimated. The estimate indicates that the remaining fatigue life of the bridge is infinite.

The reader is cautioned against using the results of this research as justification for poor welding practice. The laboratory tests show that poor welding significantly reduces the fatigue life of a beam. The infinite remaining life which is estimated for this particular bridge is a result of the low stress ranges in the bridge, which compensate for the inferior quality of the welds. The same result should not be expected in every case.

A separate part of the project involves construction of a data acquisition system for use by the Oklahoma Department of Transportation. This part of the project is underway and will be the subject of a second interim report when it is complete.

ACKNOWLEDGMENTS

TABLE OF CONTENTS

LIST OF TABLES

LIST OF FIGURES

CHAPTER 1

INTRODUCTION

1.1 Problem Statement

U.S. Highway 69 crosses the South Canadian River on the western side of Lake Eufaula. The bridge at this location was recently widened by closing the gap between the north- and southbound spans and by extending the deck outward on both spans. To close the gap in the center, it was necessary to add crossframes between existing interior girders. To extend the decks outward, it was necessary to widen the piers, add a row of plate girders on the outside of each span, and connect the added girders to the existing girders with crossframes. The process is illustrated in Figure 1.

Erection of the crossframes proved to be more difficult than expected. Plans called for welding crossframes to stiffeners on existing girders and bolting to new girders. Unfortunately, boltholes on the crossframes did not match holes on the new plate girder stiffeners, so the decision was made by the contractor and allowed by the Oklahoma Department of Transportation (ODOT) to weld at all locations. Also, because erection took place while the bridge was under traffic, movement of the girders made it difficult for the welders to maintain an arc. As a result of these difficult working conditions and procedural errors by the welders (such as lack of preheat and incorrect electrodes), quality of the field welds is very poor.

The problem with weld quality is compounded by the fact that welding took place at unintended locations. According to the bridge modification design, new crossframes were to be welded to stiffeners on existing plate girders. In practice, crossframes were welded directly to the inside of the bottom flange of the existing and new plate girders, as

1

N →

Abutment No. 1   Pier No. 1   Pier No. 2   Pier No. 3

99.25'   100'   100'
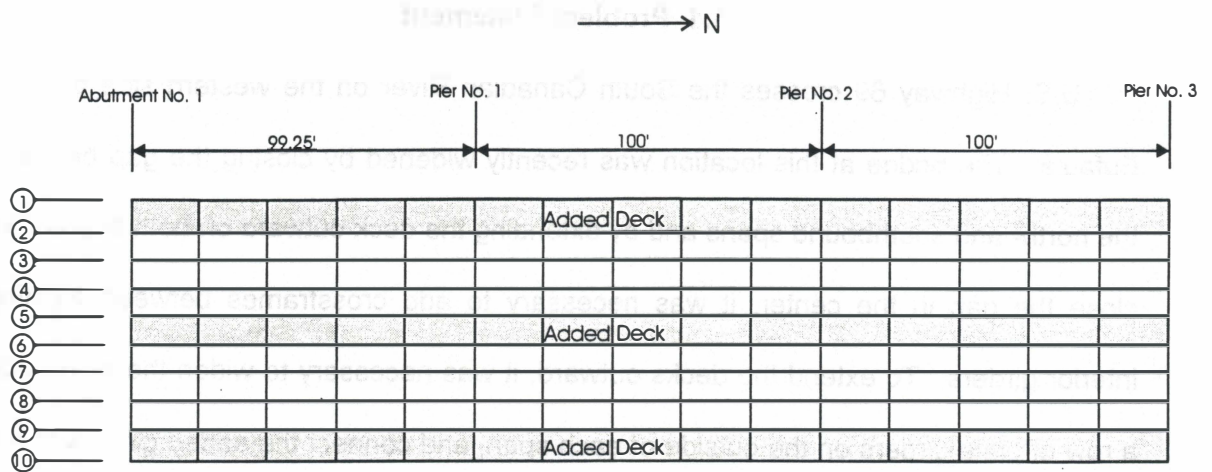
(a) Plan View of First Three Spans
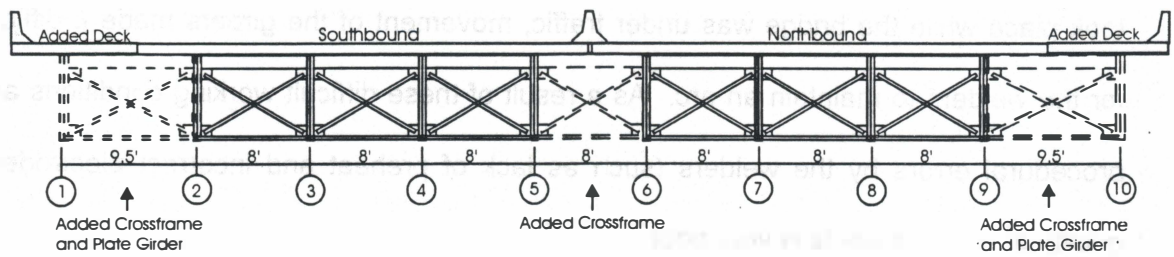
(b) Cross Section

Figure 1. U.S. Highway 69 Bridge Over South Canadian River

2

well as to the stiffeners. At most of these unintended weld locations, the bottom flange of the girder is in tension. Welding an attachment to a member in tension reduces the fatigue life of that member.

As designed, the plate girder to stiffener weld would qualify as a category C fatigue detail [American Association of State Highway and Transportation Officials, 1990]. In fact, even with the weld to the girder flange, the detail would qualify as category C if proper welding procedures had been used. Substandard welding may result in fatigue lives below category C. The extent of the reduction below category C depends on the extent to which standard practice was violated. If poor welding has reduced the detail to a category D, the calculated stress range exceeds the allowable stress range at 136 locations along the bridge, resulting in a projected fatigue life below the design life. To increase the calculated fatigue life to the desired level, it will be necessary to repair the welds at each of these locations.

Fortunately, the actual stress range in the bridge is expected to be less than the calculated stress range. The difference between actual and calculated stress ranges is the result of generally accepted conservative assumptions used in design and analysis. Conservative assumptions are made regarding load distribution, composite action, and support conditions. It may be possible to substantially reduce the number of repair locations by using actual rather than calculated stress ranges for projecting fatigue life. Actual stress ranges can be determined by instrumenting the bridge with strain gages and monitoring strains under both normal traffic and a known load.

The problem with the U.S. 69 bridge is unusual in that poor welding complicates the fatigue evaluation, but the broader problem of evaluating an existing bridge to determine remaining life or inspection intervals is commonly encountered by departments of transportation. If remaining life is based on calculated stresses, conservative

3

assumptions in the analysis can result in an unrealistically short projected life. Using calculated stresses, it is not uncommon to compute remaining lives which are negative. To assist departments of transportation in fatigue evaluations, a simplified system for in-service strain measurement is needed along with an analytical procedure using these measurements to project remaining life.

1.2 Objective of Study

This study originated out of concerns for the integrity of the U.S. 69 bridge, so the first objective is to address these concerns. Strain measurements taken from the bridge together with fatigue tests conducted in the laboratory and computer-aided analyses will provide sufficient information to estimate the remaining fatigue life of the bridge. Repair procedures will be recommended on an as-needed basis.

The second objective of this study is to develop a procedure for fatigue assessment of bridge members based on in-service stresses. Completion of this objective requires development of hardware and software for strain data acquisition in the field. The acquired data can be used to estimate the remaining fatigue life or a safe inspection interval. ODOT personnel will be trained in the use of the data acquisition system and the procedure for data analysis.

1.3 Scope of Report

This first interim report covers load tests and analyses of the U.S. 69 bridge, as well as the results of laboratory fatigue tests. Load tests include strain measurements under known loads and rainflow counts of strain ranges while the bridge is in normal service. Analyses include grid analyses and three-dimensional finite element analyses for comparisons with strains measured under known loads. Fatigue tests were conducted on laboratory specimens containing good and bad welds to assess the influence of weld quality on fatigue life.

4

A second interim report will be prepared describing the development and operation of the data acquisition system. This second interim report will be accompanied by a separate stand-alone document serving as a user's manual for the system.

CHAPTER 2

LITERATURE SEARCH

2.1 Weld Quality

A welded joint must be capable of performing reliably throughout the service life of the structure of which it is a part. The level of quality obtained in a welded joint is determined by the base materials, welding materials, and fabrication process. Employing skilled welders, selecting proper welding materials, and specifying correct welding procedures will encourage quality; however, all welds will contain some discontinuities.

2.1.1 Discontinuities

Various types and sizes of fusion weld discontinuities exist; Table 1 presents the most common. Weld discontinuities are categorized as either procedure-related or metallurgical [American Welding Society, 1987]. Both categories adversely affect the weld by introducing stress concentrations.

Table 1. Fusion Weld Discontinuities

Type of Discontinuity	Identification
Procedure Related	
Undercut	UC
Incomplete Fusion	IF
Overlap	OL
Undersize	US
Slag Inclusions	SI
Metallurgical	
Porosity	P
Cracking	CR

In addition, metallurgical discontinuities may affect chemical properties such as corrosion resistance. Weld discontinuities may be found in the weld metal, base metal, or weld heat-affected zone. The T-joint shown in Figure 2 depicts the weld discontinuities listed in Table 1.

Determining the type and extent of a discontinuity is the basis for judging weld quality. Below some acceptable level, the discontinuity is not considered harmful. Above that level, the discontinuity is a defect. Acceptable levels are generally determined by code specifications. Most notable is the ANSI/AWS Structural Welding Code [American Welding Society, 1990]. Specifications typically permit latitude by defining a tolerance for weld discontinuities. Tolerance levels are based on experience and engineering judgment. During inspection, the extent to which a given discontinuity affects the size, shape, contour, and soundness of a weld is determined and compared to code provisions. Consequently, the inspector's understanding of the features and occurrences of weld discontinuities is of critical importance.

2.1.1.1 Undercut. Undercut is the term used to describe a reduction in thickness of base metal. The reduction occurs at the edge of a bead of weld metal joining the surface of the base metal. Undercut is generally caused by improper welding technique; however, a high amperage and a long arc increase the tendency. Typically, the welder incorrectly manipulates the electrode while depositing weld material, and undercut results [American Welding Society, 1991]. In addition to a reduction in cross-sectional area, the joint may experience local yielding at the tip of the undercut due to high stress concentrations. If excessive, undercut can significantly reduce the strength of the joint. Strength reduction is most prevalent in joints subject to severe fatigue conditions [Tsai et al., 1984].
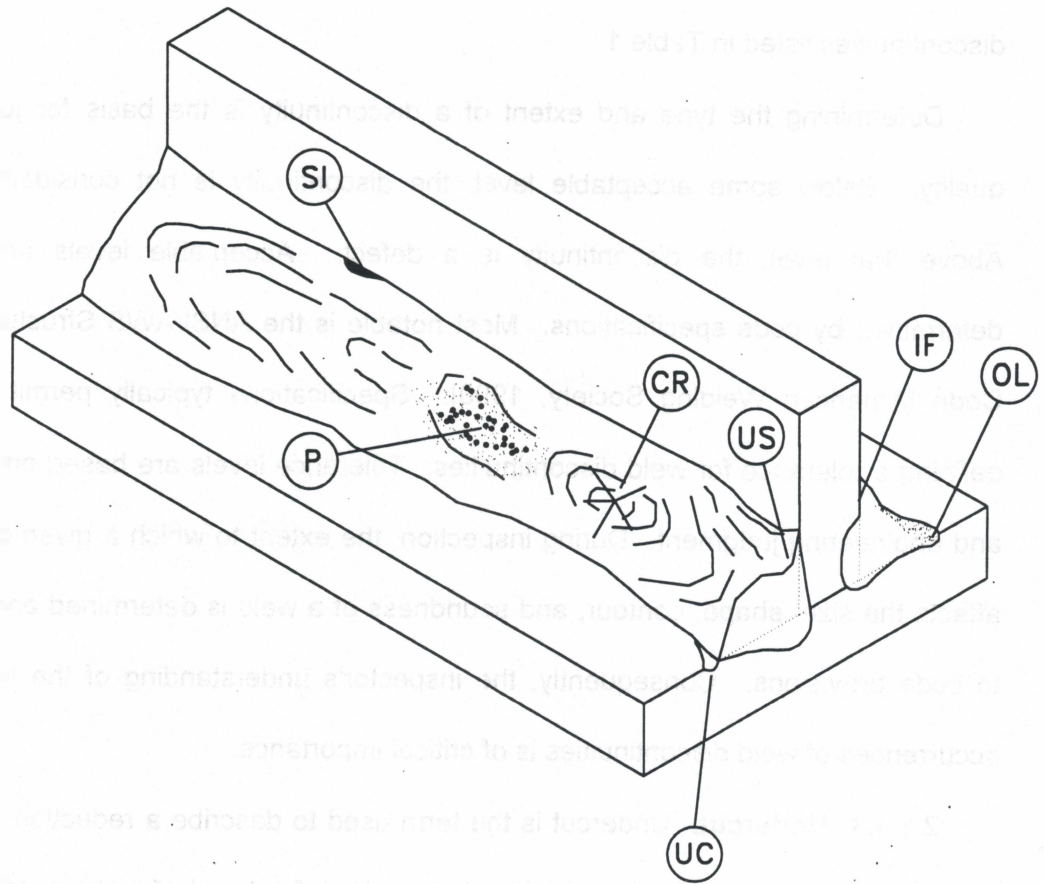
Figure 2. Fillet Weld Discontinuities in a T-Joint

2.1.1.2 Incomplete Fusion. The failure to fuse together adjacent layers of weld metal or weld metal and base metal is termed incomplete fusion. The welding arc must sufficiently penetrate the joint surfaces and raise the temperature of the base metal or previously deposited weld metal to the melting temperature or incomplete fusion will occur [Rodgerson, 1983]. Penetration problems causing incomplete fusion can result from improper electrode manipulation or incorrect arc current. The electrode travel speed must not be too high, and the arc current must not be too low. Additionally, poor surface preparation can cause incomplete fusion. Preweld cleaning must be sufficient to remove slag, oxides, or other foreign material [Gurney, 1979].

2.1.1.3 Overlap. The term overlap is used to describe a surface discontinuity that forms a severe mechanical notch parallel to the weld axis. Overlap is commonly caused by incorrect welding technique, wrong selection of welding materials, or improper preparation of the base metal. If slag, oxides, or other foreign matter on the base metal interfere with fusion, overlap may result along the toe, face, or root of the weld [American Welding Society, 1987].

2.1.1.4 Undersize. Undersize refers to a lack of welding material along the welded joint. It occurs when welding technique is poor. The welder simply fails to deposit enough weld material along the joint [American Welding Society, 1987].

2.1.1.5 Slag Inclusions. Non-metallic solid materials trapped in the weld metal or at the weld metal interfaces are termed slag inclusions. Many chemical reactions occur in the weld metal during deposition and subsequent solidification. Because of their lower specific gravity, non-metallic reaction products which are insoluble in molten metal will rise to the surface of the weld metal unless they become entrapped. The reaction products or slag may become entrapped below the surface of the molten metal by the stirring action of the arc. Slag may also follow ahead of the arc if the welder

9

manipulates the electrode incorrectly. Thus, slag inclusions can be prevented by employing good welding techniques [American Welding Society, 1991].

2.1.1.6 Porosity. Porosity is the presence of small voids in the weld material. The voids are created from gas being entrapped in the weld material during solidification. The voids may be either uniformly scattered throughout the weld or exist in localized clusters. Void size varies widely. Voids may be so small as not to be detectable by radiography, or they may be holes of more than 3/16 in. diameter [Gurney, 1979].

Porosity is a function of the degree of supersaturation of the gas in the weld metal. Gases, typically hydrogen and nitrogen, enter the weld pool through air entrainment in the arc atmosphere. Incidence of porosity may be reduced by using dry electrodes low in hydrogen content. In addition, correct amperage and proper arc length are required [Rodgerson, 1983].

2.1.1.7 Cracking. Cracks can exist in both the weld metal and the base metal. Two types of cracks can occur in a welded joint. Cracks which form during welding while the weld metal is in a plastic condition are termed hot cracks. Hot cracks develop as the weld metal begins to solidify. Cracks occurring in the heat-affected zone material after the joint is cooled are termed cold cracks. Both forms of cracking are influenced by the degree of restraint opposing movement during weld shrinkage. In addition, solidification rate is influential since it determines the structure and impurity distribution of the weld metal that may eventually crack. Cracking may be lessened by increasing heat input and by using preheat. Increasing heat input avoids excessive hardening of the heat-affected zone and allows hydrogen to disperse. Using preheat will help avoid cold cracking in the heat-affected zone by preventing the joint from cooling too fast. Preheat is particularly useful in thick (3/4-in.) sections of mild steel [Gurney, 1979].

10

2.1.2 Weld Profile

In addition to the discontinuities discussed, the finished profile of a weld may also adversely affect the service performance of a joint. Poor profile may cause stress concentrations as well as contribute to the formation of incomplete fusion or slag inclusions [American Welding Society, 1987]. Figure 3 shows desirable, acceptable, and unacceptable fillet weld profiles [American Welding Society, 1990].

2.1.3 Effect of Weld Discontinuities on Fatigue Strength

Weld performance is greatly affected by the weld discontinuities discussed. Most particularly affected is fatigue strength. Fatigue cracks initiate from notches which produce a stress concentration under an applied stress. In addition to promoting crack initiation, stress concentrations increase crack propagation rates. Although all discontinuities may be significant in promoting fatigue failures, incomplete fusion, cracking, and undercut are the most detrimental. In addition to fusion weld discontinuities, weld profile defects can also seriously hinder fatigue performance by increasing stress concentrations [Rodgerson, 1983].

2.2 Fatigue Strength

Current AASHTO Specifications [American Association of State Highway and Transportation Officials, 1990] contain provisions for fatigue design of welded details on steel bridges. These provisions are based on fatigue resistance curves which reflect the expected fatigue life for a given stress range. Different curves exist for different classes of welded details. Data accumulated from several major fatigue studies were used to generate the fatigue curves. The majority of data was obtained from extensive research sponsored by the National Cooperative Highway Research Program (NCHRP). In addition to providing for fatigue tests on over 800 full-sized welded steel bridge details,

11
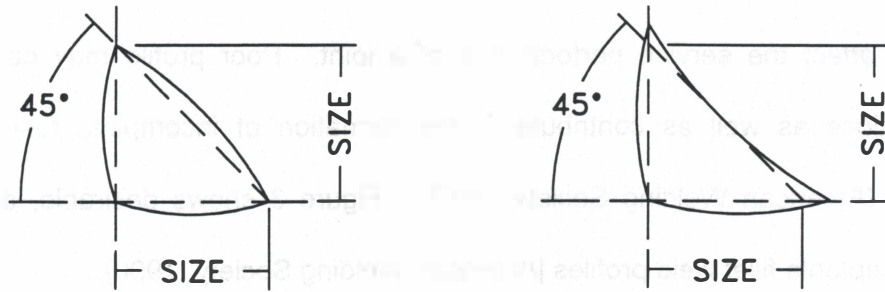
(a) Desirable

(b) Acceptable
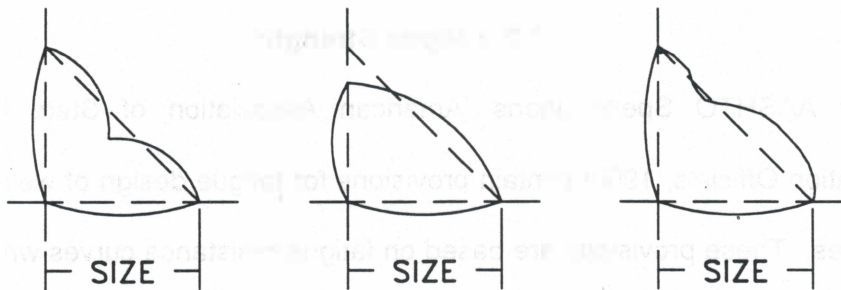
INSUFFICIENT
THROAT

INSUFFICIENT
LEG

EXCESSIVE
CONVEXITY

(c) Unacceptable

Figure 3. Fillet Weld Profiles

the fatigue studies sponsored by the NCHRP involved amassing the findings from several other fatigue studies conducted in the United States and abroad [Fisher et al., 1986].

A substantial portion of the research conducted under the NCHRP concentrated on examining the fatigue strength of transverse stiffeners and similar attachments. Efforts to fatigue test transverse stiffeners welded to steel beams were aimed at developing the AASHTO fatigue resistance curve for Category C details. Under the NCHRP, quality testing was performed in which the variables influencing fatigue strength were properly controlled and measured. The relevant test program is presented in NCHRP Report 147, Fatigue Strength of Steel Beams with Welded Stiffeners and Attachments [Fisher et al., 1974].

2.2.1 NCHRP Test Program

A total of 47 beams with one-sided transverse stiffeners were tested in the NCHRP fatigue study. Multiple stiffeners were attached to each beam. Stiffener plates were manually fillet-welded to the beam web as well as the beam flanges. Fabrication techniques, workmanship, and inspection procedures which conform to the requirements of the ANSI/AASHTO/AWS D1.5 Bridge Welding Code were employed. To simulate the restraint imposed by bridge diaphragms, lateral bracing was introduced at some stiffener locations causing an out-of-plane displacement proportional to the vertical displacement.

The two sizes of rolled steel beams studied were W14x30 and W10x25. These beam specimens were tested on simple supports with concentrated loads applied at two locations allowing for constant moment and moment gradient regions. The cyclic loading was applied through a hydraulic actuator operating at a frequency between 200 and 800 cycles per minute. Load was transmitted from the hydraulic actuator to the

13

test beam through a spreader beam. The majority of tests involved no stress reversals, and all tests were limited to constant amplitude cyclic loading. Minimum flexural stress and flexural stress range at the stiffener-to-tension flange weld were the controlling variables. Tests were continued until cracks occurring at stiffener details reduced beam stiffness and allowed for an increase in deflection. After failure at one stiffener location, beam specimens were repaired by splicing across the cracked region, and testing was continued to produce failure at other stiffener locations.

2.2.2 NCHRP Findings

Test results showed that the flexural stress range at the stiffener-to-tension flange weld was the dominant factor influencing fatigue strength. The minimum flexural stress at the stiffener-to-tension flange weld was an insignificant variable. Furthermore, it was discovered that shear stresses did not affect fatigue strength. Thus, it was concluded that principal stresses and their direction need not be considered when designing stiffened bridge members. The attachment of diagonal bracing to the beam stiffeners had no effect on fatigue strength, and out-of-plane bending at no time contributed to crack initiation or growth. Analysis of the crack growth indicated that the thickness of the flange and web was not a variable influencing the fatigue life of the stiffener details. The fatigue tests examined in this study involved between 10^5 and 10^7 cycles of loading. Furthermore, stiffeners welded to the web and flanges sustained 10.8 to 15.5 million load cycles at a stress range of 12 ksi without failure or visible crack growth.

All beam failures were the result of a large crack forming at the toe of the fillet weld connecting each stiffener to the tension flange. The large crack emerged from smaller cracks that initiated at several points along the toe of the weld. Propagating in a semielliptical shape, individual cracks grew and eventually joined. Once joined, the single crack front spread over most of the weld length before reaching the extreme fiber

of the tension flange. After breaking through the extreme fiber, the crack grew across the tension flange and up into the web. Growing the cracks through the thickness of the flange consumed approximately 96 percent of the load cycles to failure. The likelihood of crack initiation and growth was greatest at locations subjected to a high tensile stress range and where initial micro-flaws existed. The initial micro-flaws were the result of discontinuities in the fillet weld. As suspected, the rate of crack propagation was proportional to the level of stress range as well as the extent of weld discontinuities.

2.2.3 AASHTO Fatigue Resistance Curve

The AASHTO fatigue resistance curve for a Category C detail was derived from the NCHRP fatigue study on transverse stiffeners. The curve is presented in Figure 4. As previously noted, the fabrication techniques, workmanship, and inspection procedures employed in the NCHRP fatigue study comply with the ANSI/AASHTO/ AWS D1.5 Bridge Welding Code. This document places specific limits on cracking, convexity, undercut, lack of fusion, porosity, and undersizing. Such weld discontinuities are not considered weld defects until their size and frequency exceed the specified limits. The data obtained in the NCHRP fatigue study on transverse stiffeners applies to quality welds free of defects. Consequently, the AASHTO fatigue resistance curve for a Category C detail makes no allowance for substandard welding.

2.2.4 Fatigue Strength With Weld Defects

Information available on the fatigue strength of welded stiffeners containing weld defects is limited. In tests performed on beams with fillet welded stiffeners, Gurney [Fisher et al., 1974; Gurney, 1960] attributed three early failures to undercut at the toe of the weld. Although the undercutting was slight, its presence reduced the fatigue life of the detail to below a Category C. In a West German study [Fisher et al., 1986; Minner et al., 1982], fatigue tests performed on welded stiffeners consistently yielded results

The plot shows a line with the equation:

$$\log N = 9.648 - 3.0 \cdot \log S_r$$

with a fatigue limit indicated by a horizontal dashed line. The x-axis is labeled "Cycles to Failure, N" ranging from 10^5 to 10^8, and the y-axis is labeled "Stress Range, S_r (ksi)" ranging from 1 to 100.
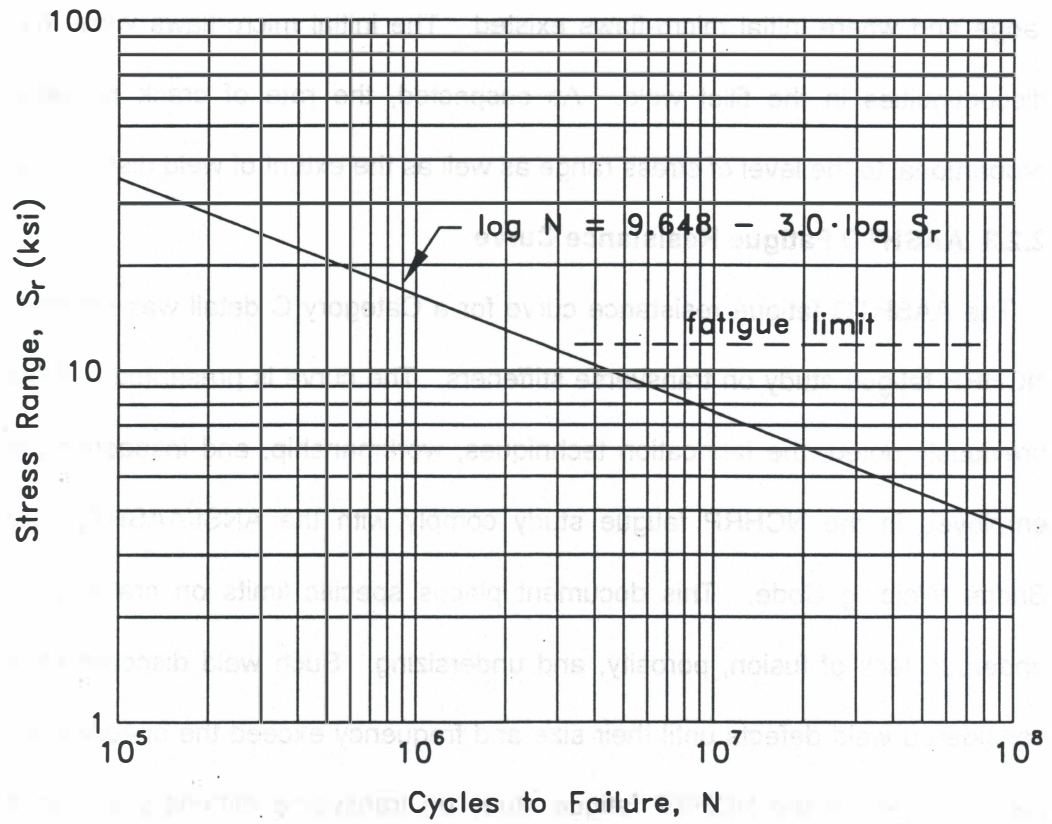
Figure 4. AASHTO Fatigue Resistance Curve for a Category C Detail

that were significantly below the predicted strength. The reduced fatigue strength was reportedly due to unintended weld defects, namely hydrogen-induced cold cracking and weld undercutting. All the test data obtained in the West German study fell below the fatigue resistance curve for a Category C detail. A comparison of the test data obtained in the West German study to the AASHTO Category C fatigue resistance curve is shown in Figure 5.

2.3 Improving the Fatigue Strength of Welded Joints

It is known from previous fatigue studies [Fisher et al., 1970; Fisher et al., 1974] on welded joints that fatigue cracks initiate and grow in areas subjected to a high tensile stress range where initial micro-flaws exist. In fillet welds, such as are used to attach transverse stiffeners, the initial micro-flaw condition is provided by discontinuities at the weld toe. The high tensile stress range is brought about by stress concentrations occurring at the weld toe. The tensile stress range may also be influenced by the presence of tensile residual stresses which result from the welding process. By lessening weld discontinuities, stress concentrations, and residual tensile stresses, the likelihood of crack initiation and growth can be reduced and fatigue strength can be improved.

2.3.1 Weld Modifying Techniques

A variety of techniques exist for modifying a welded joint and improving its fatigue strength. The most common and thoroughly examined techniques include grinding, remelting, and peening. The forms of grinding employed are either rotary burr or disc. Both forms of grinding reduce stress concentrations at the weld toe by altering the weld profile to achieve a smooth transition between the weld metal and the base metal. Grinding may also serve to reduce weld discontinuities such as undercut and slag inclusions.

17
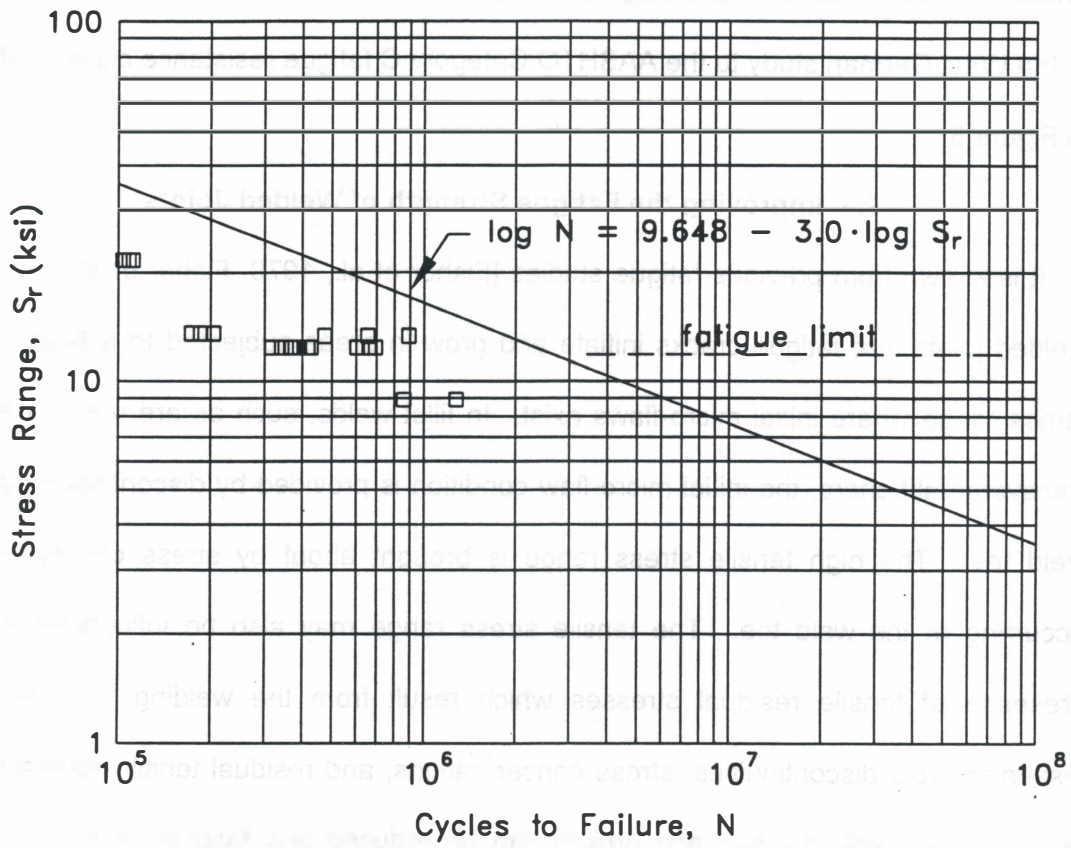
Figure 5.   West German Test Data

The technique known as remelting involves melting the weld metal to a shallow depth along the weld toe. Remelting reduces slag inclusions and modifies weld profile, thereby reducing stress concentrations and crack initiation sites at the weld toe.

Peening is a cold working process used to plastically deform the weld toe. Peening is usually accomplished by a high velocity stream of metal particles (shot peening) or by a tool (hammer peening). By peening, the weld toe profile is improved, thus reducing stress concentrations. Peening also hardens the weld and introduces residual compressive stresses; both functions can improve fatigue strength [Gregory et al., 1989].

2.3.2 Studies on Grinding, Remelting, and Peening

In two NCHRP studies [Fisher et al., 1979; Gregory et al., 1989], the relative benefit of grinding, remelting, and peening was examined. In the NCHRP study conducted by Fisher et al., only a slight increase in the fatigue strength of joints with ground fillet weld toes was reported. The average increase in the fatigue life of ground joints over as-welded joints was less than 10 percent. Poor grinding techniques may have contributed to the lack of improvement in fatigue strength. On several specimens, the weld toe surface was damaged by the grinding burr; on one specimen, slag particles were not removed but rather covered by a layer of smeared metal.

Fisher et al. achieved the greatest success with remelting. Depending on stress range, increases in the fatigue life of details with remelted welds ranged from 270 to 360 percent. On some specimens, cracks initiated and propagated from the weld root demonstrating an upper bound to the improvements that are possible by remelting the weld toe.

Fisher et al. also found that peening the weld toe increases fatigue strength. The greatest increase in fatigue strength was observed in specimens subjected to the

highest stress ranges. Although peening blunted the crack-like slag inclusion and slowed crack initiation, fatigue cracks still eventually developed in the peened region at the weld toe.

When examining the same retrofitting techniques as Fisher et al., Gregory et al. concluded that toe grinding is the most practical and economical method of achieving a significant improvement in fatigue strength. The conflict in the researchers' results may stem from the fact that Gregory et al. primarily considered stress ranges near the fatigue limit, whereas Fisher et al. was concerned with higher stress ranges. Interestingly, the slight increase in the fatigue strength of ground joints that was reported by Fisher et al. occurred in the lowest stress range tests. It is worth noting that the American Welding Society Specification [American Welding Society, 1990] also mentions remelting and peening but expresses a preference for grinding.

Gregory et al. further investigated the aspects of grinding by comparing disc and rotary burr grinding. It was found that disc grinding can be performed at almost twice the rate of burr grinding. However, burr grinding may be desirable because disc grinding suffers from two disadvantages. Being large and cumbersome, the disc grinder may be difficult to operate in tightly confined spaces. In addition, the operator of a disc grinder is more likely to remove too much material. In either case, the depth of grinding must be a minimum of 1/32 in. beneath the plate surface. The maximum depth of grinding allowed is 5/64 in. or 5 percent of the plate thickness. The final ground surfaces should be free from all traces of slag or undercut, and a smooth transition between the weld metal and the base metal should exist at the weld toe [Gregory et al., 1989].

2.4 Calculated and Actual Bridge Response

The procedures used in design and analysis of highway bridges are inherently conservative. As a result, the actual response of a bridge often varies significantly from the calculated response. In reality, bridge stresses and particularly stress ranges are almost always lower than anticipated by calculations. Consequently, an analytical model used to determine actual stress ranges must be developed from site specific data obtained from field measurements.

Structures with excessive strength stem from the designer's primary concern with safety and serviceability. During the design process, every effort is made to include safety factors to account for uncertainties in materials, loads, fabrication details, and possible construction errors. Procedures contained in the AASHTO Standard Specifications for Highway Bridges [American Association of State Highway and Transportation Officials, 1990] are governed by a static strength design, followed by fatigue checks. Because the strength design procedures must account for the worst conditions expected to occur over the life of the bridge, conservative assumptions are made in each step. Although these design procedures lead to bridge structures which are extraordinarily safe, these same procedures can predict stress ranges which are far greater than actually felt by the structure [Moses et al., 1987].

In addition to conservative design assumptions, conservative analysis assumptions can result in actual stresses being lower than calculated stresses. Analytical models of beam and slab bridges often fail to consider several ways in which load is resisted. In an investigation performed by Burdette et al. [1988], more than 50 years of bridge test data were collected and examined to determine specific load-resisting mechanisms that are typically not accounted for during design or evaluation. The investigation revealed

that conservative analysis assumptions are made with regard to load distributions, composite action, and unintended continuity.

2.4.1 Analysis Assumptions

2.4.1.1 Load Distribution. Load distribution refers to the lateral distribution of load to longitudinal supporting elements. How loads applied to the bridge deck distribute themselves laterally has a significant effect on the stress range experienced by each girder. Bridge tests indicate the usual assumption that interior girders carry most of the load can be grossly conservative. A more realistic estimate of stress range is likely obtained by examining multiple load configurations nearer to exterior girders [Burdette et al., 1988].

2.4.1.2 Composite Action. The composite action of bridges with steel girders and concrete decks is generally underestimated. Tests on bridges with shear connectors frequently exhibit full composite action. Even in the absence of shear connectors several bridges have demonstrated some composite action. Bridges examined in the AASHO Road Test [Highway Research Board, 1962] exhibited full composite action even after repeated stress cycles. In a study conducted by Viest [1960], steel beams with and without mechanical shear connectors were examined. In every test, complete interaction between slab and beam was observed so long as the bond between the concrete and steel flange remained unbroken. Though not quantitatively stated, these studies indicate that actual bridge stresses and stress ranges are lower than anticipated in design calculations.

2.4.1.3 Unintended Continuity. Unintended continuity is the tendency of a bridge to act continuous at its simply supported ends. This action would result in actual stresses being lower than design stresses which do not consider resistance to end rotation. An analysis performed by Barton and McKeel [1986] showed that some

22

allowance for end moment had to be made in order to match the bridge behavior measured in field tests. In a similar analysis performed by Burdette and Goodpasture [1971], applying approximately 35 percent full fixity at the bridge ends resulted in a much closer matching of calculated and measured bridge response. These same results were observed in tests conducted by Buckle et al. [1982].

2.4.2 Modeling

Incorrectly predicting actual bridge response is generally attributable to incorrect assumptions made in modeling. Although the theories relied upon in structural analysis are accurate, the model being examined fails to reflect the actual characteristics of the bridge structure. As a result, models derived from test data taken at the bridge site are the most realistic [Barton and McKeel, 1986]. To practically model bridge stress ranges, bridge girders are fitted with strain gages at various locations. In particular, strain gages are placed along the lower flanges of all girders where maximum stress ranges are expected to occur. A known load closely resembling the real live load is moved on the bridge and strain measurements are taken for various positions of the static load.

Once actual bridge strains have been determined at specific locations, a finite element model of the bridge structure is generated. Before calibration, every effort is made to model the bridge structure as closely as possible. The model is then calibrated by adjusting the level of composite action at the flange-deck interface, the moment restraint at the supports, and the load distribution on the deck until measured strains match calculated strains. Once the model is complete, it can be used to calculate the stresses at any point on the bridge, rather than being limited to just strain gage locations.

Several researchers [Nowak, 1990] have obtained favorable results by performing variances of the procedures described above. Although quantifying how each of the

different mechanisms affected actual response was practically impossible, generating a model which accurately predicted actual bridge response was possible. Furthermore, the models were successfully used to determine the stress ranges actually occurring on the bridge allowing for a more accurate estimate of fatigue life.

2.5 Fatigue Evaluation Procedures

Fatigue evaluation procedures for existing steel bridges were developed in a study sponsored by the NCHRP. The study collected information gained from several years of research on variable-amplitude fatigue response, high-cycle fatigue behavior, bridge detail fatigue strengths, actual traffic loadings, and bridge load distributions. This information was used to develop guidelines for calculating the remaining fatigue life of an existing bridge. These guidelines are presented in the NCHRP Report 299, Fatigue Evaluation Procedures for Steel Bridges [Moses et al., 1987].

As specified in the NCHRP report, the procedure for computing remaining fatigue life for a bridge detail begins with determination of a nominal stress range for the truck traffic crossing the bridge. This stress range is then applied to a fatigue resistance curve generated from laboratory testing. The fatigue resistance curve reflects the number of load cycles a particular detail can sustain at a given stress range before failing. After determining the number of load cycles corresponding to this stress range, the life of the detail is calculated from an estimated truck volume and the present age of the bridge.

Two different procedures for estimating the remaining fatigue life of a detail are available. The two procedures are identified as remaining mean life and remaining safe life. Both estimates are calculated using the detail's fatigue data generated from laboratory tests. The remaining mean life estimate is based on the mean stress range versus number of cycles curve. The mean curve is developed from a linear regression

analysis of the fatigue test data. The remaining safe life estimate is based on the allowable stress range versus number of cycles curve. The allowable curve is defined two standard deviations below the mean curve. A standard deviation is calculated for the number of load cycles test data after transferring each of the values of the number of load cycles to the same stress range value. These values are transferred using the slope of the mean curve. When determining the allowable curve in this manner, it is assumed that the allowable curve is parallel to the mean curve on a log-log plot. Hence, the allowable curve corresponds only approximately to the lower bound of the 95 percent confidence limit for the test data. The 95 percent confidence limit is the statistical limit which defines the interval of cycle life within which the fatigue test data are expected to occur 95 percent of the time.

The best possible estimate of the actual remaining life is reflected in the remaining mean life calculation. There is a 50 percent chance that the actual remaining life will exceed the remaining mean life. The remaining mean life is the same for redundant and nonredundant members.

A much higher degree of safety is provided by the remaining safe life calculation. In calculating the remaining safe life, different levels of safety are provided for redundant and nonredundant members. The probability that the actual remaining life will exceed the remaining safe life is 97.7 percent for redundant members and 99.9 percent for nonredundant members.

The fatigue life evaluation procedures derived from the NCHRP study were designed to provide consistent levels of reliability for different conditions. This is accomplished by providing basic procedures along with alternative procedures that may be better suited to the data available on a particular bridge. Although the alternative procedures may require more effort, they generally provide greater accuracy resulting in a longer

calculated fatigue life. The NCHRP report provides an alternative procedure which relies on stress range measurements taken at the bridge site. Since measurements were taken on the U.S. 69 bridge under investigation, this procedure is included in the discussion that follows.

To calculate the remaining fatigue life for an estimated lifetime average daily truck volume, the following equation is used:

$$Y_f = \frac{f\,K \times 10^6}{T_a C (R_s S_r)^b} - a \qquad (2.1)$$

where Y_f = remaining fatigue life in years; S_r = effective stress range; R_s = reliability factor; C = stress cycles per truck passage; K, b, and f = fatigue curve constants; T_a = estimated lifetime average daily truck volume; and, a = present age of the bridge in years. Further discussion of each of the variables in Equation 2.1 is provided in the sections which follow.

2.5.1 Effective Stress Range (S_r)

In the general procedure, the nominal stress range is calculated from a rigorous analysis of the bridge structure. To determine the stress range, a model of the bridge structure is developed, and its response to a fatigue truck load is examined. As an alternative procedure, the effective stress range may be used. The effective stress range is calculated from stress-range histograms obtained from field measurements on the bridge under normal traffic. The histograms should reflect effective stress ranges at critical locations along the bridge. The effective stress range, S_r, for each histogram is calculated from the following equation:

$$S_r = \left(\sum p_i S_{ri}^3 \right)^{1/3} \qquad (2.2)$$

where p_i = fraction of stress ranges within an interval; and S_{ri} = midwidth of the interval.

2.5.2 Reliability Factor (R_s)

The reliability factor is used to ensure an adequate level of safety. It is derived from a statistical analysis performed to determine the probability that the actual life will exceed the safe life. When determining the remaining safe life, multiply the computed stress range, S_r, by a reliability factor:

$$R_s = R_{so}(F_{s1})(F_{s2})(F_{s3}) \qquad (2.3)$$

where R_s = reliability factor associated with calculation of stress range, 1.0 for remaining mean life; and R_{so} = basic reliability factor, 1.35 for redundant members, 1.75 for nonredundant members.

The effective stress range is considered more accurate if calculated using stress-range histograms. The factor F_{s1} accounts for this increased accuracy by reducing the effective stress range. Thus, if the effective stress range is calculated using stress-range histograms obtained from field measurements on the bridge, F_{s1} = 0.85. In all other cases, F_{s1} = 1.0. The factor F_{s2} is used when stresses are computed rather than measured. If loads used in the computations are for site-specific weigh-in-motion measurements, F_{s2} = 0.95; if the AASHTO fatigue truck is used, F_{s2} = 1.0. The AASHTO fatigue truck is a model truck used to represent the variety of trucks of different types and weights in actual traffic. The factor F_{s3} accounts for the level of accuracy in lateral load distribution when stresses are computed. If a rigorous analytical method is used, F_{s3} = 0.96. If an approximate method based on parametric studies is used, F_{s3} = 1.0.

2.5.3 Stress Cycles Per Truck Passage (C)

The number of stress cycles per truck passage, C, can be determined from the values that follow:

For longitudinal members:

(a) Simple-span girders:

    40-ft or above = 1.0

    Below 40-ft = 1.8

(b) Continuous-span girders within a distance equal to 0.1 of the span on each side of an interior support:

    80-ft or above = 1 + (span - 80)/400 in feet

    40-ft or above but below 80-ft = 1.0

    Below 40-ft = 1.5

(c) Continuous-span girders elsewhere:

    40-ft or above = 1.0

    Below 40-ft = 1.5

(d) Cantilever (suspended span) girders = 2.0

(e) Trusses = 1.0

For transverse members:

(a) 20-ft or above spacing = 1.0

(b) Below 20-ft spacing = 2.0

2.5.4 Fatigue Curve Constants (K, b, and f)

Data obtained from fatigue tests on laboratory specimens are used to evaluate the fatigue life of details similar to the one tested. The fatigue test data consist of the number of load cycles, N, a detail can sustain at a given stress range, S_n before failing. The relationship between the number of load cycles, N, and the stress range, S_n has been determined from extensive test data obtained in fatigue studies sponsored by the NCHRP [Fisher et al., 1985]. The relationship determined from the NCHRP fatigue

studies is given by

$$NS_r^b = A \tag{2.4}$$

When plotted on a log-log scale, a straight line with an intercept A and a negative slope b is obtained. This straight line defines the fatigue resistance curve for the detail. In log form, the relationship is given by

$$\log N = \log A - b \cdot \log S_r \tag{2.5}$$

In the discussion that follows, the constant A is the intercept value of the allowable fatigue curve. As previously discussed, the allowable fatigue curve is used to calculate the remaining safe life and is derived from the lower bound of the approximate 95 percent confidence limit for 95 percent survival based on a regression analysis of the test data. For convenience in calculating the remaining life in years, a constant K is used rather than A. This constant is related to A by

$$K = \frac{A}{365 \times 10^6} \tag{2.6}$$

In the denominator, the constant 365, when multiplied by T_a and C in Equation 2.1, converts fatigue life from cycles to years; the constant 10^6 simply reduces the number of digits required to display K.

When calculating the remaining mean life, the constant f is used to modify the constant K. The constant f = the ratio of the mean curve intercept, A', and the allowable curve intercept, A. As previously discussed, the mean curve is simply derived from a regression analysis of the fatigue test data. No modification to the constant K is necessary when calculating the remaining safe life. Thus, when calculating the remaining safe life, f = 1.0.

29

The allowable stress range curve and the mean stress range curve are assumed to be parallel on a log-log plot. Consequently, the slope for both curves is the same. Thus, b = the slope of either curve.

2.5.5 Lifetime Average Daily Truck Volume (T_a)

Using Figure 6, the lifetime average daily truck volume in the outer lane, T_a, can be determined from the present average daily truck volume in the outer lane, T, the annual growth rate, g, and the present age of the bridge, a.

The present average daily truck volume in the outer lane, T, can be calculated from the ADT at the site as follows:

$$T = (ADT)F_T F_L \tag{2.7}$$

where ADT = present average daily traffic volume (both directions) on the bridge; F_T = fraction of trucks in the traffic; and F_L = fraction of trucks in the outer lane. A value for ADT must be obtained from Department of Transportation data for the location of interest. It is suggested [Moses et al., 1987] that for rural interstate highways $F_T = 0.20$, for rural highways and urban interstate highways $F_T = 0.15$, and for urban highways $F_T = 0.10$. The variable F_L may be determined from Table 2.

Table 2. Fraction of Trucks in Outer Lane [Moses et al., 1987]

No. of Lanes	2-Way Traffic	1-Way Traffic
1	-	1.00
2	0.60	0.85
3	0.50	0.80
4	0.45	0.80
5	0.45	0.80
6 or more	0.40	0.80

The annual growth rate, g, should be estimated by combining a knowledge of local conditions with historical data on growth rates. Table 3 presents growth rate values that
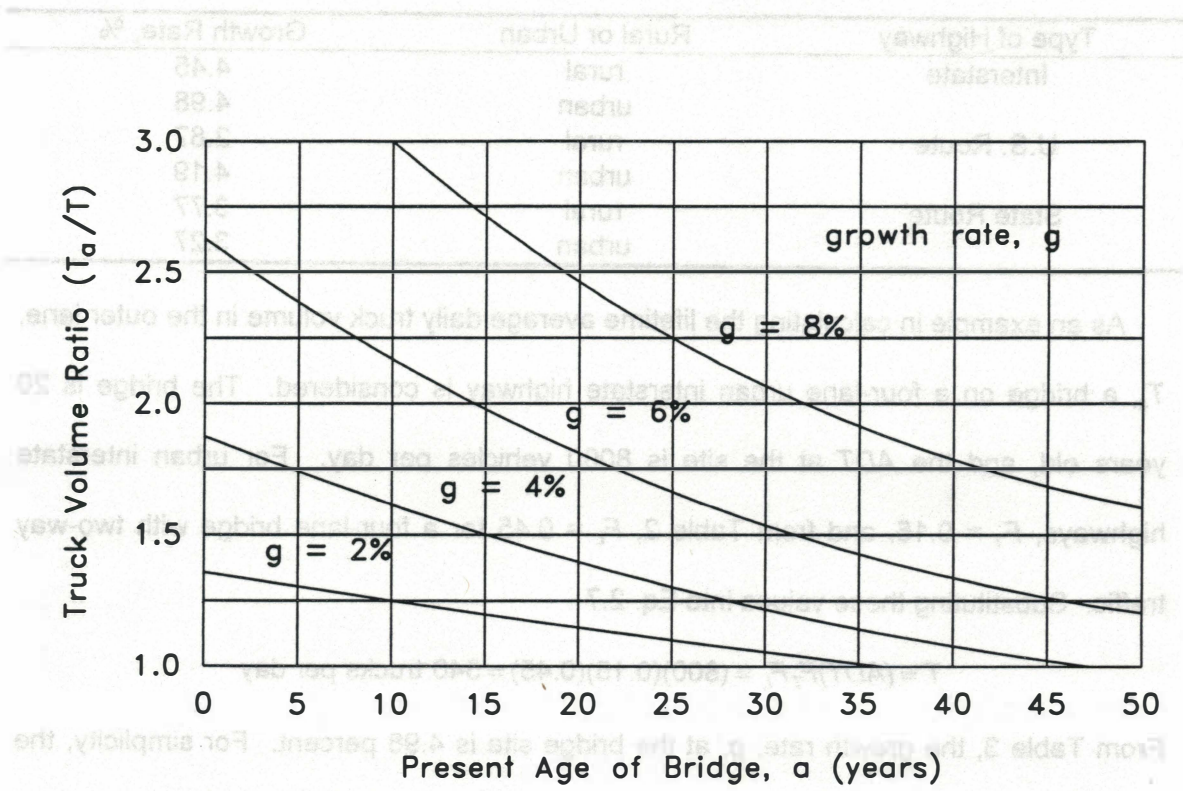
Figure 6. Truck Volume Ratio (Ta/T) [Moses et al, 1987]

were estimated from Annual Average Daily Traffic (*AADT*) data taken at counting stations throughout the United States between the years 1938 and 1985.

Table 3. Observed Average Daily Traffic (ADT) Growth Rates [Moses et al., 1987]

Type of Highway	Rural or Urban	Growth Rate, %
Interstate	rural	4.45
	urban	4.98
U.S. Route	rural	2.87
	urban	4.19
State Route	rural	3.77
	urban	3.27

As an example in calculating the lifetime average daily truck volume in the outer lane, T_a, a bridge on a four-lane urban interstate highway is considered. The bridge is 20 years old, and the *ADT* at the site is 8000 vehicles per day. For urban interstate highways, $F_T = 0.15$, and from Table 2, $F_L = 0.45$ for a four-lane bridge with two-way traffic. Substituting these values into Eq. 2.7

$$T = (ADT)F_T F_L = (800)(0.15)(0.45) = 540 \text{ trucks per day}$$

From Table 3, the growth rate, g, at the bridge site is 4.98 percent. For simplicity, the growth rate is rounded to 5.0 percent. Thus, $T = 540$ trucks per day, $g = 5.0$, and $a = 20$ years. Using Figure 6, the truck volume ratio $(T_a/T) = 1.7$ resulting in a lifetime average daily truck volume, $T_a = 918$ trucks per day.

A complete set of calculations for determining remaining fatigue life based on Equation 2.1 is provided in Section 3.5 of this report.

CHAPTER 3

EVALUATION OF U.S. 69 BRIDGE

3.1 Field Testing

A plan view of the U.S. 69 bridge is provided in Figure 7(a) and a cross section in Figure 7(b). Field testing focused on the northbound continuous spans between abutment one and pier three. End spans were chosen for study to simplify moving work vehicles on and off the bridge, and to capture the impact loading caused by a vehicle bouncing as it moves onto the bridge. A plan view of the relevant portion of the bridge is reproduced in Figure 8.

3.1.1 Instrumentation

In Figure 8, general locations of three groups of eight strain gages are indicated. Gages were installed in groups of eight to conform to the eight channel limitation of the data acquisition equipment. All gages were installed on the center span of the three span section because stresses from a preliminary analysis were highest in this span. Gages in Group 1 were installed in a negative moment region (compression on the bottom flange of the girder) and gages in Groups 2 and 3 were installed in a positive moment region (compression on the top flange of the girder). A fourth group, which is not shown in Figure 8, was created by combining half of the gages each from Groups 2 and 3.

Two groups of gages were installed in the positive moment region, where the bottom flanges of the plate girders are under high tension, since this is the critical region for fatigue. One group of gages was installed in a negative moment region to provide

Abutment No. 1   Pier No. 3   Pier No. 7   Abutment No. 2

← Southbound

Northbound →

Instrumented Span

Continuous Girders ◄─────────────────► Continuous Girders ◄─────────────────► Continuous Girders

(a) Plan View

Southbound   Northbound

├─Shoulder─┼─Driving Lane─┼─Driving Lane─┼Shoulder┼Shoulder┼─Driving Lane─┼─Driving Lane─┼─Shoulder─┤

9.5'   8'   8'   8'   8'   8'   8'   8'   9.5'

① ② ③ ④ ⑤ ⑥ ⑦ ⑧ ⑨ ⑩
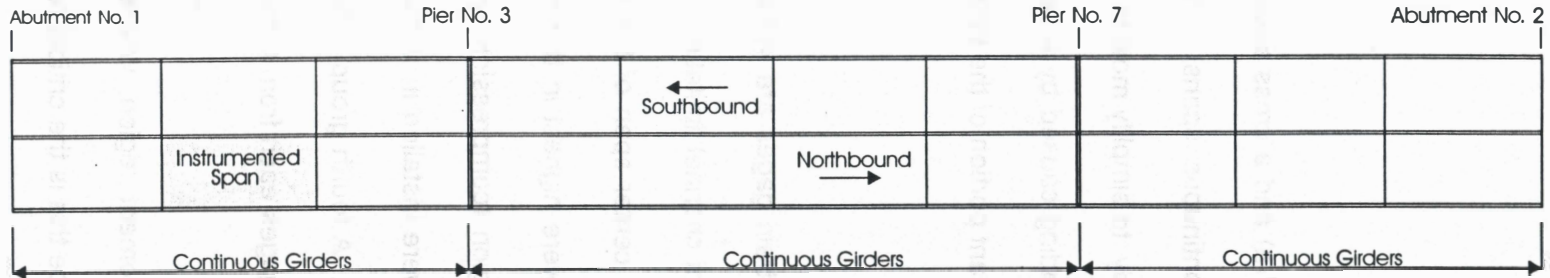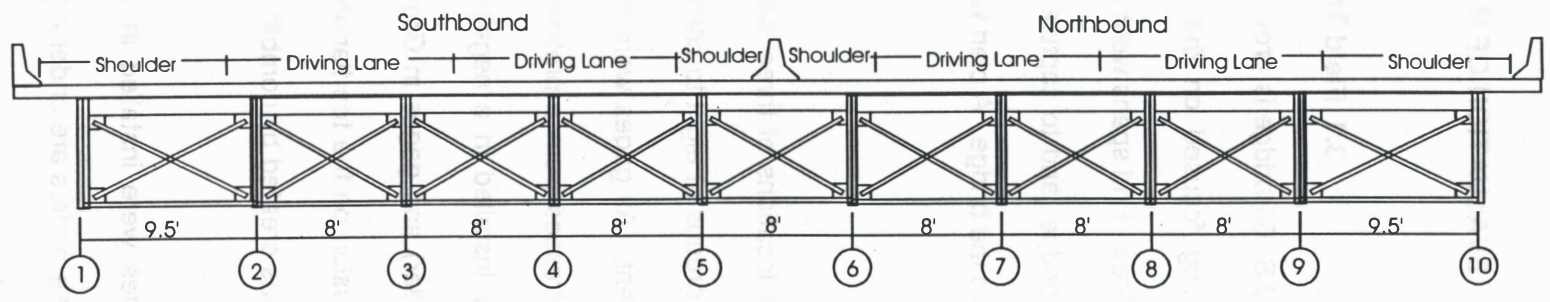
(b) Cross Section

Figure7. Plan View and Cross Section of U.S. 69 Bridge Over South Canadian River

Figure 8. Strain Gage Locations in Plan View

information on the level of composite action occurring in this region; this information is useful for computer modeling. Gages were installed under the shoulder since this was the area of new construction and because the outside girder is the easiest to load with heavy static loads. A truck can be positioned to straddle the outside girder and there is framing on only one side of the girder to help carry the load. Gages were installed under the center lane to acquire data for a rapidly moving load immediately above instrumented girders and to provide information on transverse load distribution.

Locations of individual gages within each group are shown in Figure 9. All gages on girder flanges are centered 1 ft north of the crossframes. Gages were placed away from crossframes because fatigue design is based on nominal stresses at the detail location. Stresses immediately adjacent to a welded attachment are expected to be above the nominal level due to stress concentrations. Gages are attached on the inside of the top and bottom flanges. Gages were placed on the inside of the bottom flange because this is the location of the welded details in question and because it is easier to work in this position. Two gages were placed on bottom flanges since this is the critical flange for fatigue. Having two gages provides some redundancy in data. If one gage fails, the second can provide the necessary information. Only one gage is attached to the top flange since stresses at this location are expected to be small and/or compressive. Gage Group 4 is made up of the bottom flange gages from Groups 2 and 3.

All gages on crossframes are attached to the vertical leg of the angle at approximately the centroid of the angle. These gages are intended to measure tensile strain. Bending strains are substantially avoided by attaching near the centroid.
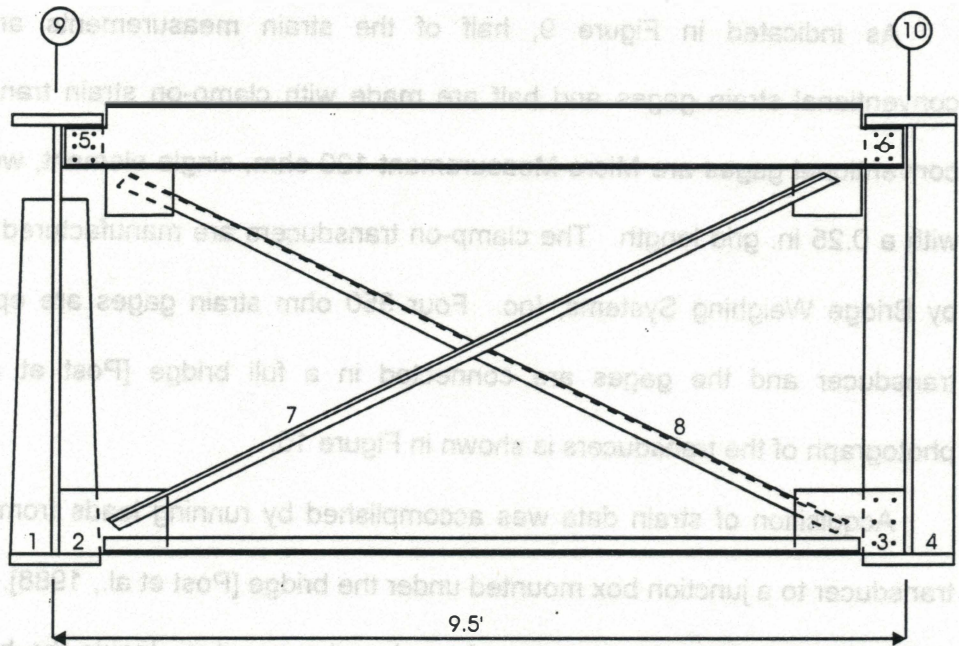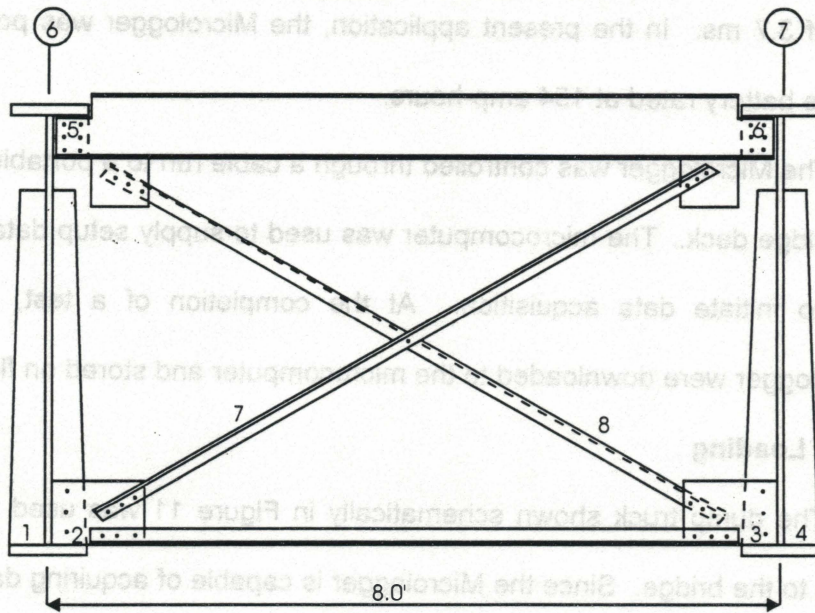
36

1,4,7,8 are clamp-on transducers
2,3,5,6 are strain gages

1,2,3,4,5,6 are attached to the inside flange of the plate girder 1 ft north of the crossframe
7,8 are attached to the vertical leg of the crossframe angle

(a) Gage Positions for Groups 1 and 3

1,4,7,8 are clamp-on transducers
2,3,5,6 are strain gages

1,2,3,4,5,6 are attached to the inside flange of the plate girder 1 ft north of the crossframe
7,8 are attached to the vertical leg of the crossframe angle

(b) Gage Positions for Group 2

Figure 9. Gage Positions on Structural Framing

As indicated in Figure 9, half of the strain measurements are made with conventional strain gages and half are made with clamp-on strain transducers. The conventional gages are Micro-Measurement 120 ohm, single element, weldable gages, with a 0.25 in. grid length. The clamp-on transducers are manufactured and marketed by Bridge Weighing Systems, Inc. Four 350 ohm strain gages are epoxied to each transducer and the gages are connected in a full bridge [Post et al., 1988]. A photograph of the transducers is shown in Figure 10.

Acquisition of strain data was accomplished by running leads from each gage or transducer to a junction box mounted under the bridge [Post et al., 1988]. The leads are attached to the box with an external amphenol connector. Inside the box, signals are routed to a Campbell Scientific 21X Micrologger. The Micrologger is a microcomputer based datalogger with eight differential analog input channels and a maximum sample rate of 3.7 ms. In the present application, the Micrologger was powered by a 12-volt marine battery rated at 154 amp-hours.

The Micrologger was controlled through a cable run to a portable microcomputer on the bridge deck. The microcomputer was used to supply setup data to the Micrologger and to initiate data acquisition. At the completion of a test, data stored in the Micrologger were downloaded to the microcomputer and stored on floppy disks.

3.1.2 Loading

The dump truck shown schematically in Figure 11 was used to apply a series of loads to the bridge. Since the Micrologger is capable of acquiring data from a maximum of eight channels, it was necessary to repeat the series of loads for each of the gage groups identified in Figure 8. The load series included truck speeds increasing from 0 to 5 to 25 to 40 mph, and truck transverse positions moving from the shoulder to the right
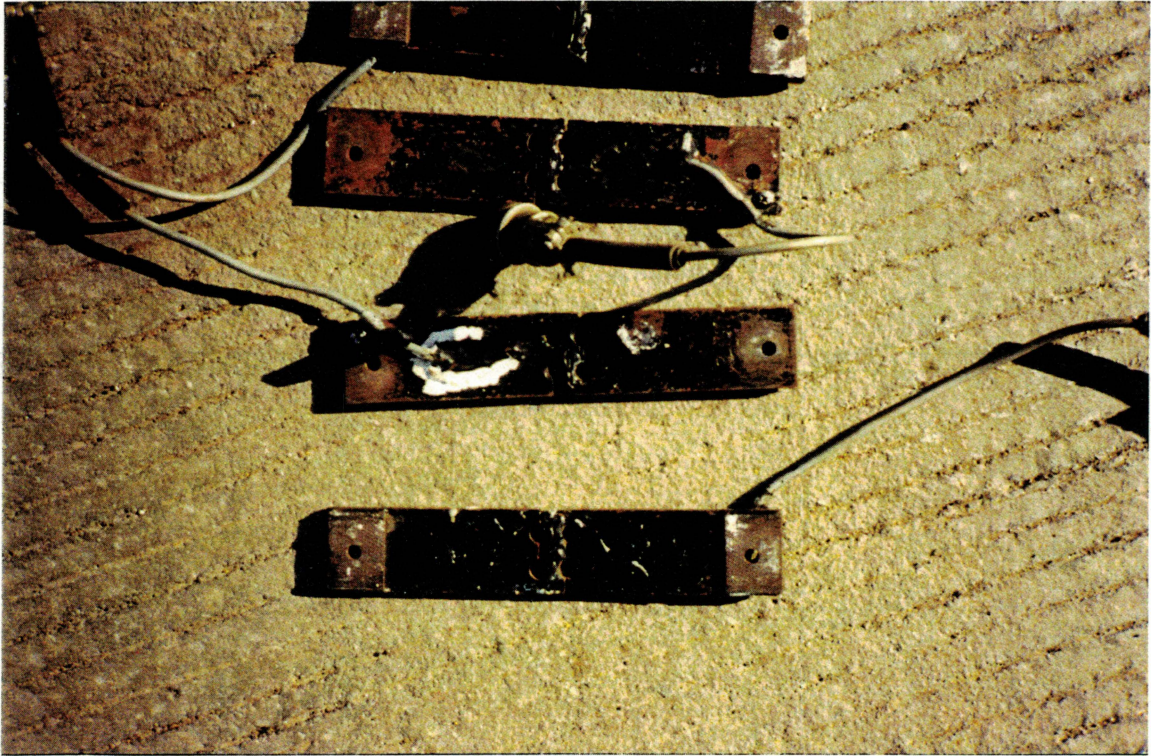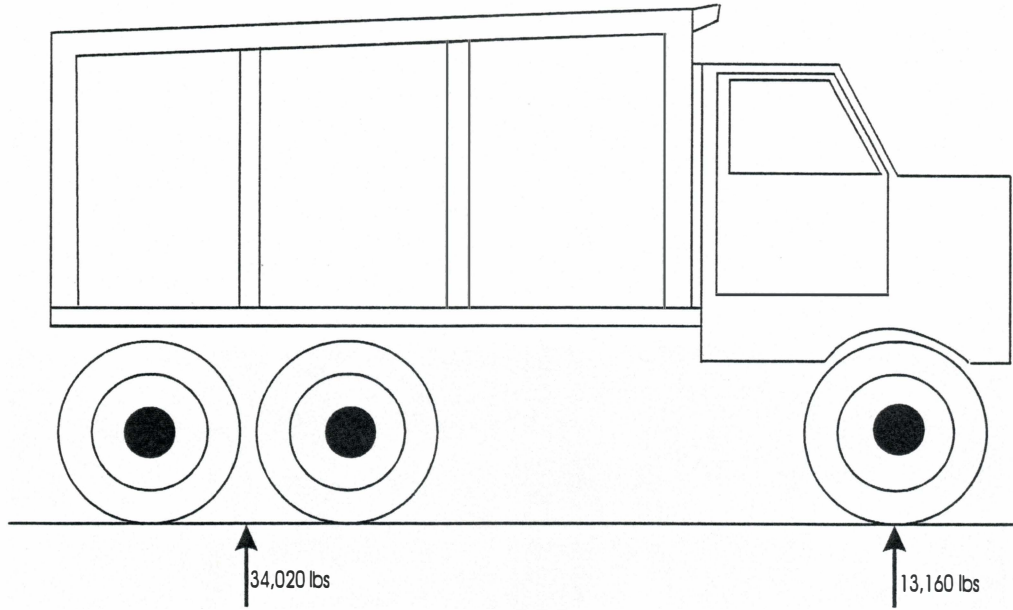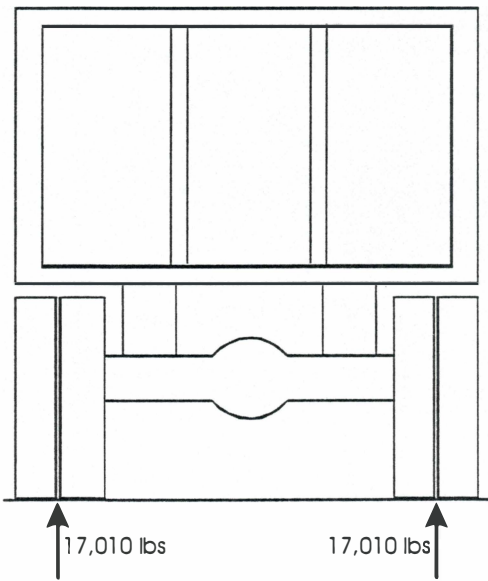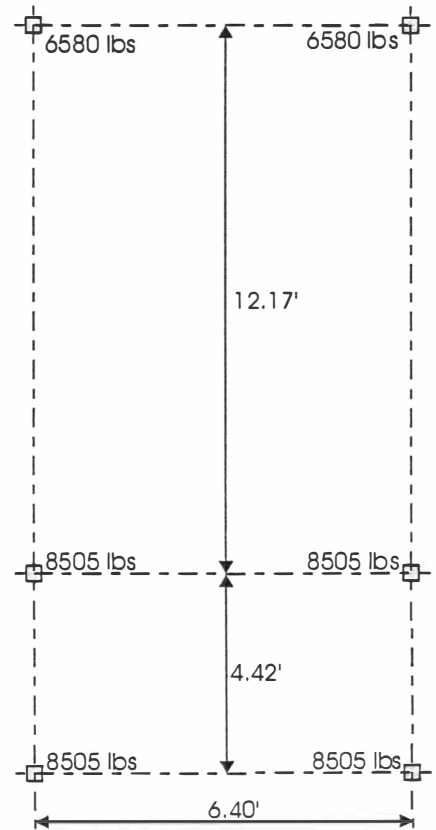
Figure 10. Clamp-on Strain Transducers

(a) Side View

34,020 lbs   13,160 lbs

6580 lbs   6580 lbs

12.17'

8505 lbs   8505 lbs

4.42'

8505 lbs   8505 lbs

6.40'

17,010 lbs   17,010 lbs

(b) Rear View

(c) Wheel Loads

Figure 11. Dump Truck Used to Load Bridge

40

lane to the left lane. For static loads, the middle axle of the truck was always placed directly above the Group 2/3 crossframe.

Tests were not conducted for each gage group at all four truck speeds in each of the three transverse truck positions. For Group 1, data were recorded for the truck traveling at 0 and 5 mph in the shoulder; and, 0, 5, and 25 mph in the right lane. For Group 2, data were recorded for the truck traveling at 0 mph in the shoulder; 0, 5, and 25 mph in the right lane; and, 25 and 40 mph in the left lane. For Group 3, data were recorded for the truck traveling at 0 mph in the shoulder; 0, 5, 25 mph in the right lane; and, 25 and 40 mph in the left lane. The truck was driven down the shoulder only for the Group 1 gages because personnel and instrumentation occupied the shoulder during the test and, after the first test, it was decided that safety could be compromised by having a moving truck too close to personnel. The maximum velocity in the right lane was limited to 25 mph because that was the maximum velocity the truck could reliably obtain in the length of highway which had been closed to normal traffic. The left lane was kept open to traffic throughout the tests, so the test truck was able to start well in advance of the bridge and reach a stable velocity of 40 mph over the instrumented sections. Minimum velocity for the left lane was set at 25 mph to avoid the danger associated with slow traffic in a high speed lane.

Data were recorded only if the dump truck was able to pass alone over the continuous three-span region of interest. To accomplish this, it was necessary to close the shoulder and right traffic lane. Static measurements were obtained by parking the truck with the middle axle directly above the Group 2/3 crossframe and waiting for both north- and southbound traffic to clear. Dynamic measurements were obtained by waiting for traffic to clear both before and after the continuous three-span region, starting the truck far enough behind the bridge to allow the driver to attain the desired

41

speed, and manually triggering the Micrologger just before the truck entered the span. Time required for the truck to pass over the continuous three-span region was estimated and provided as setup information to the Micrologger. Data acquisition stopped at the end of this time period.

3.2 Analytical Model

Two different types of analysis were performed at significantly different levels of complexity. The first analysis described below is a grid analysis performed on a microcomputer. As discussed below, simplifying assumptions were made in the model to maintain the model size at a workable level. The second analysis was a three-dimensional finite element analysis performed on a workstation. Separate elements were used to model the girder flanges, the girder web, the concrete deck, and the crossframe members.

3.2.1 Grid Analysis

3.2.1.1 Grid Model. The grid analysis was performed using version 19.1 of STAAD-III/ISDS running on a personal computer with an Intel 90 Mhz pentium processor and 16 MB RAM. Only the three spans between abutment 1 and pier 3 (see Figure 7) are included in the model. The total number of joints in the model is 160 and the total number of members is 294.

Grid elements running longitudinal with the bridge are located along girder lines. Girders are treated as prismatic between supports with the cross sections shown in Figure 12. The deck is assumed to be fully composite with the girders in both the positive and negative moment regions, and section properties are computed assuming elastic behavior. Assuming a prismatic girder between supports reduces the modeling effort and minimizes the number of joints and elements in the model. Girders are

42
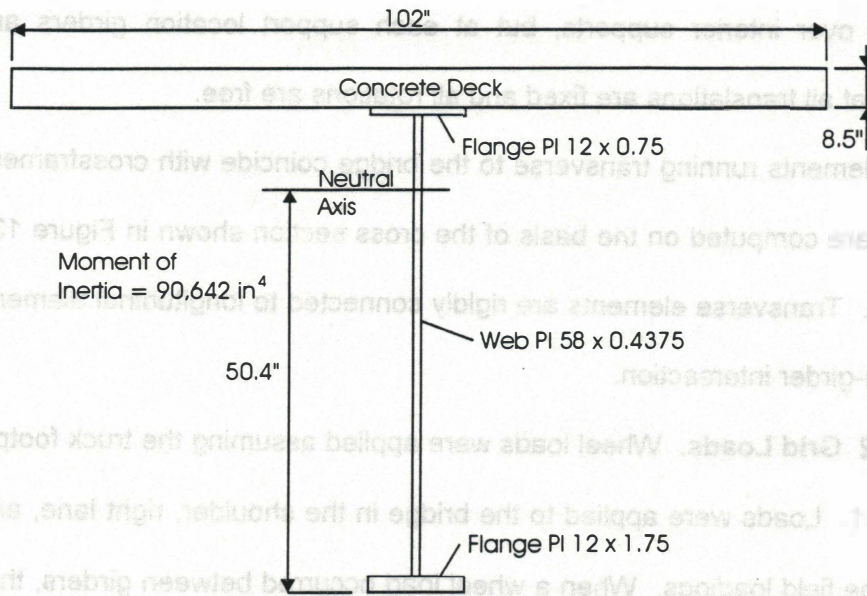
(a) Between Abutment No. 1 and Pier No. 1 and Between Pier No. 2 and Pier No. 3
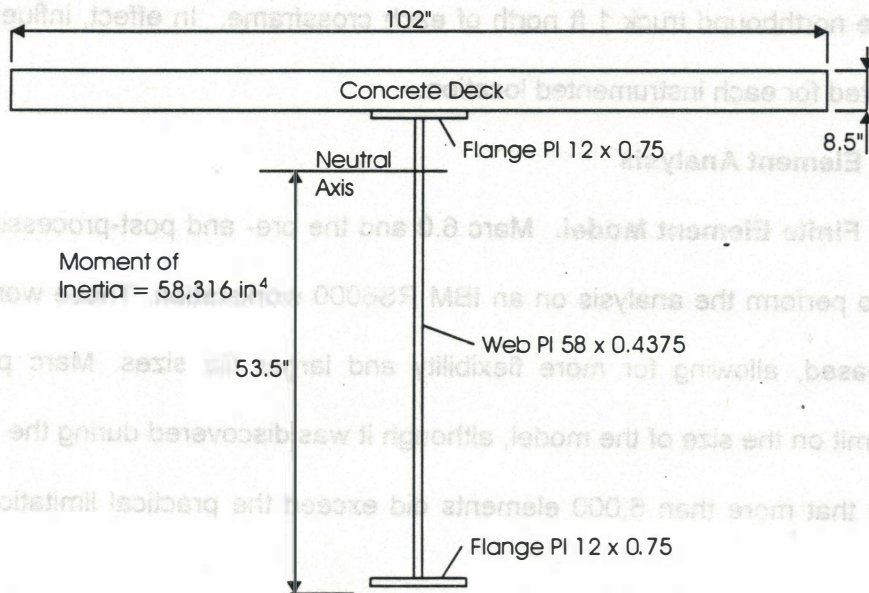
(b) Between Pier No. 1 and Pier No. 2

Figure 12. Composite Section for Grid Analysis

continuous over interior supports, but at each support location girders are pinned, meaning that all translations are fixed and all rotations are free.

Grid elements running transverse to the bridge coincide with crossframes. Section properties are computed on the basis of the cross section shown in Figure 13 acting as a solid unit. Transverse elements are rigidly connected to longitudinal elements at each crossframe-girder intersection.

3.2.1.2 Grid Loads. Wheel loads were applied assuming the truck footprint shown in Figure 11. Loads were applied to the bridge in the shoulder, right lane, and left lane to match the field loadings. When a wheel load occurred between girders, the load was distributed to girders on either side of the wheel assuming the wheel to be simply supported by the deck between the girders. For comparison to strains measured under moving loads, girder moments at instrumented locations were computed with the rear wheels of the northbound truck 1 ft north of each crossframe. In effect, influence lines were generated for each instrumented location.

3.2.2 Finite Element Analysis

3.2.2.1 Finite Element Model. Marc 6.0 and the pre- and post-processor Mentat were used to perform the analysis on an IBM RS6000 workstation. These workstations are UNIX based, allowing for more flexibility and larger file sizes. Marc places no theoretical limit on the size of the model, although it was discovered during the course of the analysis that more than 6,000 elements did exceed the practical limitations of the RS600's.

Initially three continuous spans were modeled, similar to the grid analysis. This model required 18,792 elements and 17,999 nodes in order to keep the aspect ratio of all elements less than 2 to 1. Output files exceeded 100 megabytes in size; this was beyond the limitations of the system which caused the model to run incessantly. In order

W12x30

Neutral
Axis

60"

Moment of
Inertia = 7712 in^4

37.75"

Crossframe Angles
(not included in
moment of inertia)

2 - L3x2.5x0.375

Figure 13. Crossframe Section Properties

to complete the analysis, the model was divided along both longitudinal and transverse lines of symmetry, reducing the model to 25 percent of its original size. The reduced model has 4,802 elements and 4, 685 nodes.
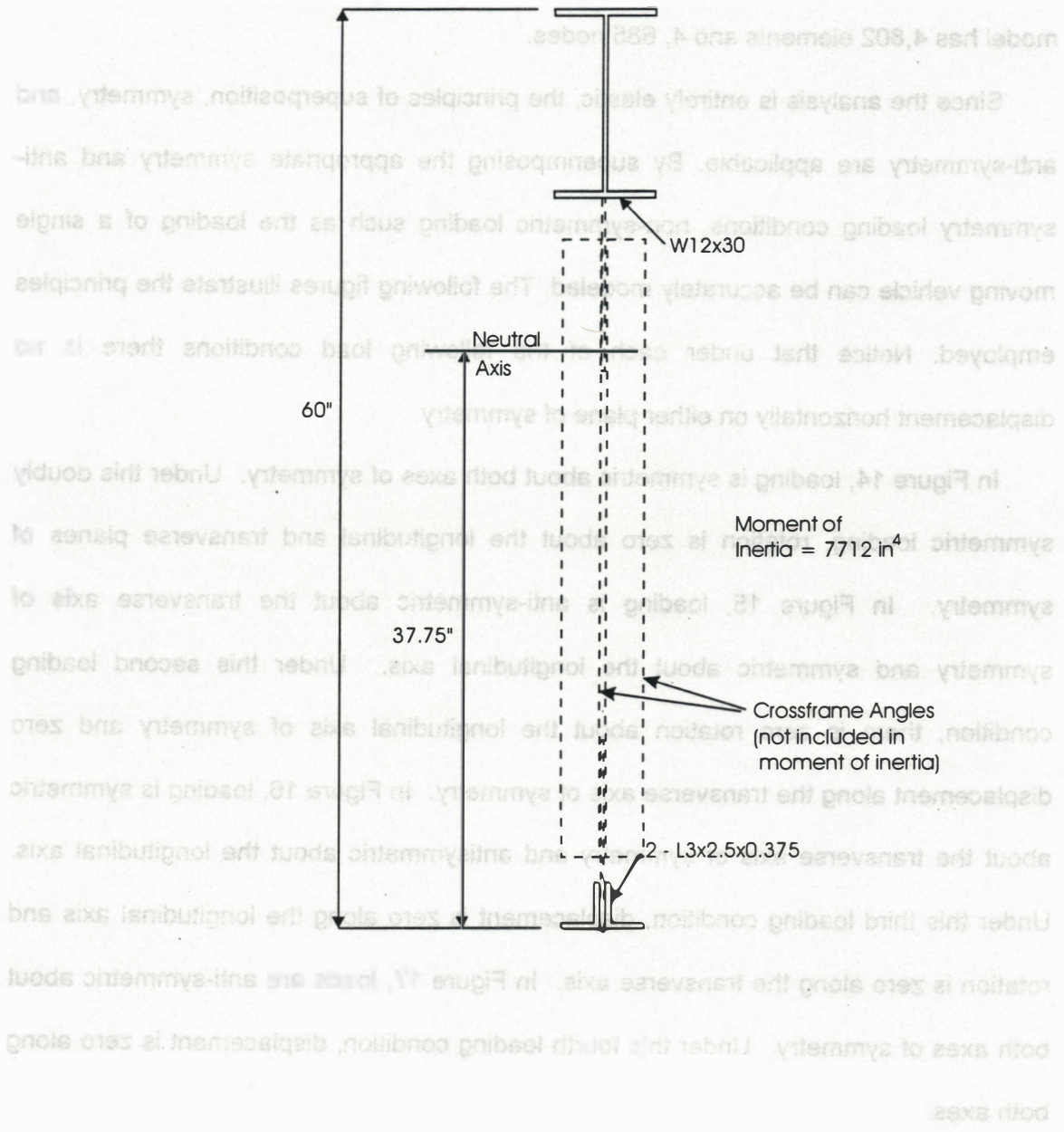
Since the analysis is entirely elastic, the principles of superposition, symmetry, and anti-symmetry are applicable. By superimposing the appropriate symmetry and anti-symmetry loading conditions, non-symmetric loading such as the loading of a single moving vehicle can be accurately modeled. The following figures illustrate the principles employed. Notice that under each of the following load conditions there is no displacement horizontally on either plane of symmetry.

In Figure 14, loading is symmetric about both axes of symmetry. Under this doubly symmetric loading, rotation is zero about the longitudinal and transverse planes of symmetry. In Figure 15, loading is anti-symmetric about the transverse axis of symmetry and symmetric about the longitudinal axis. Under this second loading condition, there is zero rotation about the longitudinal axis of symmetry and zero displacement along the transverse axis of symmetry. In Figure 16, loading is symmetric about the transverse axis of symmetry and antisymmetric about the longitudinal axis. Under this third loading condition, displacement is zero along the longitudinal axis and rotation is zero along the transverse axis. In Figure 17, loads are anti-symmetric about both axes of symmetry. Under this fourth loading condition, displacement is zero along both axes.

Notice that, under all four loading conditions, the load in the bottom right quarter of each figure always acts down. All other loads act down in two figures and up in two figures. Therefore, superimposing the four loading conditions will provide a result identical to performing one analysis with one load equal to four times the magnitude of the individual loads in the four load cases, applied only in the bottom right quarter of the
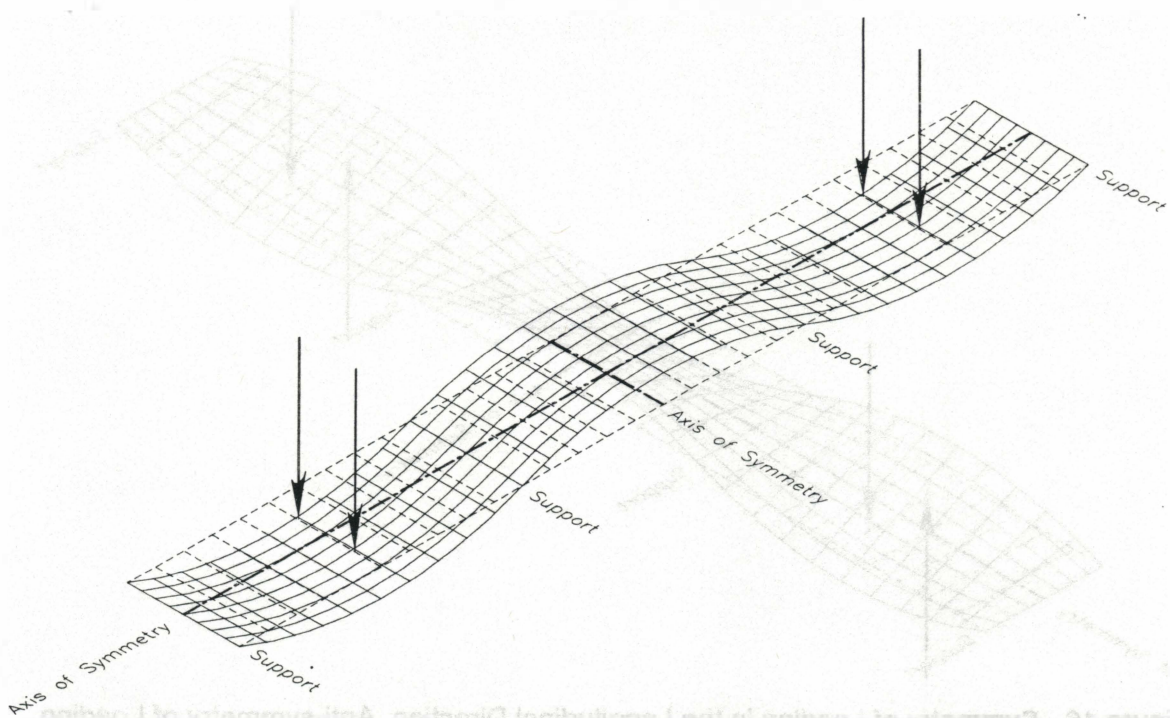
Figure 14. Symmetry of Loading in Transverse and Longitudinal Directions
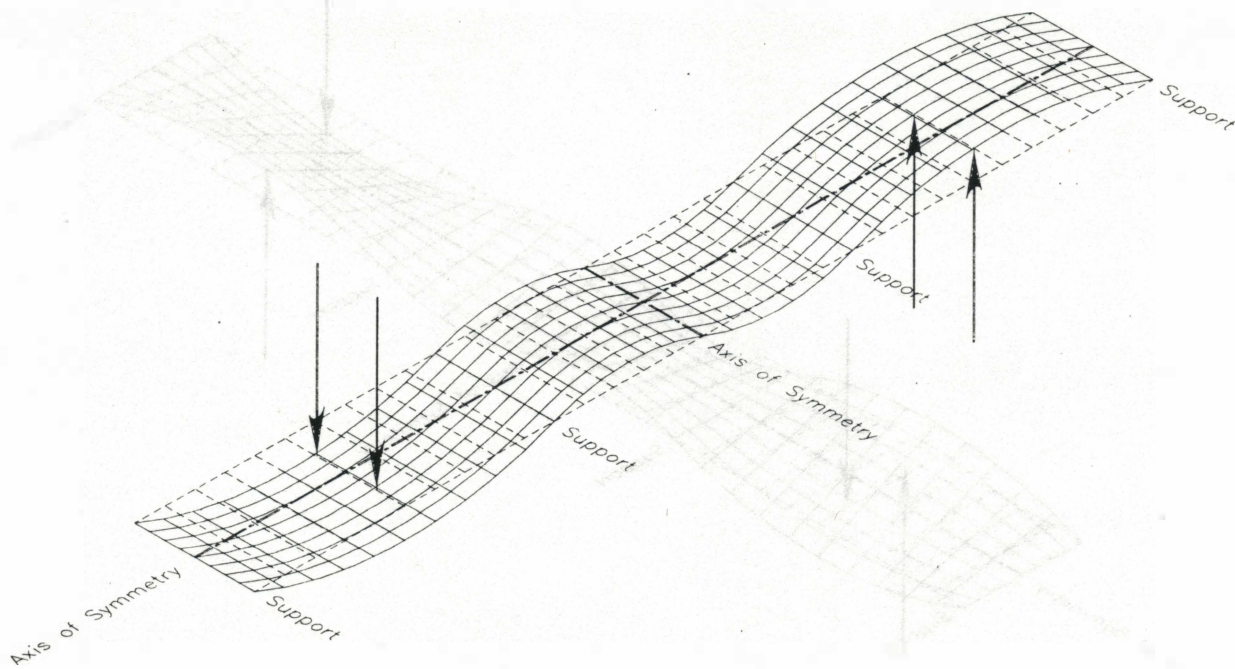

Figure 15. Anti-symmetry of Loading in Longitudinal Direction, Symmetry of Loading in Transverse Direction
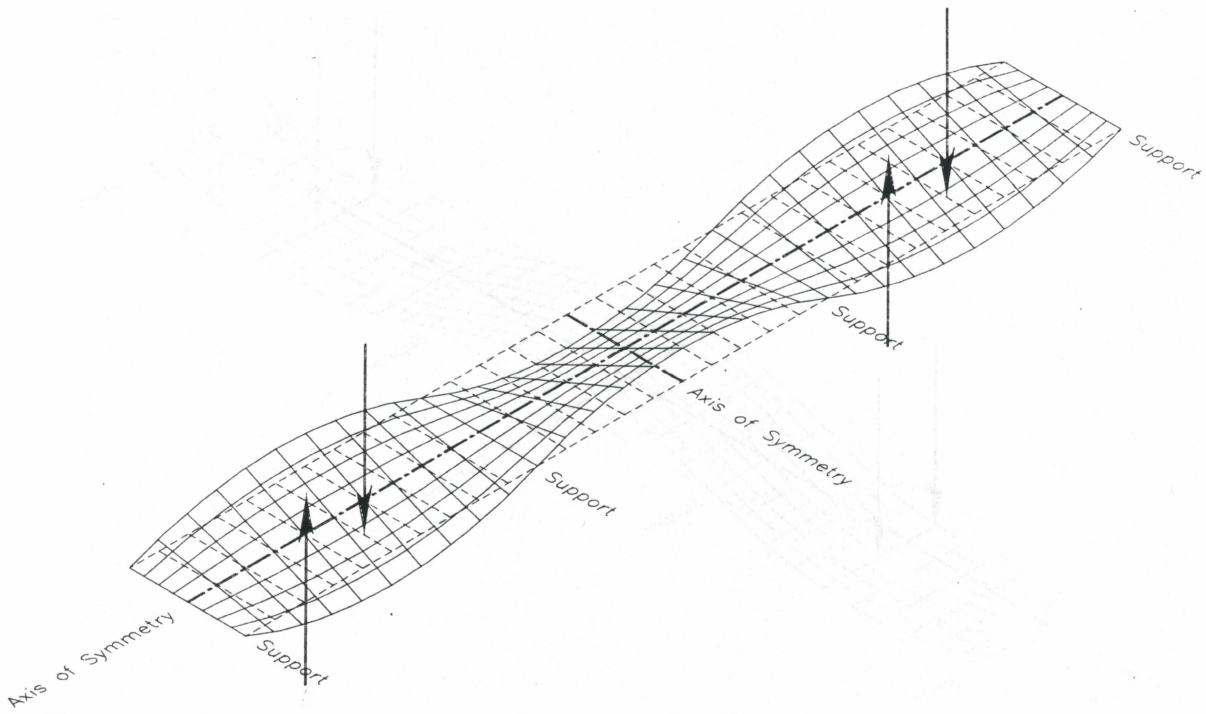
Figure 16. Symmetry of Loading in the Longitudinal Direction, Anti-symmetry of Loading in the Transverse Direction
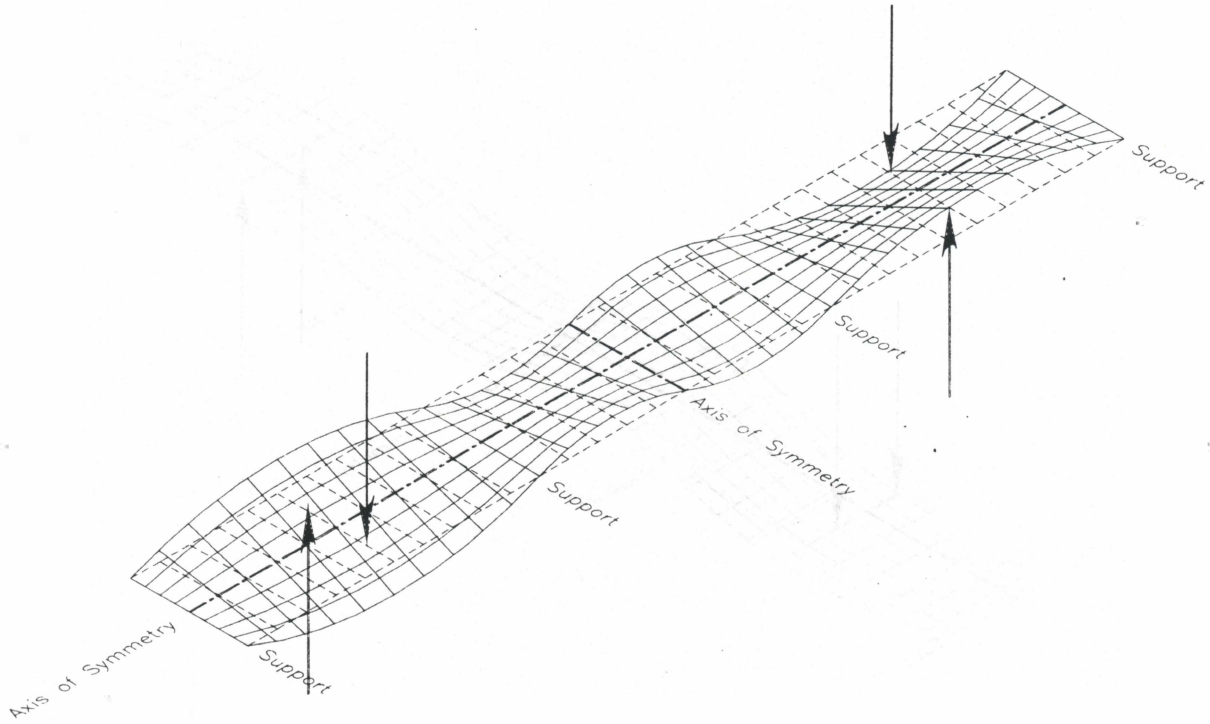

Figure 17. Anti-Symmetry of Loading in Both the Longitudinal and Transverse Directions

three-span model. More importantly for purposes of reducing the model size, it is also possible to arrive at the same result by superimposing four analyses using only a quarter of the model as long as the each of the boundary conditions described in the preceding paragraph are applied in one of the analyses.

By superimposing these four cases it is possible to ascertain the effect of a concentrated load source anywhere on the three spans of interest by modeling only one quarter of the total continuous structure. It is merely necessary to add and subtract stresses to cancel unwanted loads while simultaneously letting the cases sum to unity for the desired load position, provided that position has been evaluated in the four reduced models.

The model used in the analysis accounts for the presence of stiffeners and the varying of flange thickness along the length of the bridge. All of the girders were modeled using the same geometric properties with the exception of additional stiffeners on the exterior girders as directed by the bridge plans. The girder flanges, web, stiffeners, and the deck were modeled using Marc's type 75 element. Element 75 is a bilinear thick-shell element. This element is comprised of four nodes which each have six degrees of freedom. Bilinear interpolation is used for the coordinates, displacements and rotations. This element was chosen for two reasons; it is relatively simple and efficient, and the element is well suited to the analysis of complex plate structures.

The diaphragms were modeled using two node 3-D truss elements. The particular element chosen was Marc's element type 9. The only stiffness modeled by this element is axial stiffness; therefore, bending stresses were not accounted for in these members.

Several assumptions were necessary in order to perform the analysis. No attempt was made to account for possible cracking or existing cracks in the deck concrete. The deck was modeled as a homogeneous isotropic shell with a constant thickness of 8

49

inches. Modulus of elasticity of the concrete was computed using the basic ACI equation [American Concrete Institute, 1995] assuming concrete with a unit weight of 145 pounds per cubic foot and a compressive strength of 4000 pounds per square inch. At service load it was assumed that the deck and girders were fully composite. Supports were assumed to provide vertical restraint only; restraint in other directions was provided only as necessary to maintain a stable structure. Care was taken to ensure that restraints did not induce axial stress.

3.2.2.2 Finite Element Loads. Loads were applied in a manner similar to the grid analysis. The truck footprint was applied at 16 locations each on the shoulder, right lane, and left lane. The first data point corresponds to the rear wheels of the truck on the abutment. To generate each succeeding data point, wheel loads were stepped at 18.75 ft intervals along the bridge deck. Wheel loads were applied directly to the shell elements modeling the deck.

3.3 Field and Analytical Test Results

Comparisons between field test and analytical results are made on the basis of stresses. In the case of the field test results, stresses are computed from measured strains assuming that the measured strains are principal strains. In the case of the grid analyses, stresses are computed from output girder moments using simple beam theory. For the finite element analyses, requested outputs were principal stresses at element centroids.

In the figures which follow, a cross section of the bridge is shown at the top of the sheet. In this cross section, the truck is placed in the correct transverse position for the data plotted below. Dimensions from the side barrier to the truck wheel are approximate for those load cases where the truck is moving, and assume that the truck is in the middle of the driving lane. Gage numbers corresponding to the legend for the plot are

50

shown on the cross section. Gage numbers on the cross section apply only to the plot immediately below that cross section, not necessarily to the plots shown in any other figures.

The grid model does not include individual crossframe members, so data for crossframes are not included in the plots of the grid analysis data. Also, in the grid analysis, stresses on opposite sides of the same flange are identical, so data are reported as a single gage.

3.3.1 Test Truck

In the following figures, all data from the field measurements are presented first, followed by all data from the grid analyses, followed by all data from the finite element analyses. Field data are presented in the same chronological order as the tests were conducted. In all figures except 29, 36, 48, and 50, the range of the vertical axis is -2 ksi to +2 ksi; in Figures 29 and 36 the range is -2 ksi to +3 ksi and in Figures 48 and 50 the range is -2 ksi to +2.4 ksi. The choice of ranges is based on a desire to be consistent between figures to allow easier visual comparisons while at the same time providing sufficient detail within each figure.

Results for Group 1 are shown in Figures 18 through 22. Recall that Group 1 gages are in the negative moment region north of pier 1. Note that bottom flange stresses are compressive while top flange stresses are tensile (as expected in a negative moment region) and of a smaller magnitude than bottom flange stresses. This behavior indicates that the girder is acting compositely with the concrete deck, even in the negative moment region. Also note that the stresses are very low, with the highest recorded stress magnitude being 1.2 ksi.

Figures 18 and 19 are for the truck in the static load position. The static position has the truck parked with its middle axle directly above the Group 2/3 crossframe, not

51
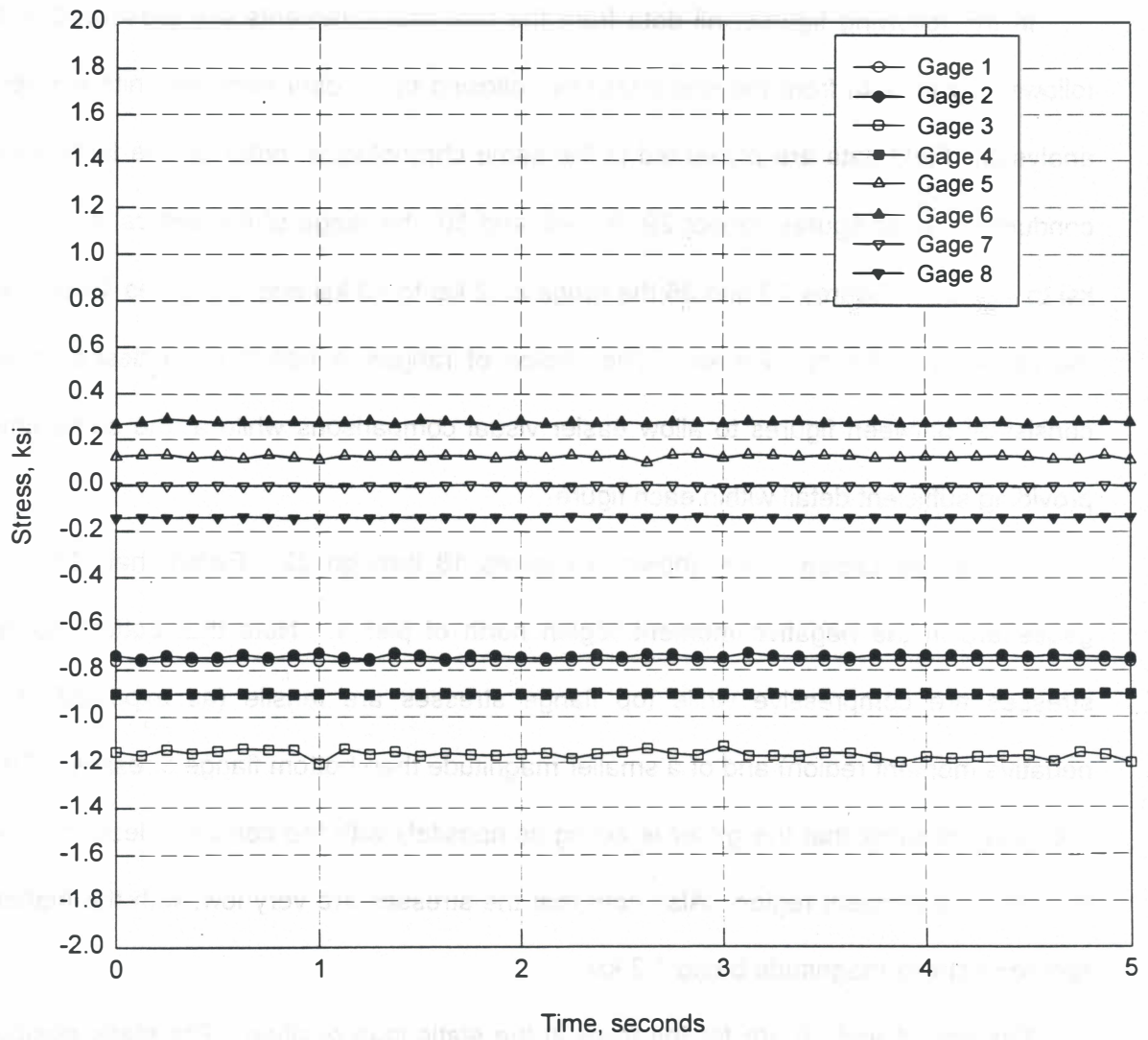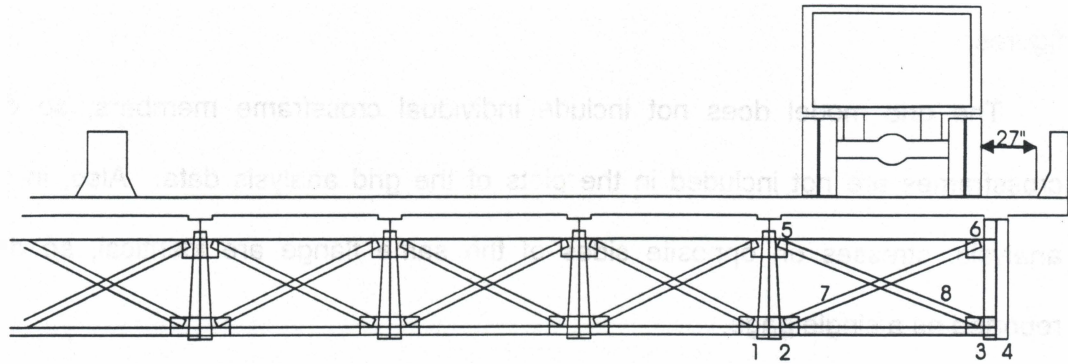
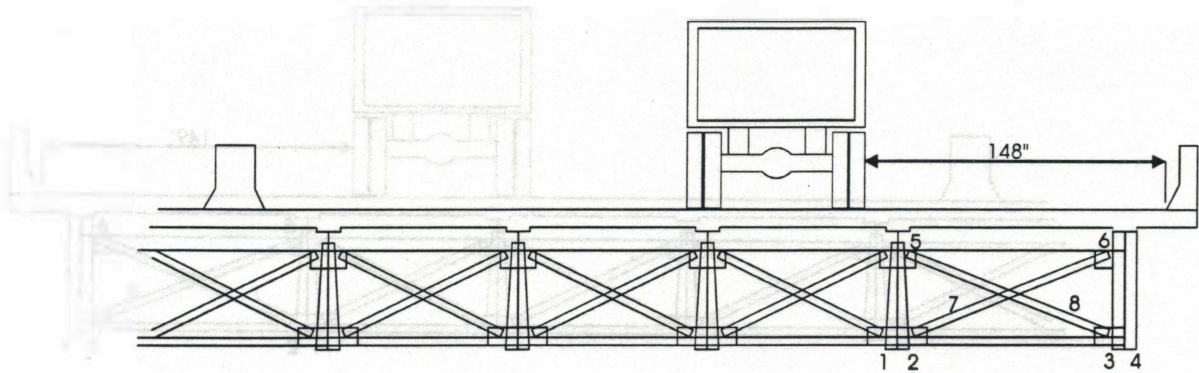Figure 18. Stationary Truck in Shoulder, from Measurements at Group 1 Location
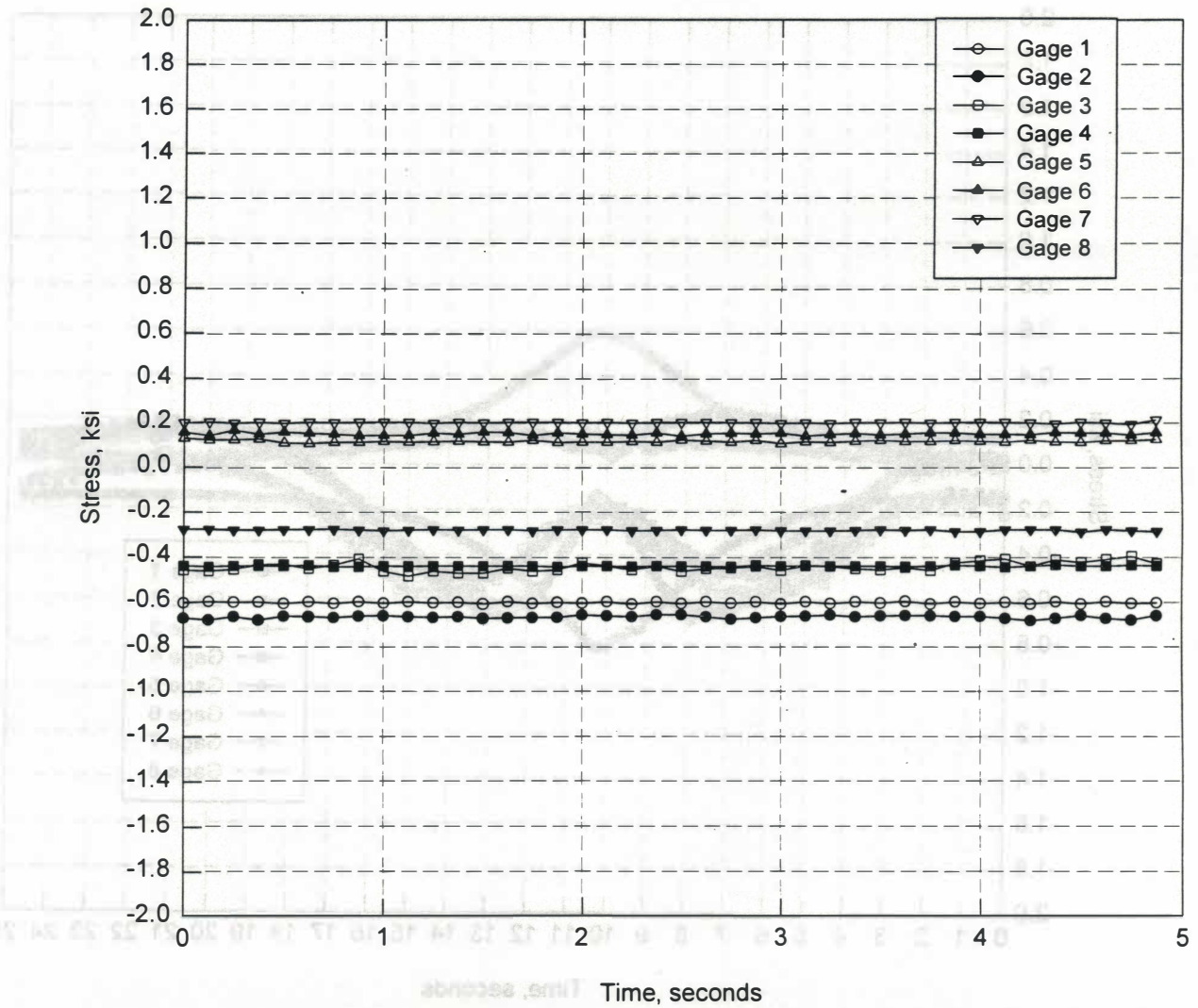
Figure 19. Stationary Truck in Right Lane, from Measurements at Group 1 Location
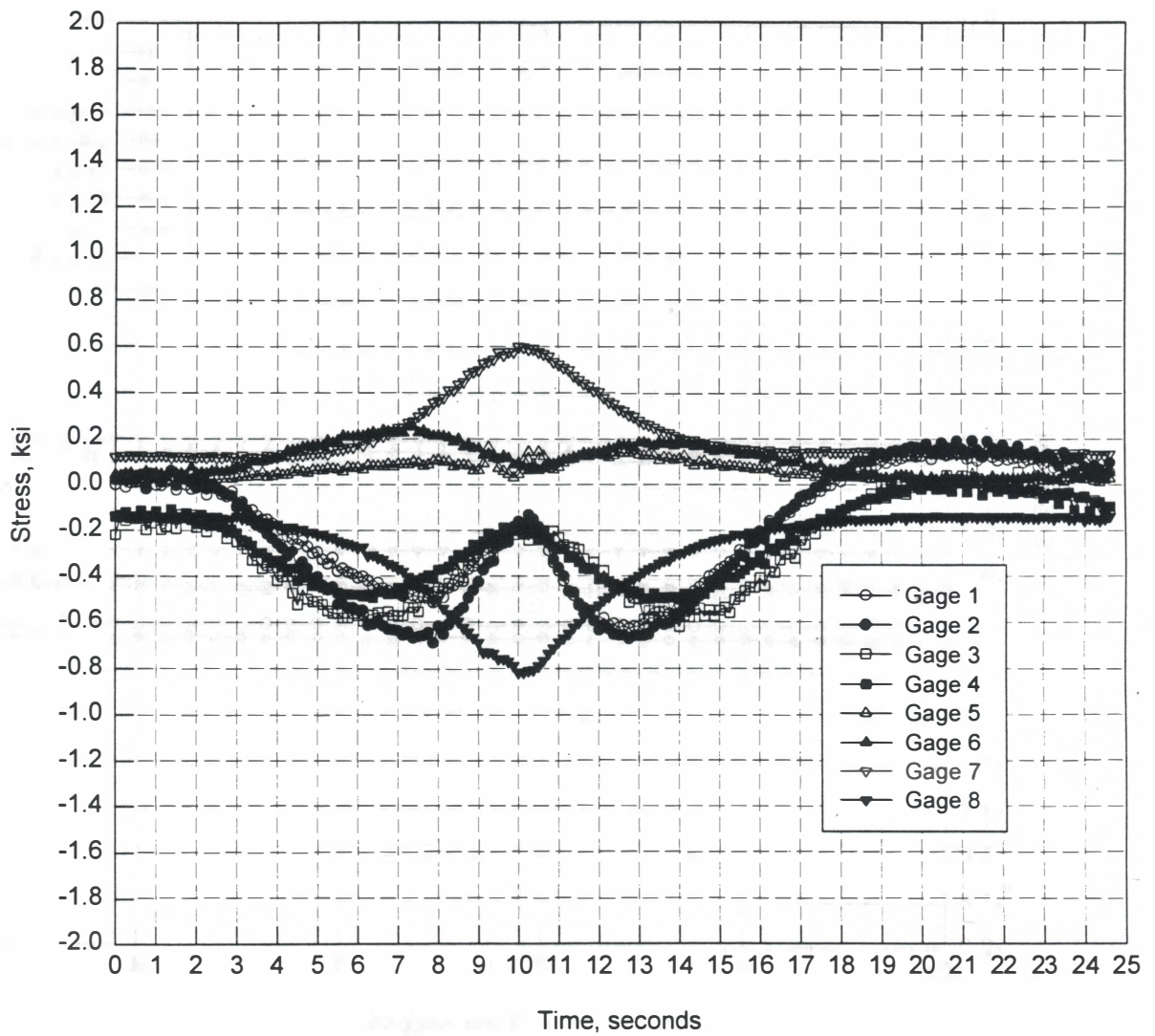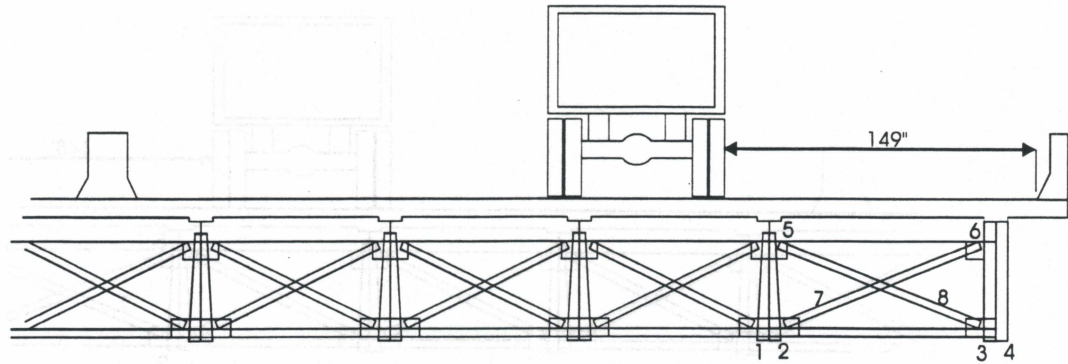
Figure 20. Truck Moving at 5 mph in Right Lane, from Measurements at Group 1 Location
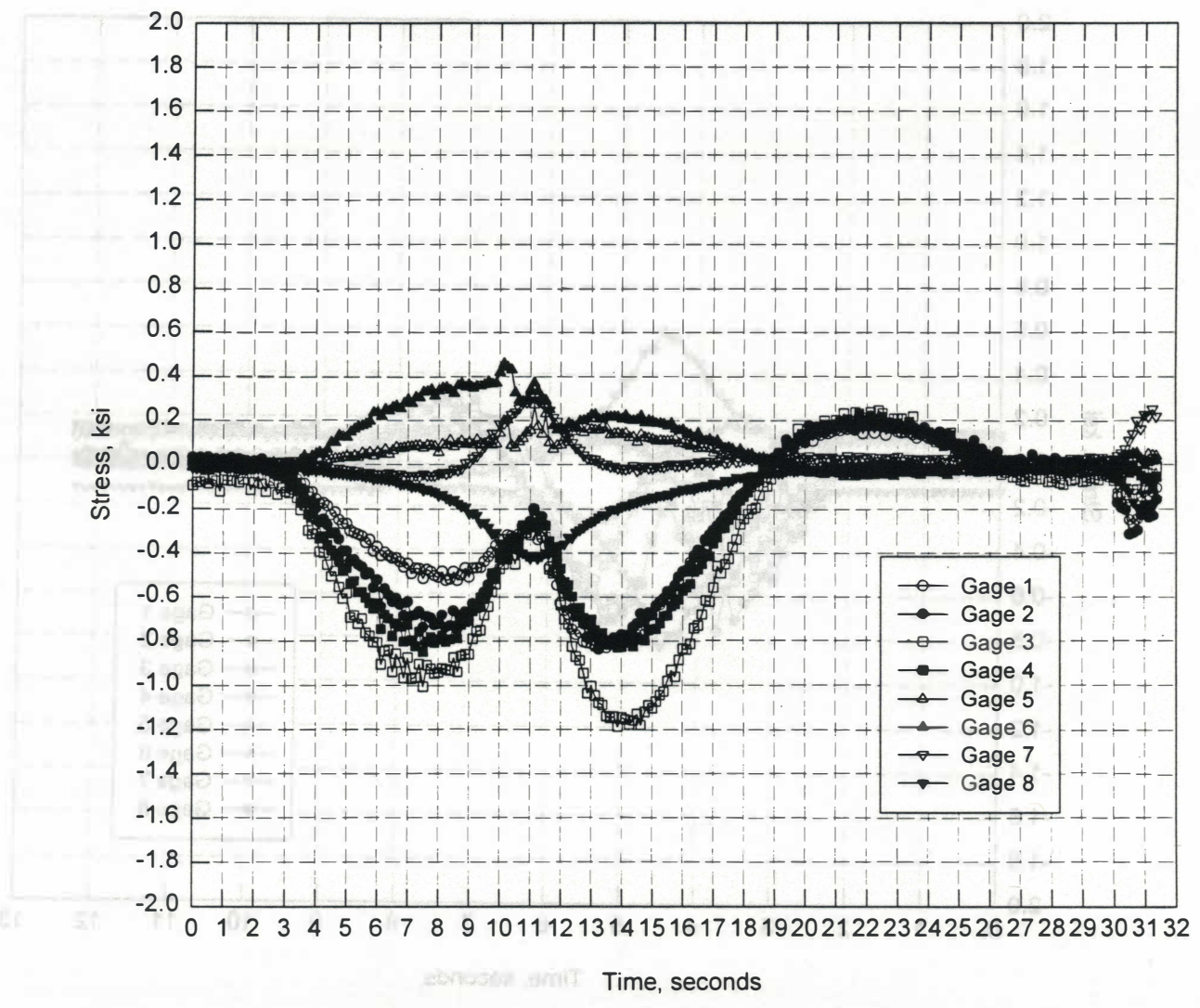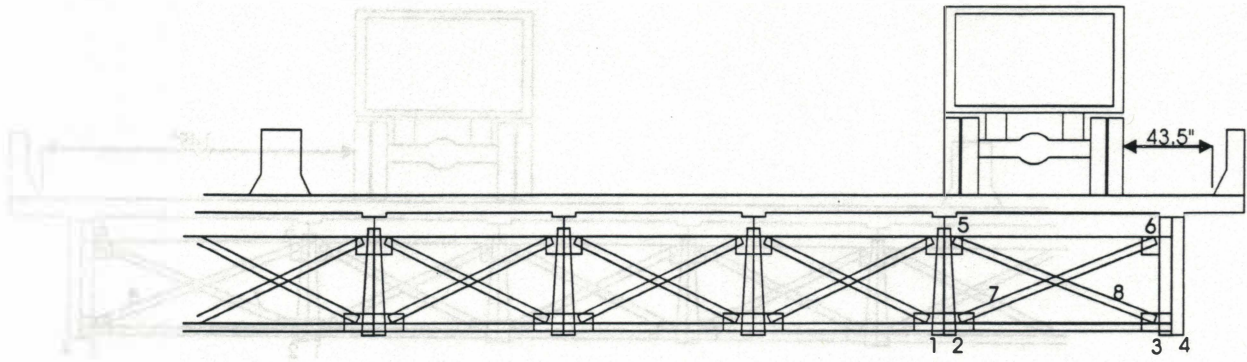
Figure 21. Truck Moving at 5 mph in Shoulder, from Measurements at Group 1 Location
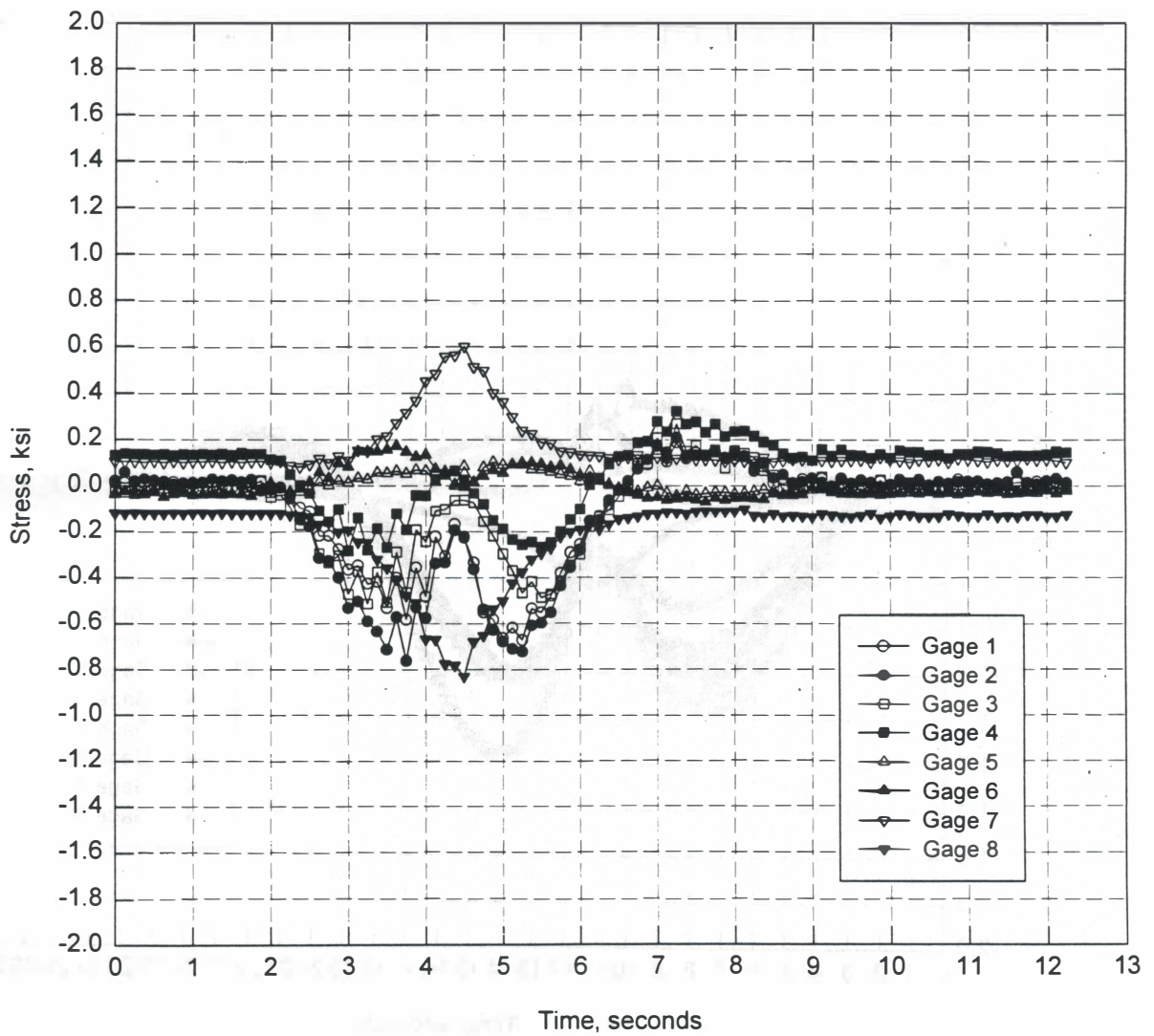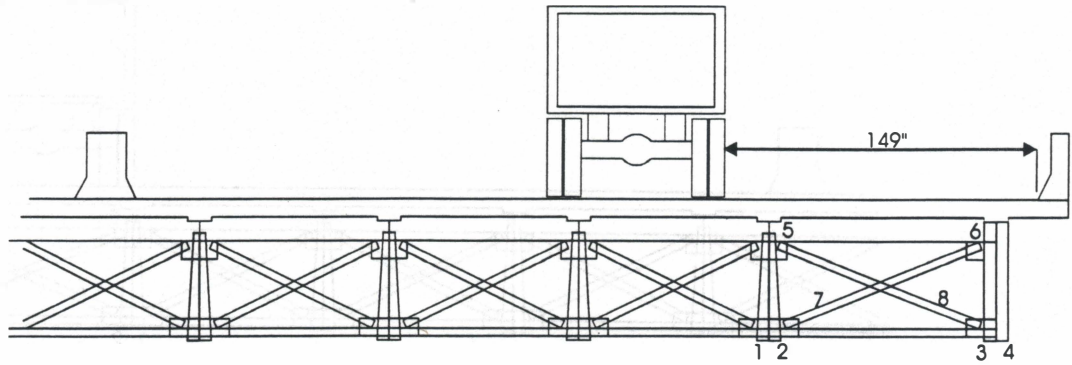
Figure 22. Truck Moving at 25 mph in Right Lane, from Measurements at Group 1 Location

above the Group 1 crossframe. There is very little fluctuation in the data over the recorded time interval, indicating that the gages are working properly. It was expected that data from gage 1 would closely match data from gage 2, and data from gage 3 would closely match data from gage 4 since these gages are on opposite sides of the same flange. It can be seen that gages 1 and 2 provide almost identical output while 3 and 4 differ by at most 0.4 ksi, providing further support for the validity of the field data. Also as expected, stresses at 3 and 4 are higher than at 1 and 2 when the truck is in the shoulder, while stresses at 1 and 2 are higher when the truck is in the right lane.

Figures 20 through 22 show the variation of stress with time as the truck moves along the bridge. Since it was necessary to preset the time interval for data collection and manually trigger the system as the truck approached, data collection may not begin exactly as the truck enters the bridge or end exactly as the truck moves off the continuous three-span segment. Also notice that in Figure 22, data points are more widely spaced than in Figures 20 and 21. This occurs because the truck velocity was greater in Figure 22. Data are collected every 0.125 seconds regardless of truck velocity, so fewer points are collected when the truck spends less time on the bridge.

Comparison of static and dynamic data shows that the absolute maximum flange stress at each gage under dynamic load is in close agreement with corresponding flange stresses measured under static load. This indicates that dynamic amplification of stresses was negligible and that the static truck was properly positioned to produce the greatest effect in the flanges.

Comparison of the data also shows that the static truck was not properly positioned to produce the greatest effect in the crossframe members. As can be seen in Figure 20, crossframe stresses reach a maximum when the truck is directly above the instrumented crossframe. Recall that the static truck is above the Group 2/3

crossframe, not the Group 1 crossframe currently under consideration. Crossframes are loaded by differential displacement of adjacent girders, and such displacement would be greatest when the load is longitudinally positioned above the crossframe.

Results for Group 2 gages are shown in Figures 23 through 28. Group 2 gages are under the left lane and left shoulder in the positive moment region between piers 1 and 2. As expected, bottom flange stresses are positive and top flange stresses are negative and small. The highest stress range (sum of peak compressive and tensile stresses) measured in any girder is 2.4 ksi, as seen in Figure 27. Crossframe stresses peak at the same time as the flange stresses and are greater than the flange stresses when the truck is not over the instrumented girders. However, the maximum stress of 2.0 ksi occurs in the bottom flange when the truck crosses the bridge at 25 mph in the left lane. Similar to the Group 1 gages, comparison of Figure 24 with Figures 25 and 26 provides no evidence of dynamic amplification of stresses.

Results for Group 3 gages are shown in Figures 29 through 36. Group 3 gages are under the right lane and shoulder at the same longitudinal position as the Group 2 gages. Through all the figures for Group 3, the obviously erratic behavior of gage 2 indicates a problem with installation and requires that all data from this gage be disregarded. It also appears, in Figure 34, that gage 3 is failing; data from Figure 34 are replotted in Figure 35 without gages 2 and 3.

Many of the same observations made on the basis of the Groups 1 and 2 data can be made from the Group 3 data. Under the static load, the bottom flange stresses are positive and much larger than the top flange stresses. The highest stress of 2.6 ksi occurs in the outside girder when the truck is parked in the shoulder over the crossframe. The highest stress range measured in any girder with substandard welds is approximately 1.9 ksi, as seen in Figures 31 and 32. There is no evidence of dynamic
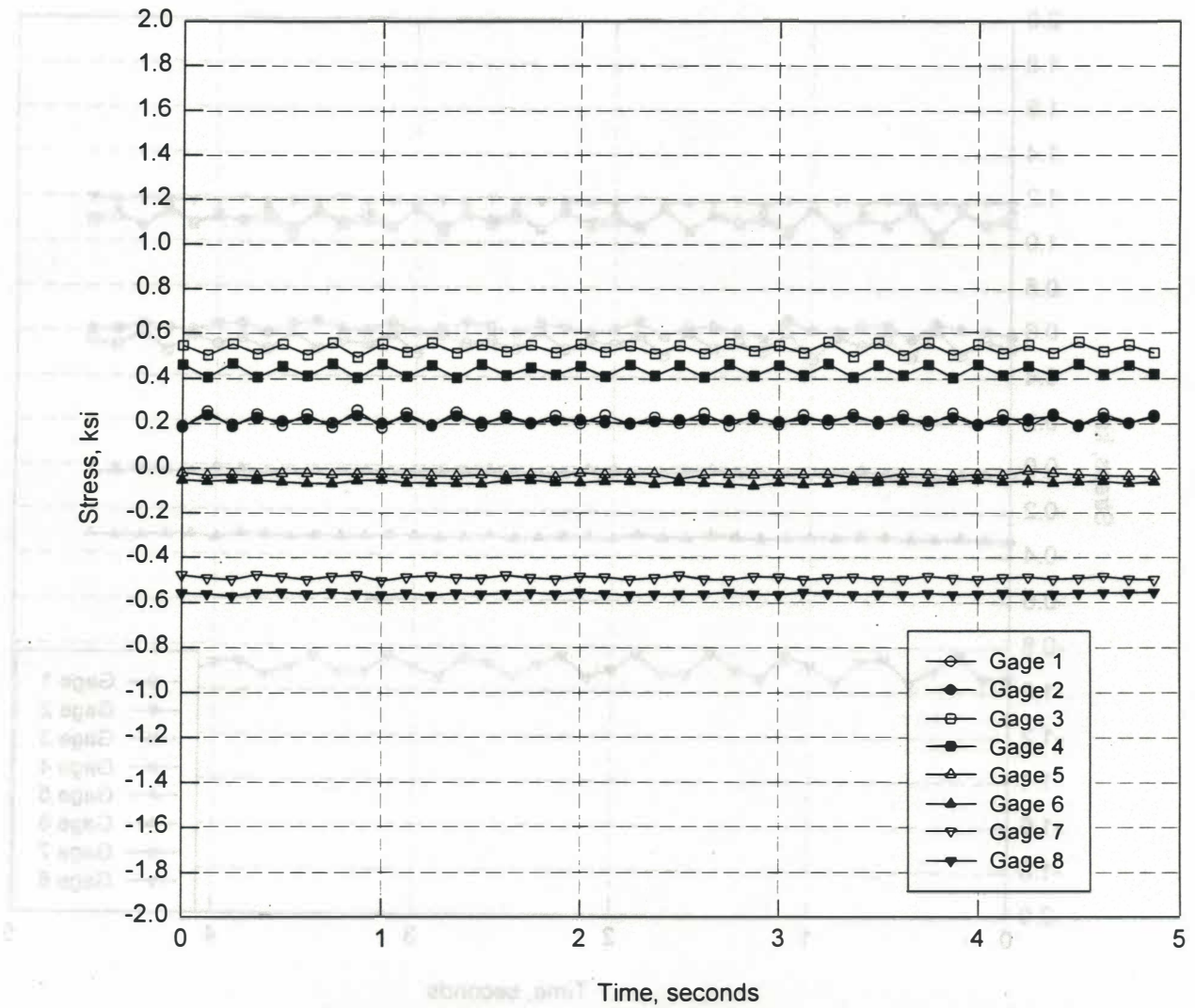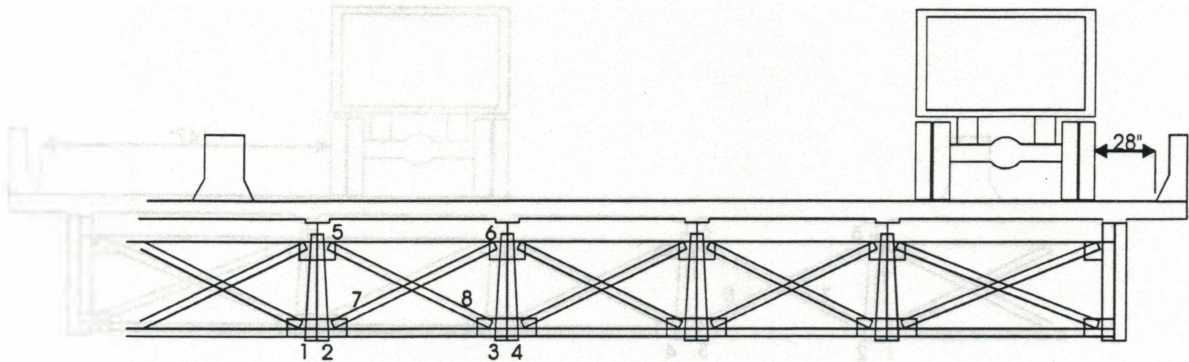
Figure 23. Truck Stationary in Shoulder, from Measurements at Group 2 Location
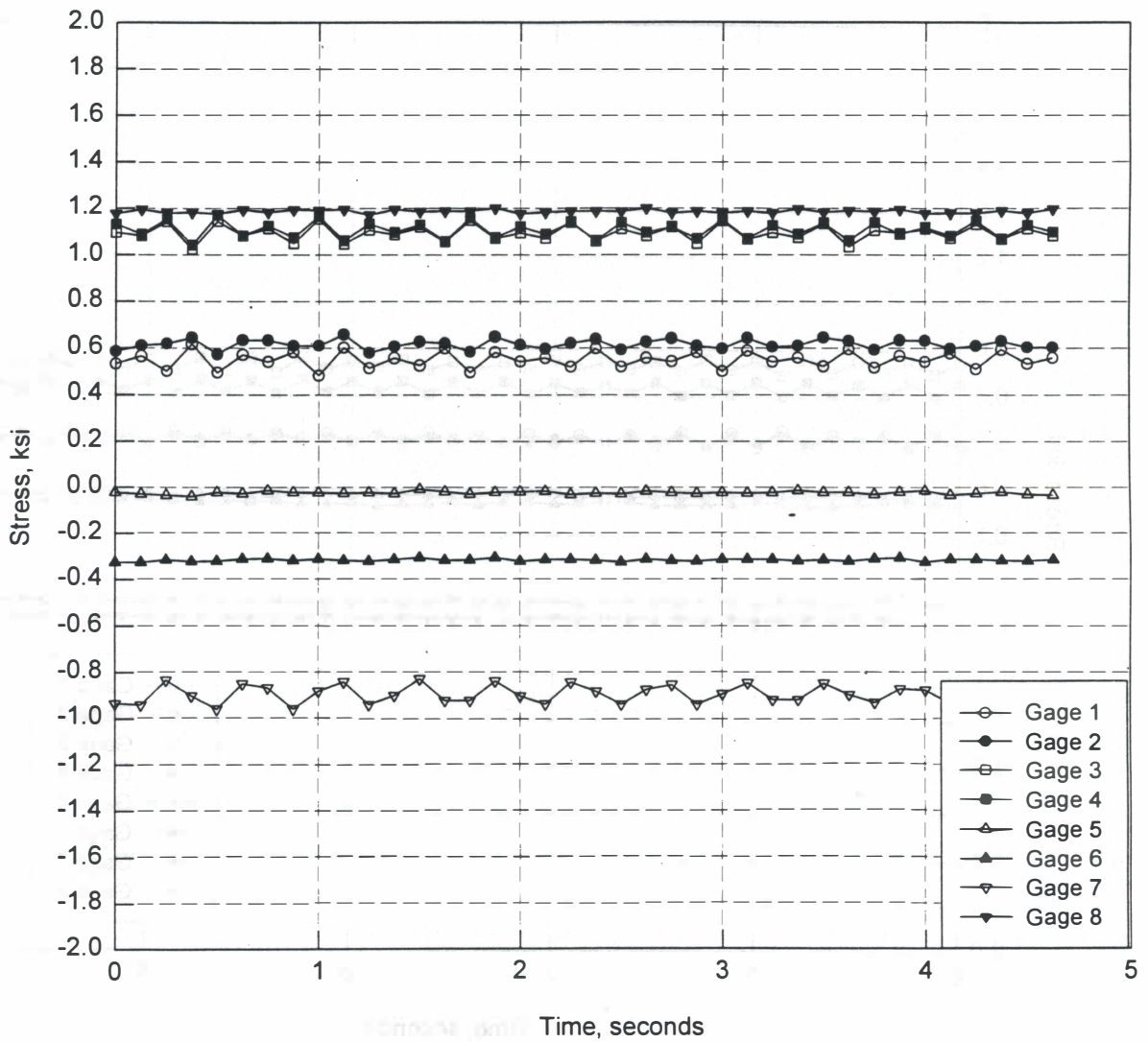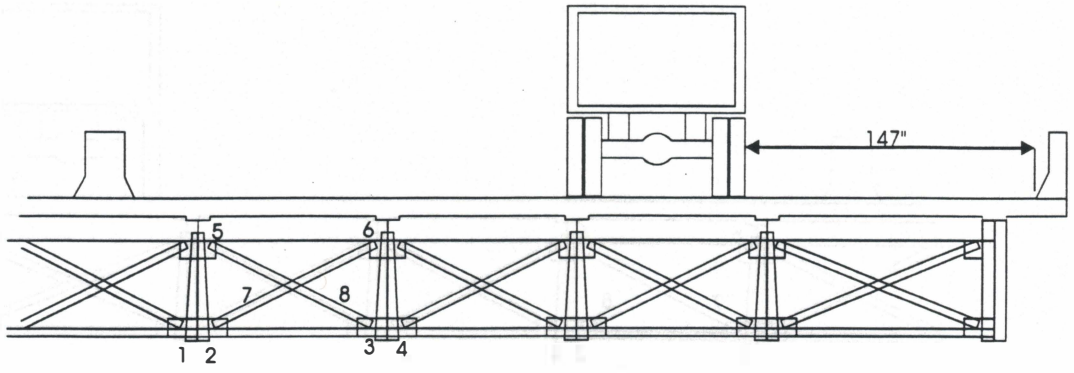
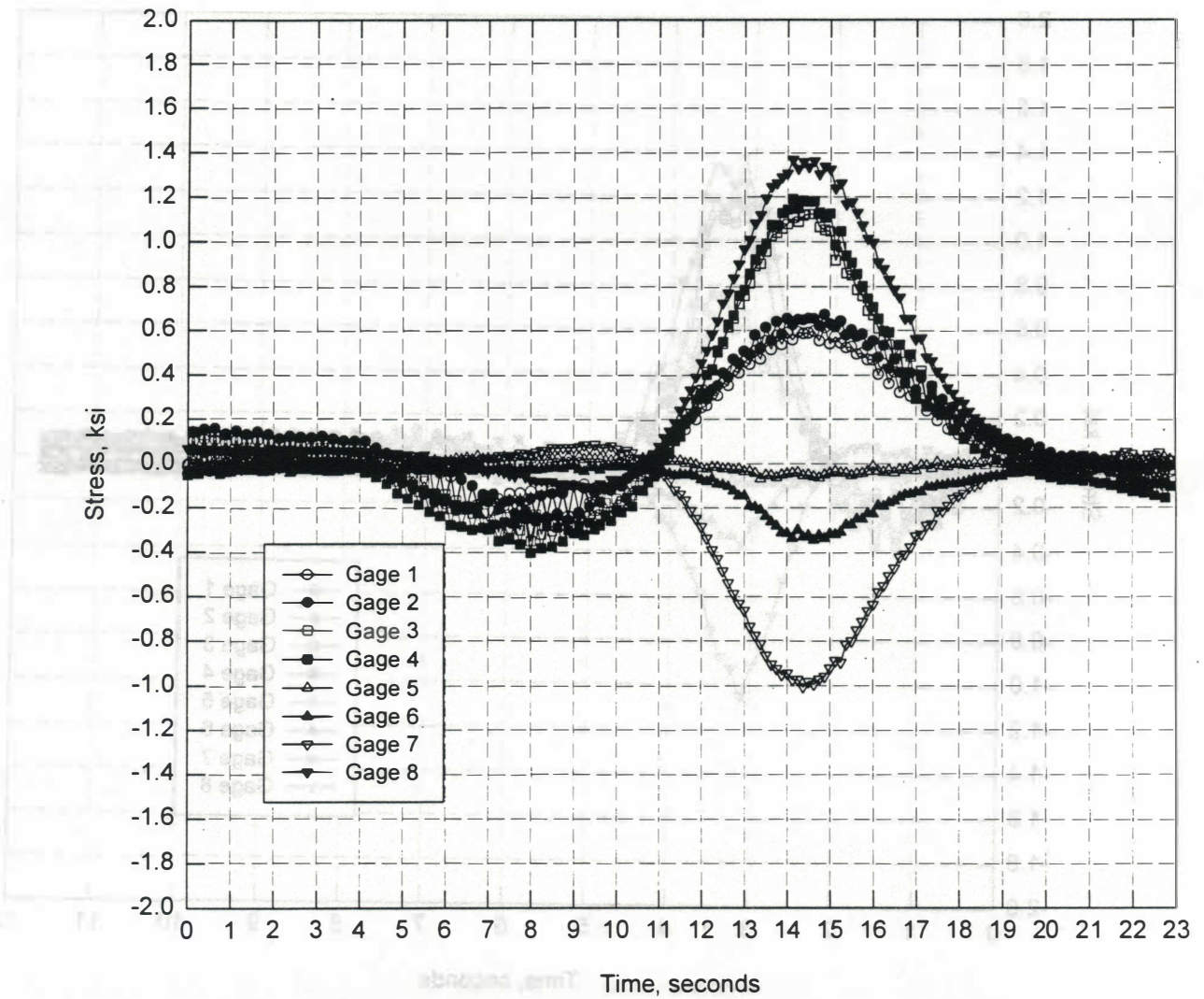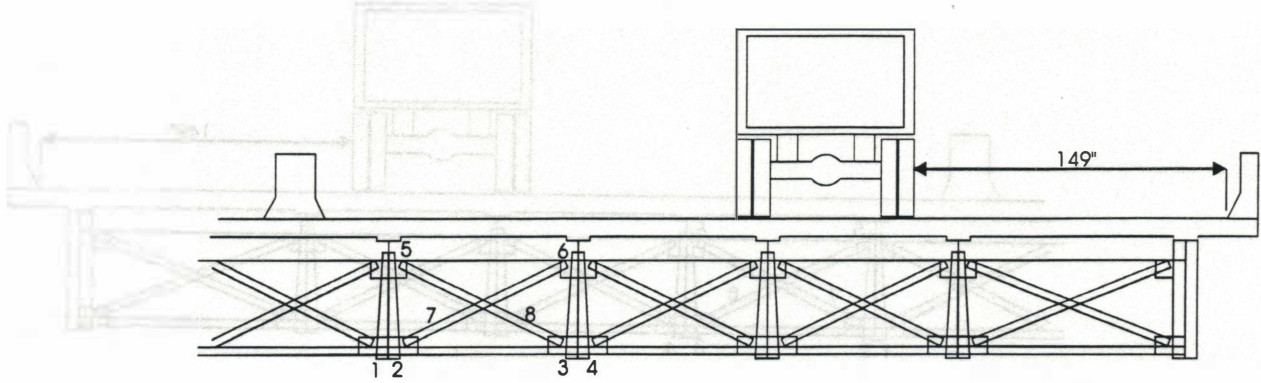Figure 24. Truck Stationary in Right Lane, from Measurements at Group 2 Location

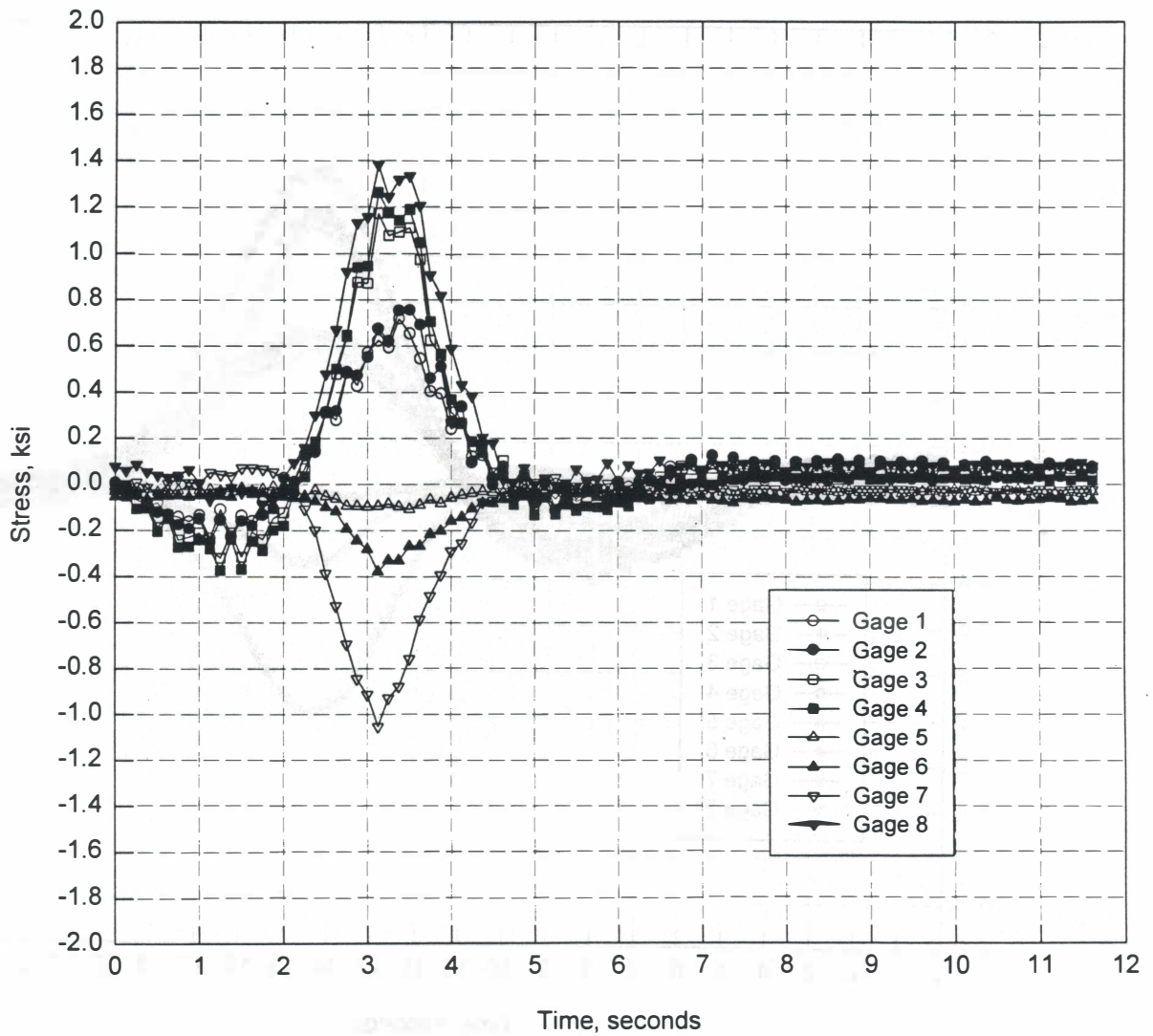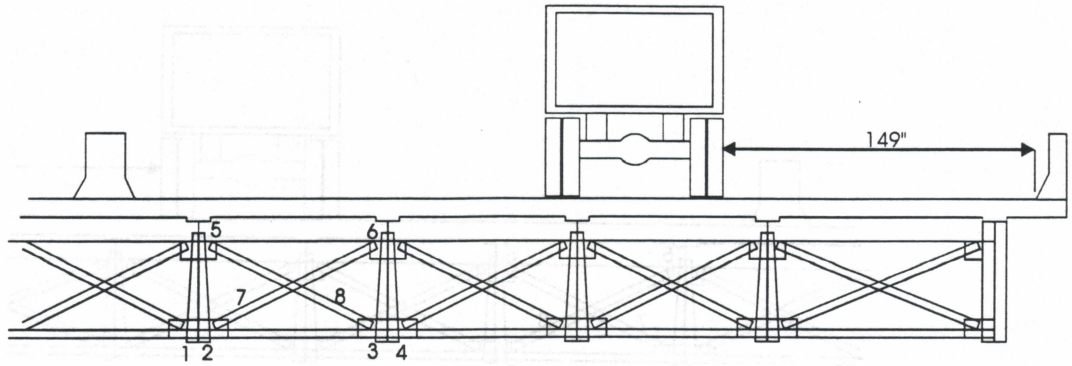Figure 25. Truck Moving at 5 mph in Right Lane, from Measurements at Group 2 Location

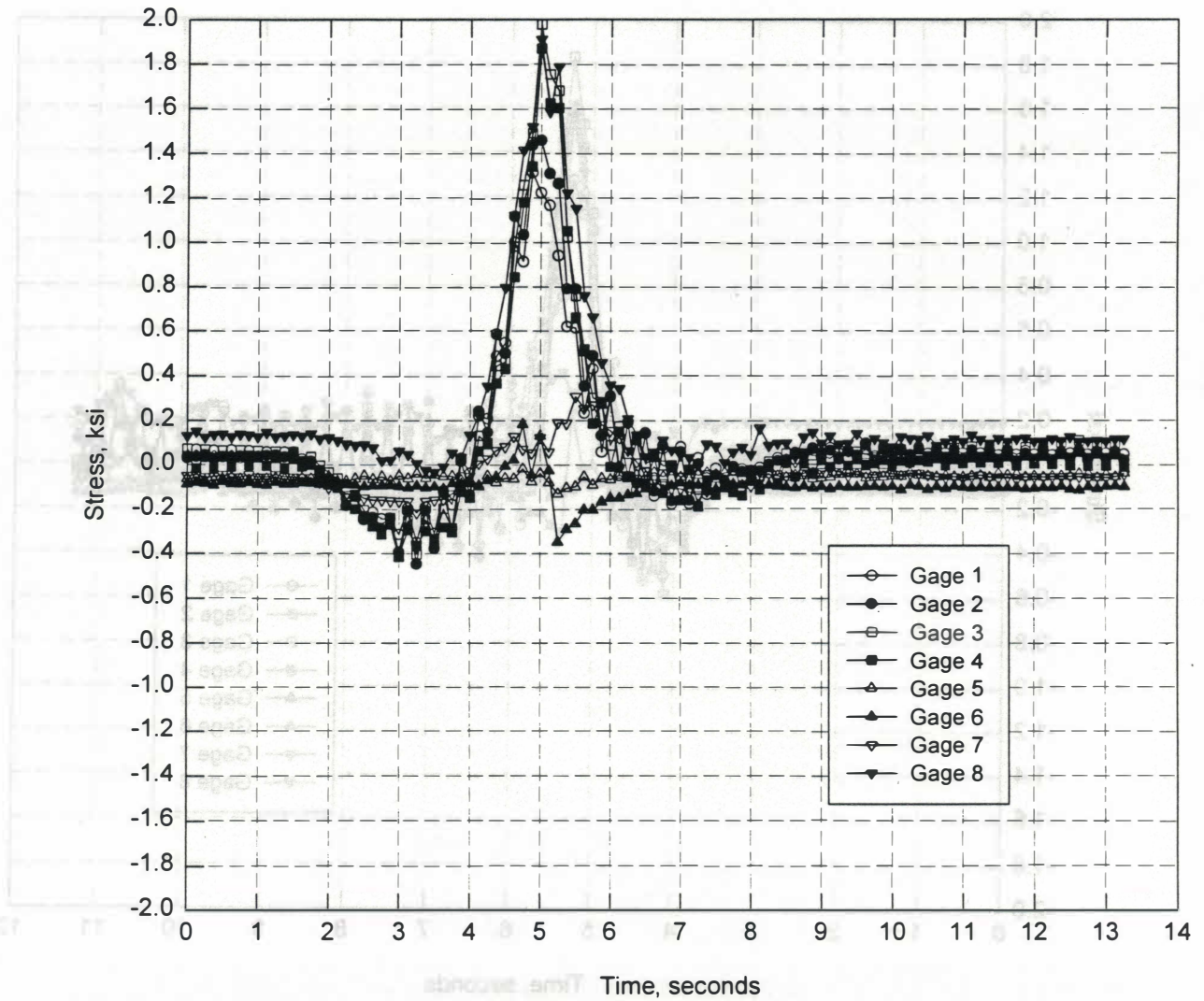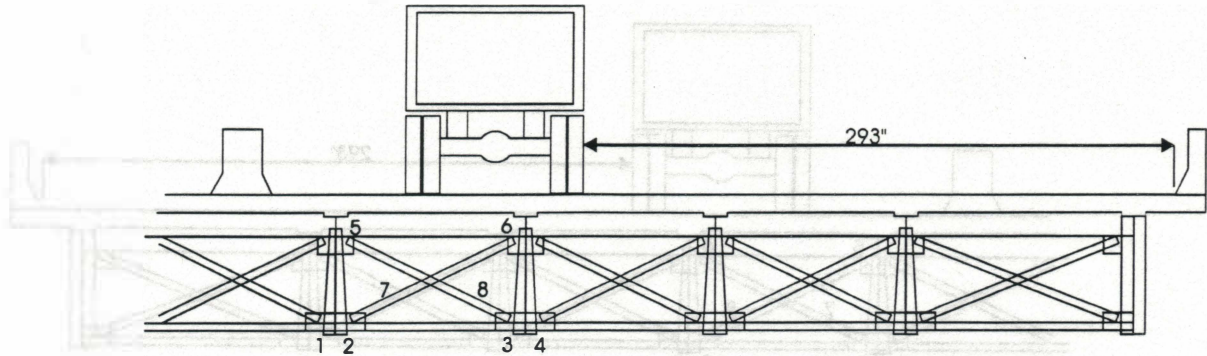Figure 26. Truck Moving at 25 mph in Right Lane, from Measurements at Group 2 Location

Figure 27. Truck Moving at 25 mph in Left Lane, from Measurements at Group 2 Location
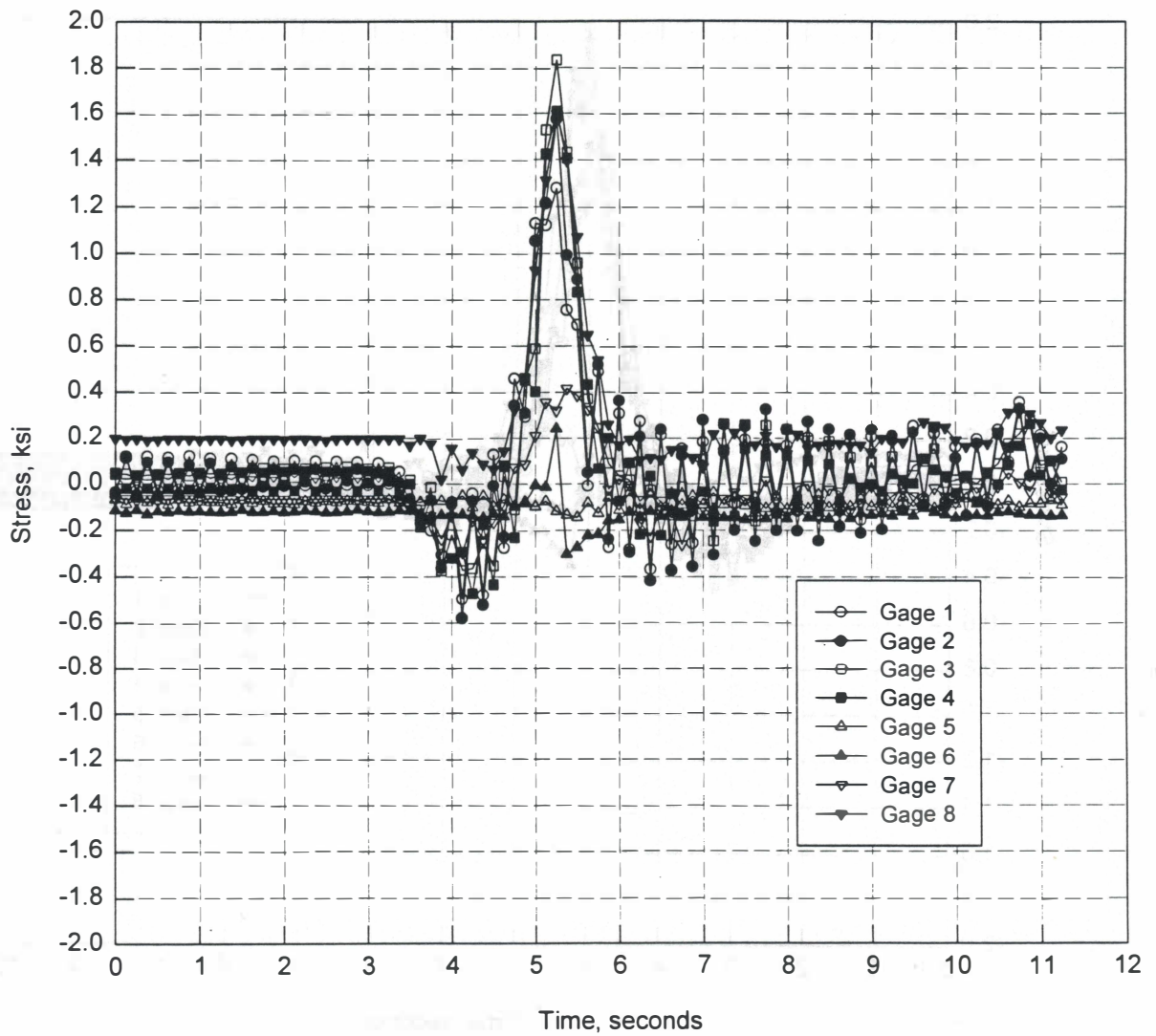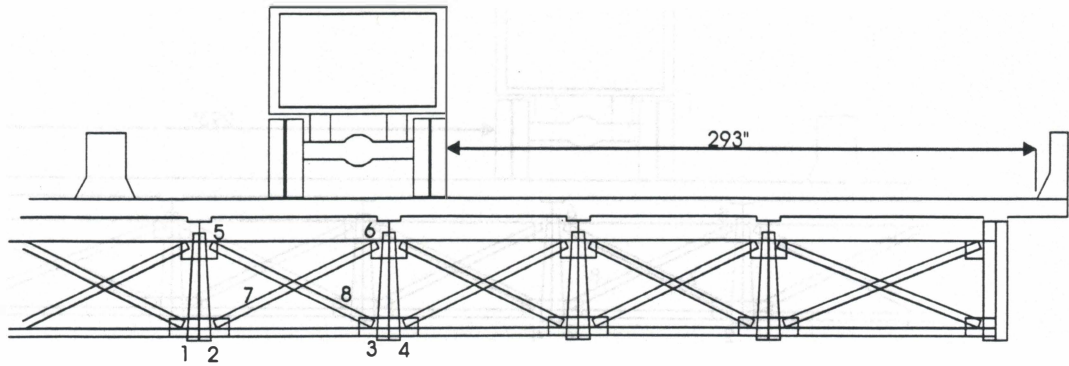
Figure 28. Truck Moving at 40 mph in Left Lane, from Measurements at Group 2 Location
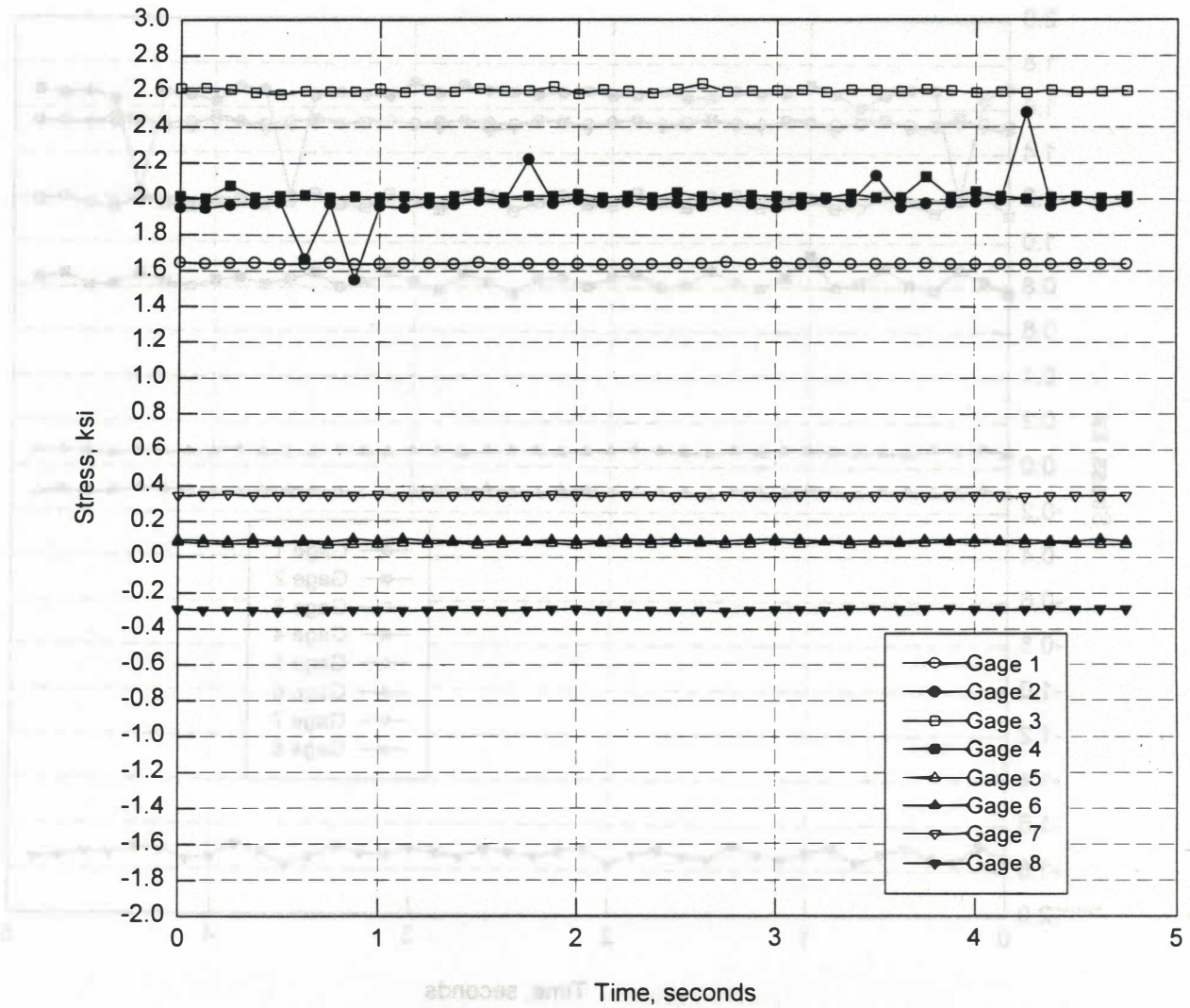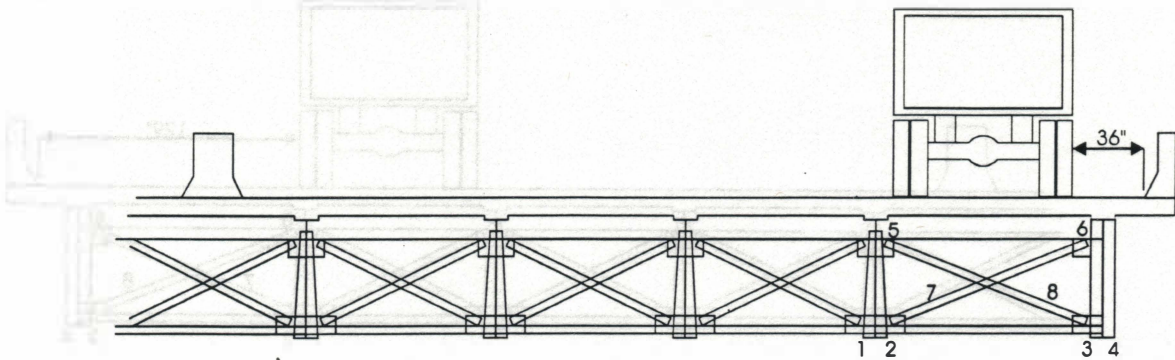
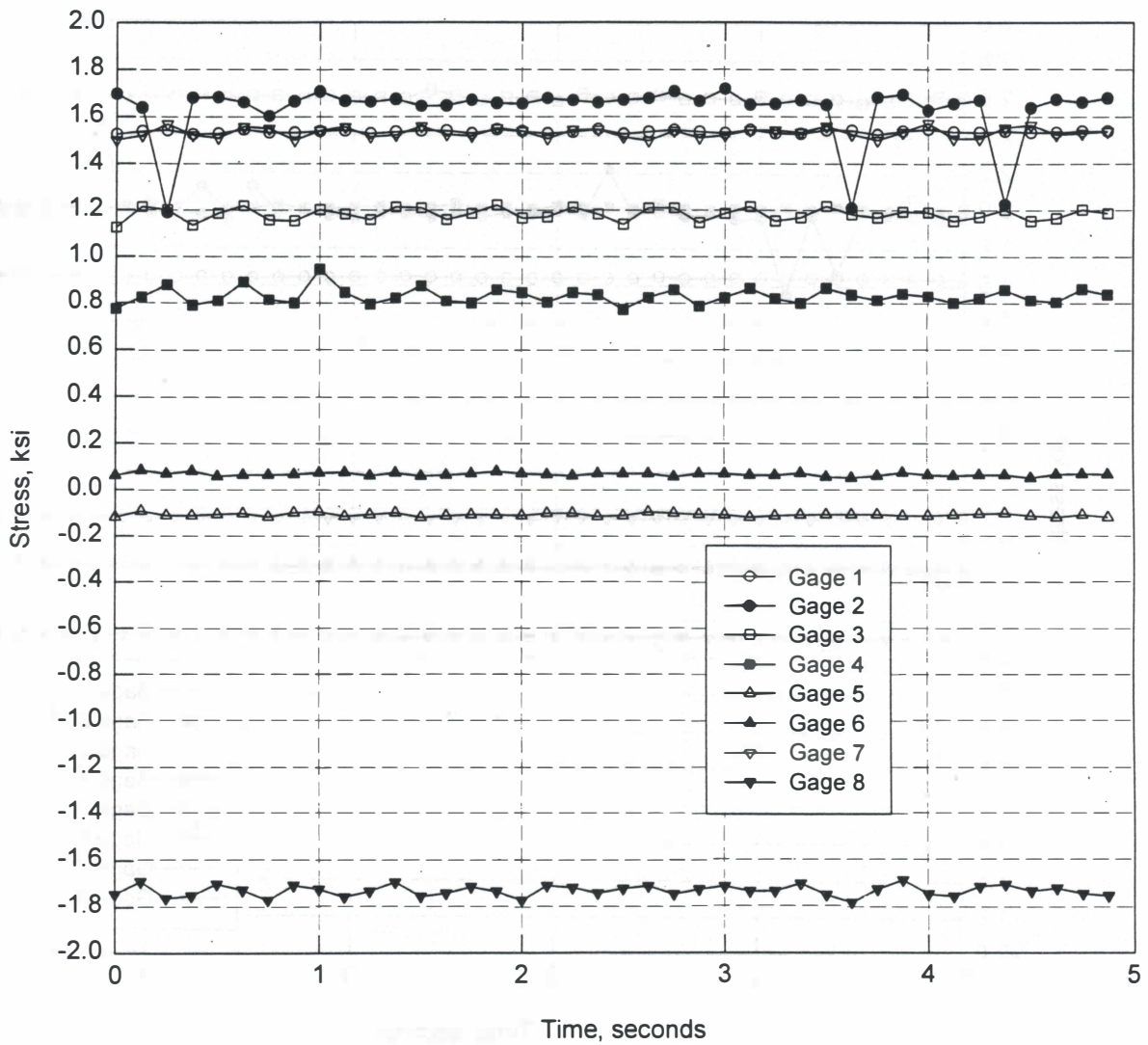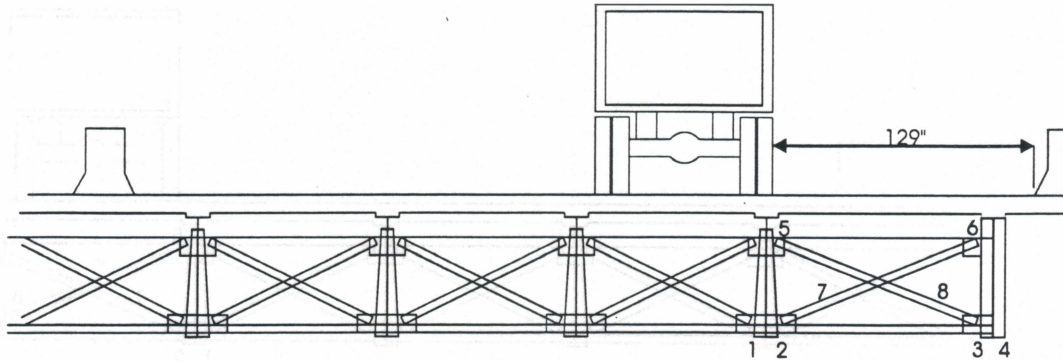Figure 29. Stationary Truck in Shoulder, from Measurements at Group 3 Location

Figure 30. Truck Stationary in Right Lane, from Measurements at Group 3 Location
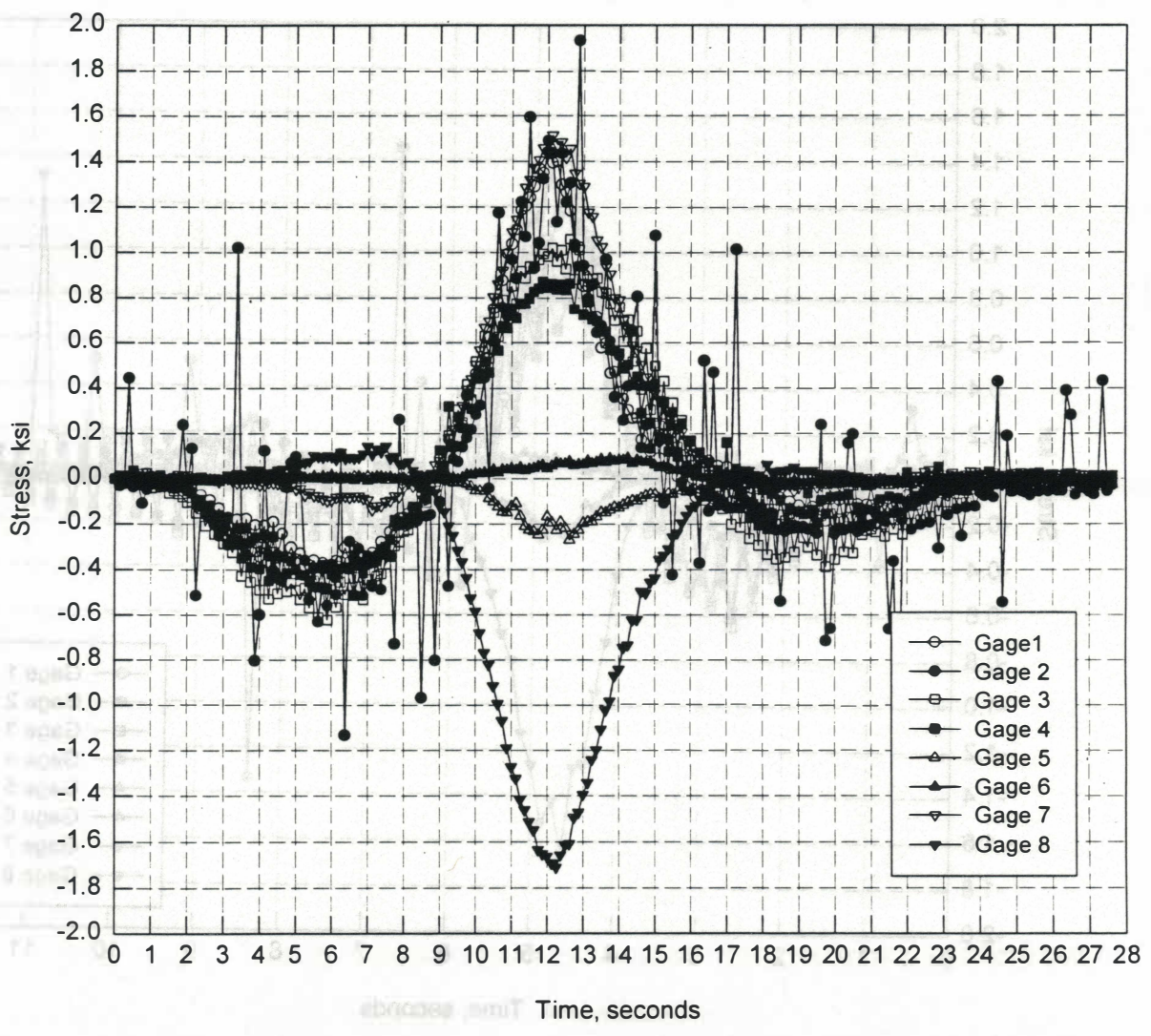
66

Figure 31. Truck Moving at 5 mph in Right Lane, from Measurements at Group 3 Location
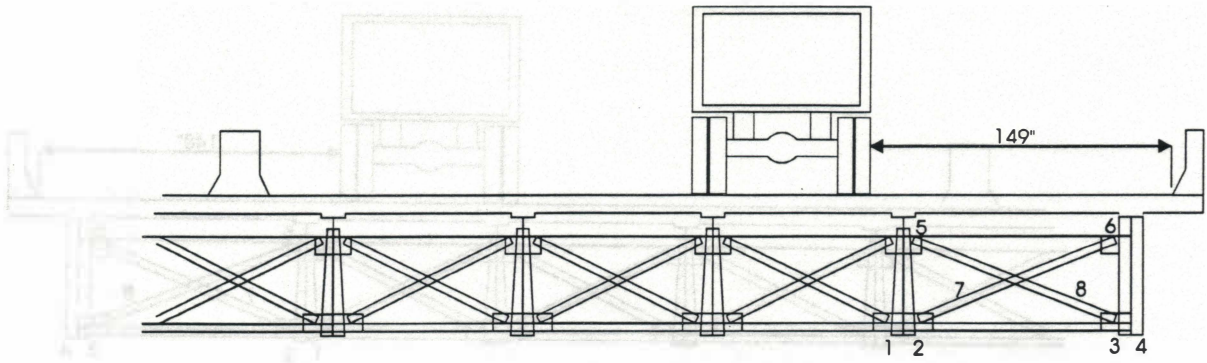
Figure 32. Truck Moving at 25 mph in Right Lane, from Measurements at Group 3 Location
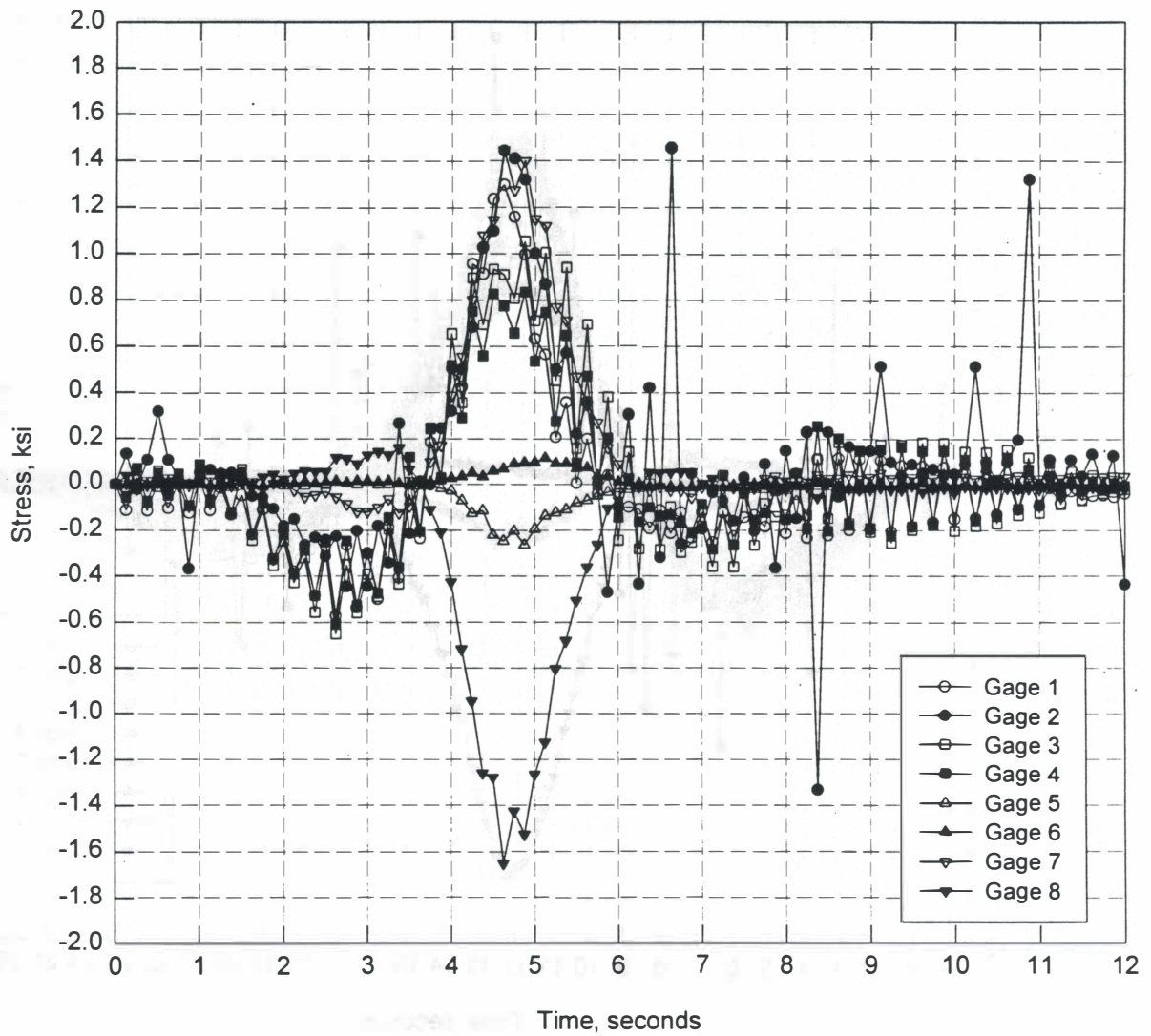
Figure 33. Truck Moving at 25 mph in Left Lane, from Measuremets at Group 3 Location
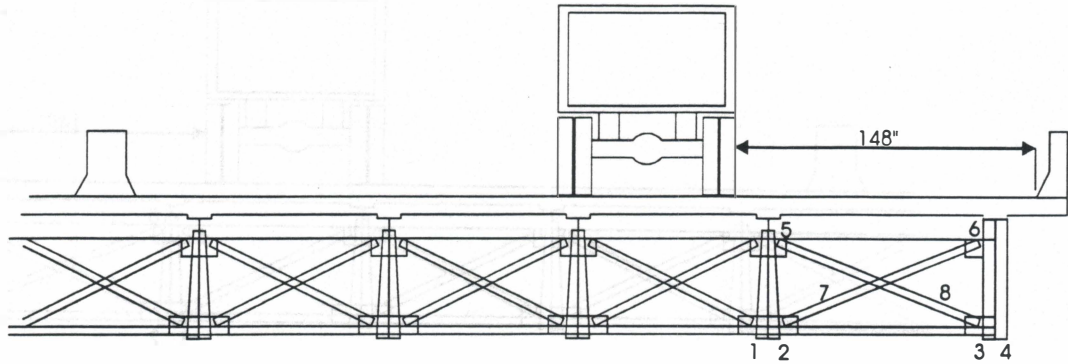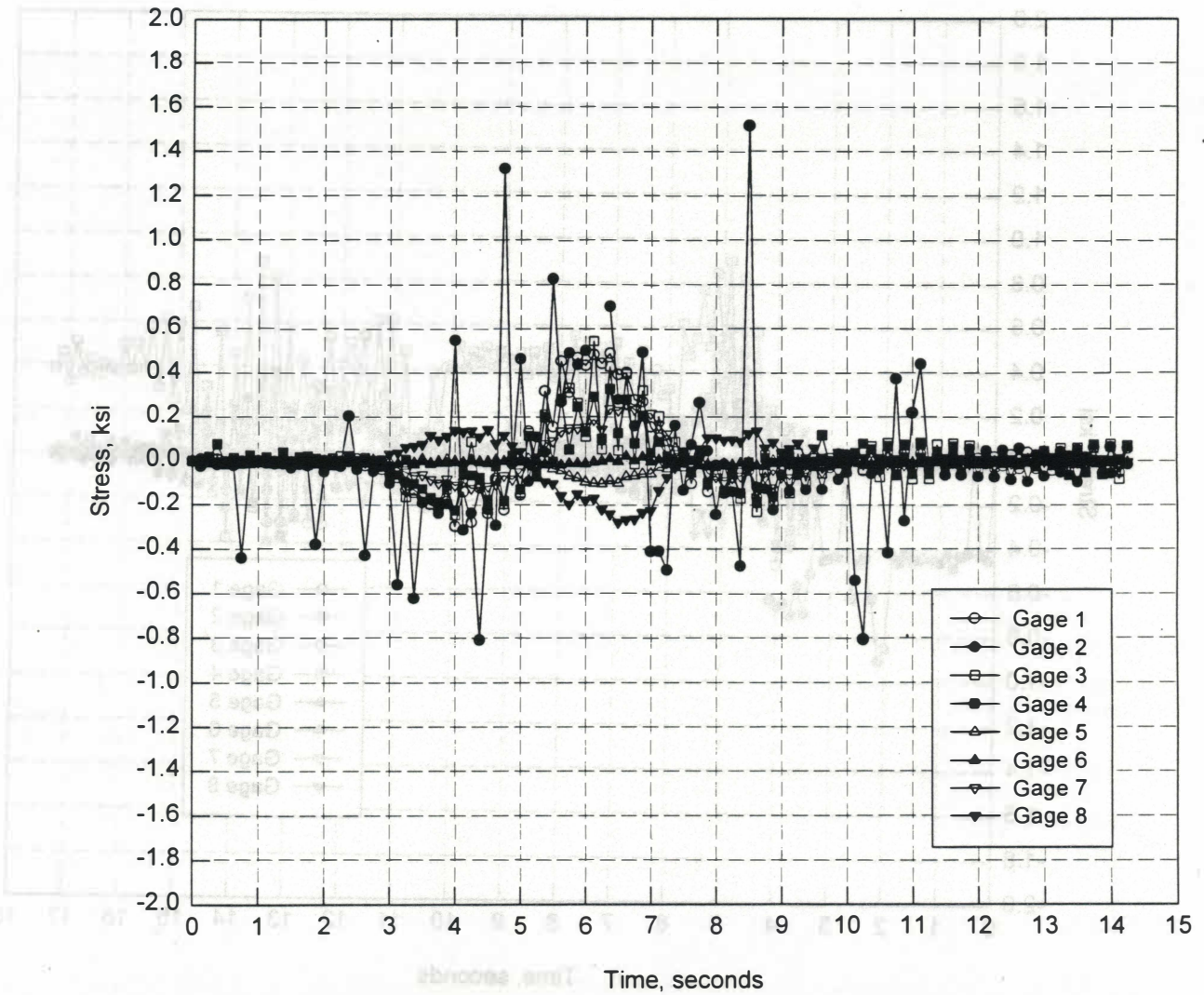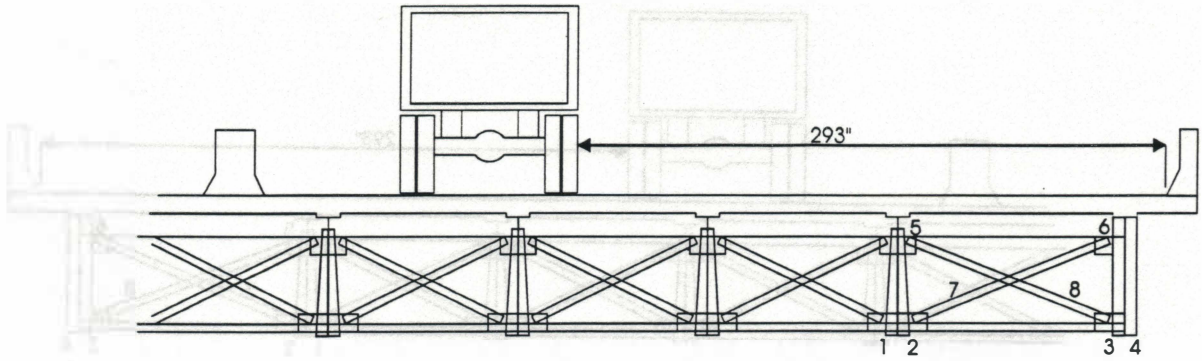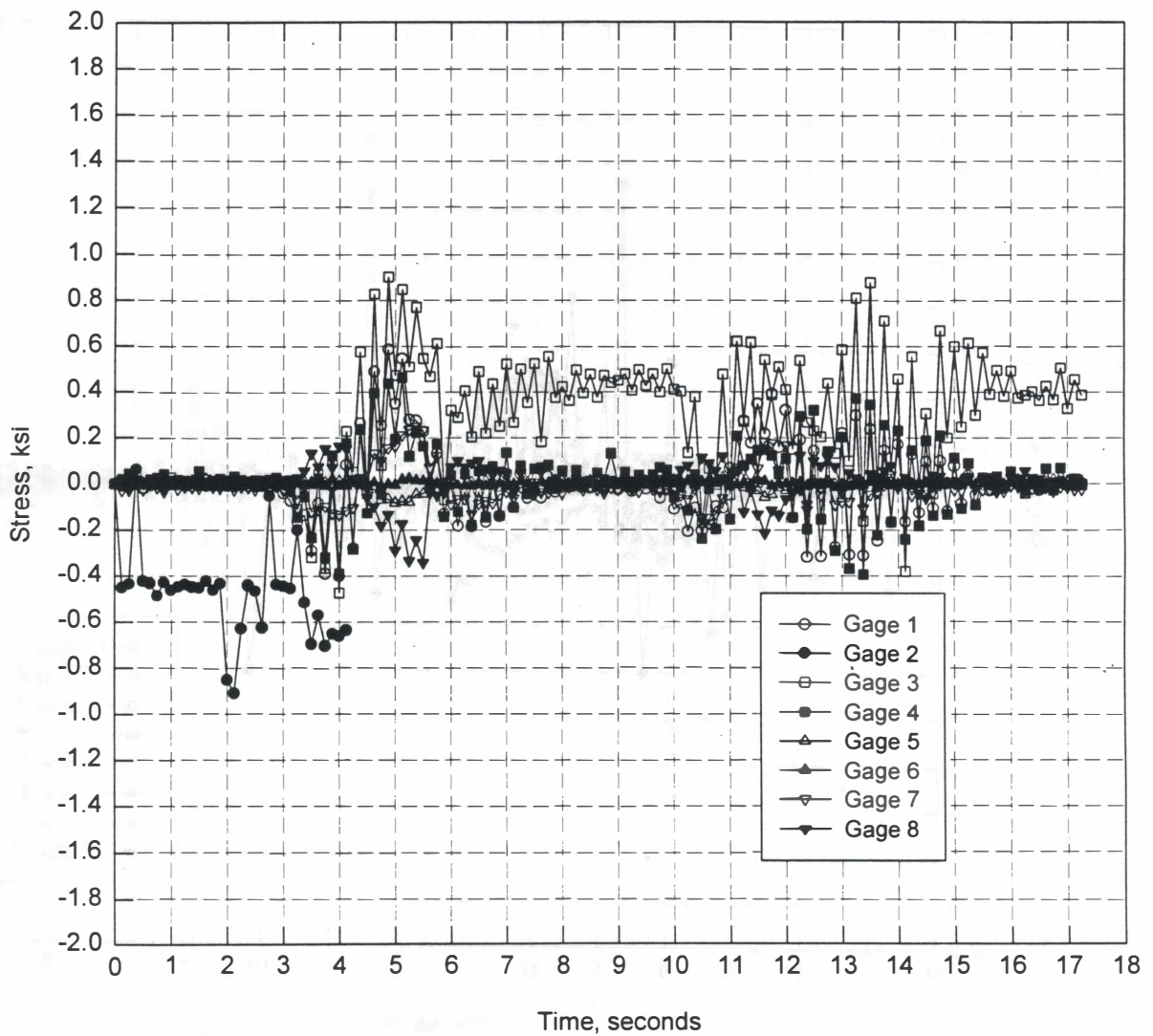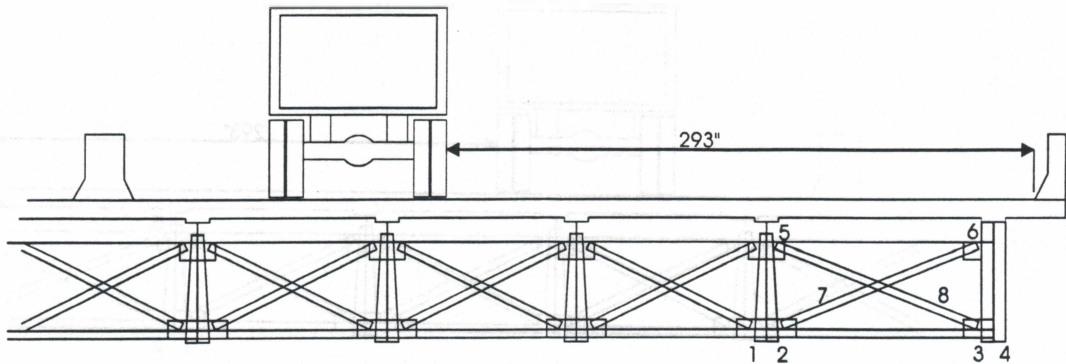
Figure 34. Truck Moving at 40 mph in Left Lane Followed by Tractor-Trailer, from
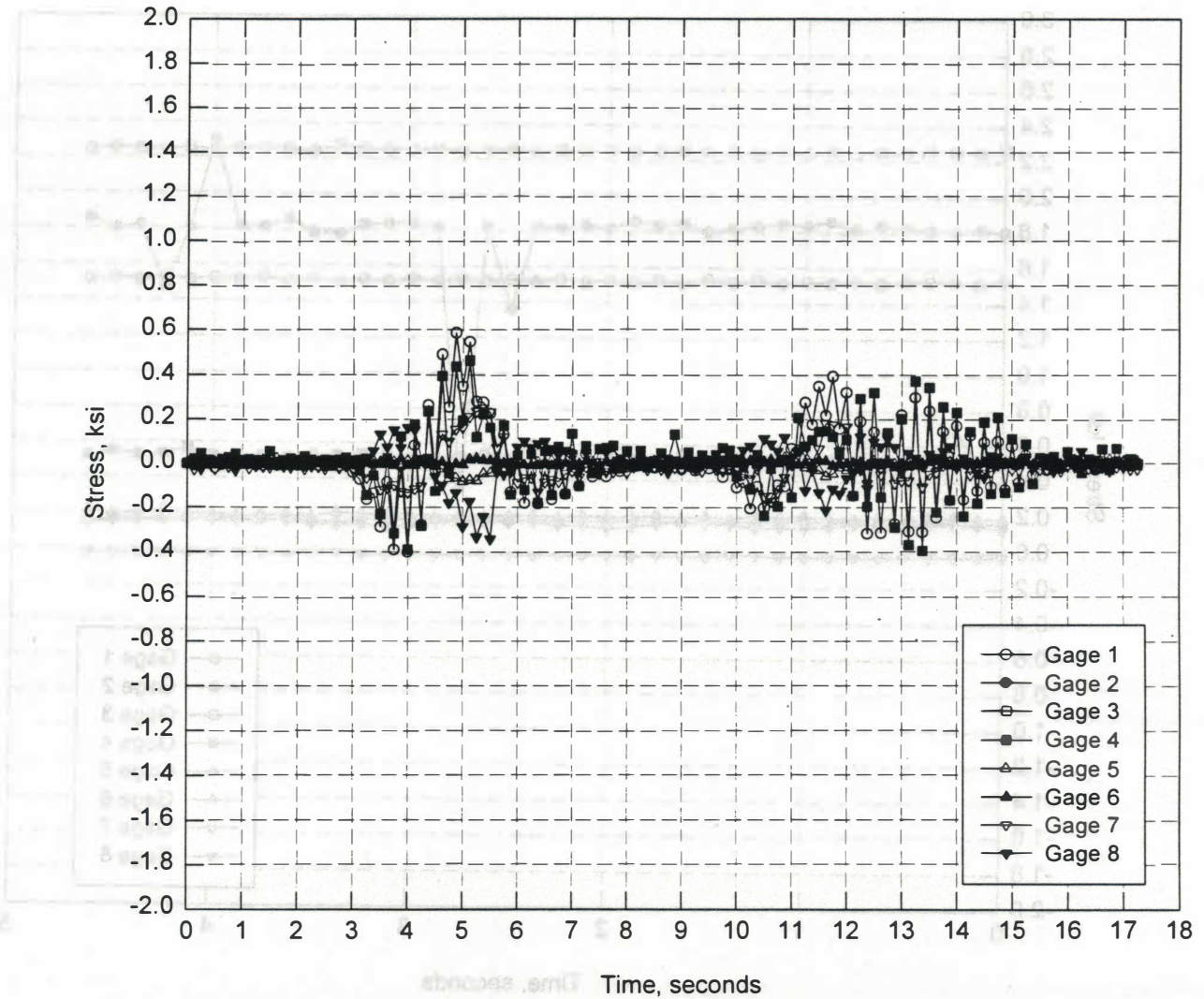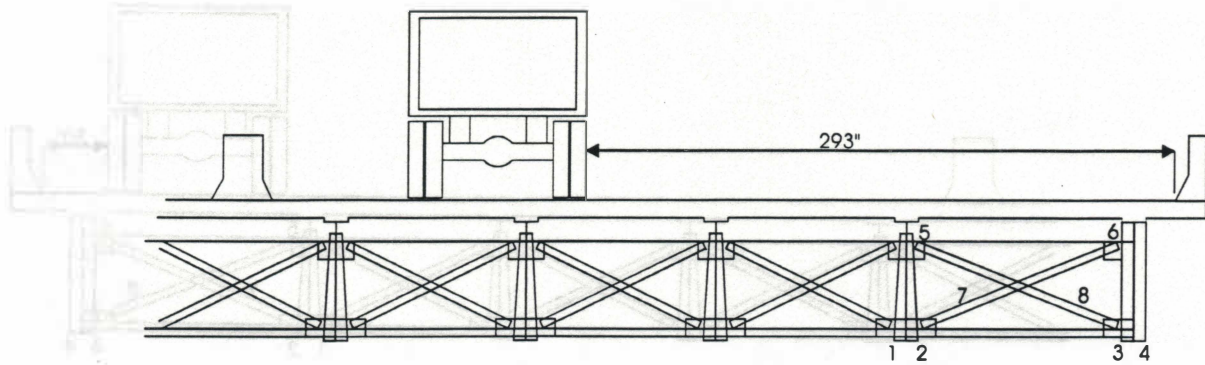Measurements at Group 3 Location

Figure 35. Truck Moving at 40 mph in Left Lane Followed by Tractor-Trailer, Without Gages 2 and 3
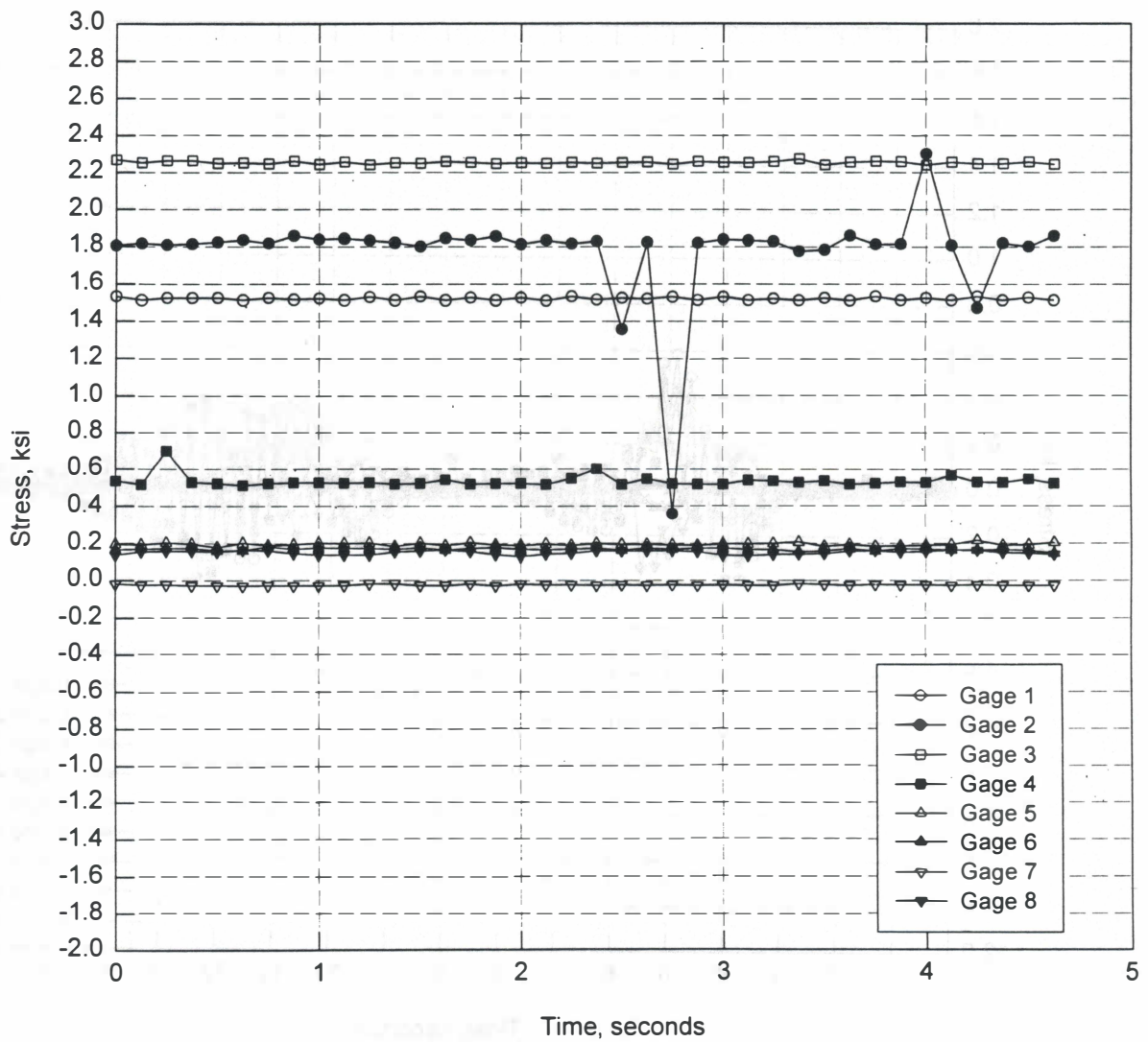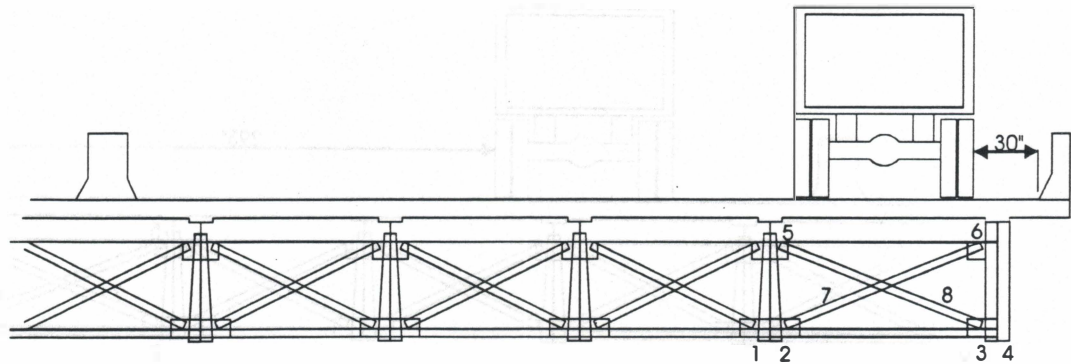
Figure 36. Stationary Truck in Shoulder, from Measurements at Group 3 Location

amplification of stresses, but the number of minor stress cycles associated with a truck crossing increases as velocity increases. Crossframe stresses are very low when the truck is directly above the instrumented girders (Figures 29 and 36), but equal or exceed the flange stresses when the truck is in the lane adjacent to the instrumented girders. The crossframes act to distribute the load when one girder is more heavily loaded than its neighbors.

An additional static test was performed after the Group 3 dynamic tests to determine if gage responses other than 2 and 3 had changed. In Figure 36, gage 2 continues to show evidence of instability while gage 3 appears to be functioning properly. The problem with gage 3 may only show itself when the bridge and leadwires are moving under load. Gage 4 appears to have slipped or shifted, showing a stress of 2.0 ksi in Figure 29 and a stress of 0.5 ksi in Figure 36.

Figures 37 through 42 show results of grid analyses which were conducted for comparison to field data. Recall that the four members making up a crossframe were lumped into one bending element for the grid model, so crossframe stresses equivalent to the field data are not available from the grid model. Also recall that, from the grid analysis, stresses at gage 1 are exactly equal to stresses at gage 2 and stresses at gage 3 are exactly equal to stresses at gage 4, so only gages 1 and 3 are shown on the plot. It should also be noted that all of the analyses conducted are static analyses, which should provide a valid comparison since the field data showed no evidence of dynamic amplification of stresses.

Figure 37 compares to Figures 20 and 22, 38 to 21, 39 to 25 and 26, 40 to 27 and 28, 41 to 31 and 32, and 42 to 33 and 35. Both the shape of the curves and the peak magnitudes are remarkably similar. The maximum stress computed with the grid model is 1.7 ksi, and the maximum stress range is 2.1 ksi; both can be seen in Figure 41. The

Figure 37. Truck Moving in Right Lane, Grid Analysis at Group 1 Location
(Compare to Figures 20 and 22)

Figure 38. Truck Moving in Shoulder, Grid Analysis at Group 1 Location
(Compare to Figure 21)

75

Figure 39. Truck Moving in Right Lane, Grid Analysis at Group 2 Location
(Compare to Figures 25 and 26)
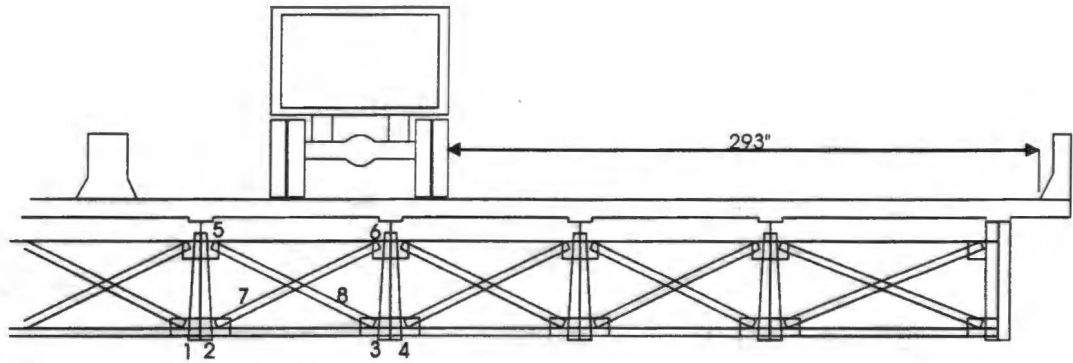
Figure 40. Truck Moving in Left Lane, Grid Analysis at Group 2 Location
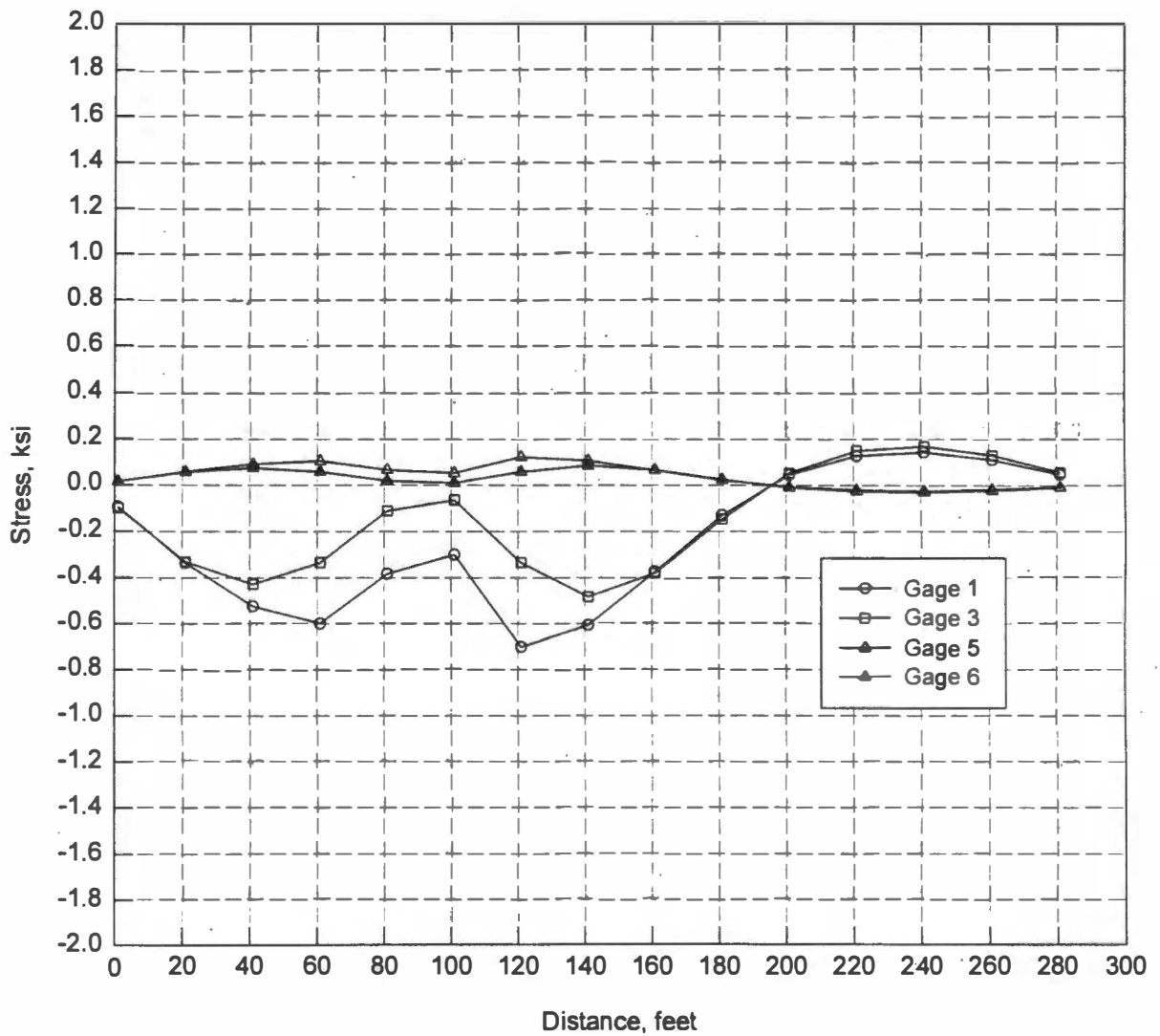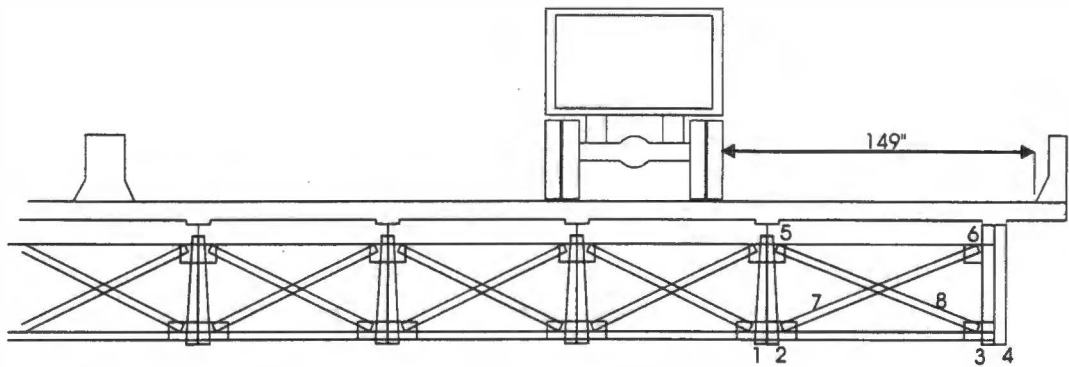(Compare to Figures 27 and 28)

Figure 41. Truck Moving in Right Lane, Grid Analysis at Group 3 Location
(Compare to Figures 31 and 32)
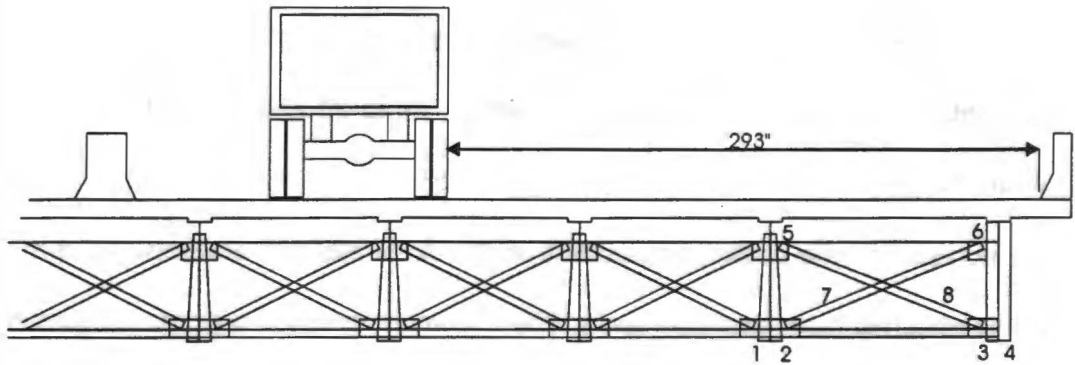
Figure 42. Truck Moving in Left Lane, Grid Analysis at Group 3 Location
(Compare to Figures 33 and 35)

grid model provides a relatively simple and effective means of computing flange stresses for the bridge under investigation.

Results of finite element analyses are provided in Figures 43 to 51. Similar to the grid results, Figure 43 compares to Figure 21, 44 to 20 and 22, 47 to 25 and 26, 48 to 27 and 28, 50 to 31 and 32, and 51 to 33 and 35. As with the grid analysis, the shape of the curves and the peak magnitudes from the finite element analysis are very similar to those obtained from measurements. The maximum stress in a grider computed with the finite element model is 1.9 ksi and the maximum stress range is 2.4 ksi; both can be seen in Figure 49.

3.3.2 Normal Traffic

To monitor stresses carried by the bridge in normal service, it was decided to gage the bottom flanges of the plate girders as shown at the top of Figure 52. Gages 1, 4, 5, and 8 are full bridge strain transducers and 2, 3, 6, and 7 are single element strain gages. All of the gages are located at the Group 2/3 crossframe.

The bottom of Figure 52 shows the stresses produced by the passage of a tractor-trailer in the left lane. The weight of the tractor-trailer is not known; based subjectively on the "feel" of the bridge vibrations as the truck passed, it was typical of a loaded tractor-trailer. As expected, stresses are highest in the girder under the driving lane. However, the magnitude of the maximum stress is only 0.9 ksi. There are numerous minor cycles superimposed on and following the major cycle. In the cycles which follow the major cycle, stresses are actually higher in the girder furthest from the driving lane. Vibrations may damp more rapidly in the interior girders.

Following acquisition of the strain data for the tractor-trailer, the equipment was reconfigured for long term data acquisition. In this configuration, the datalogger is programmed to count cycles over a two week period for a stress range histogram. A
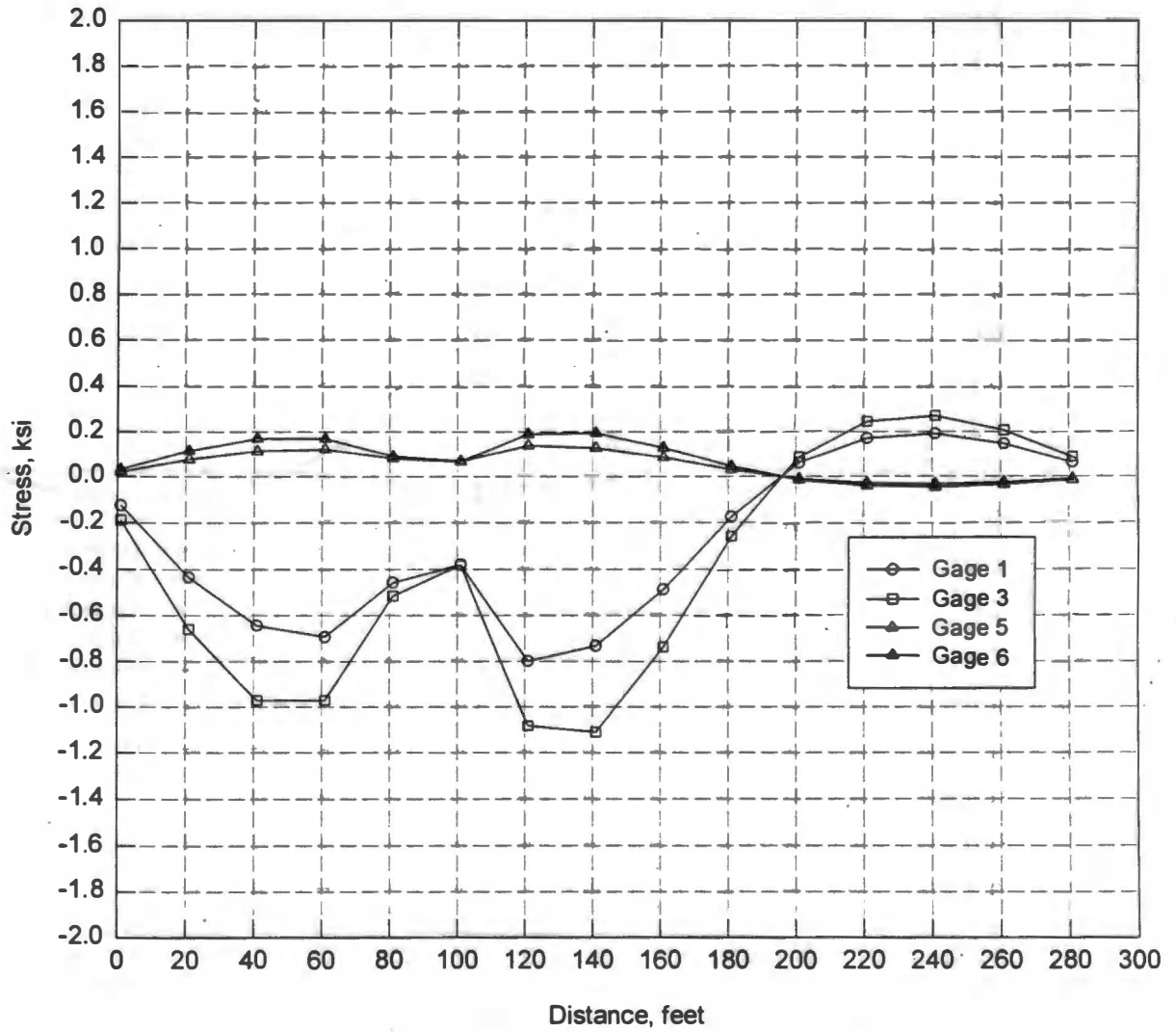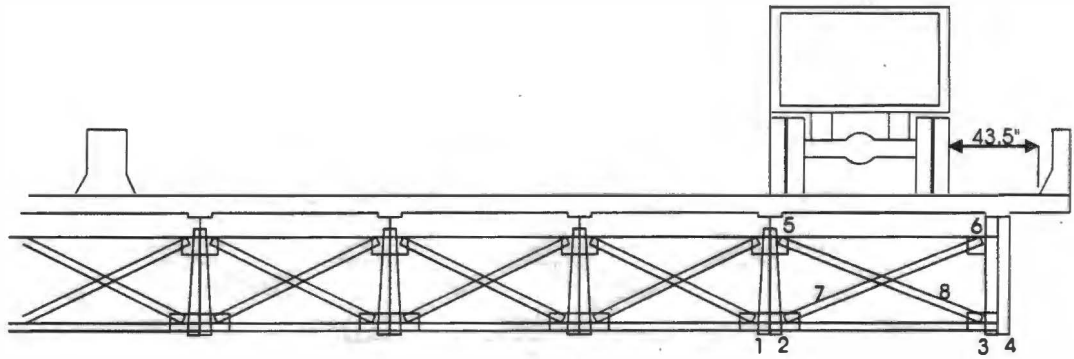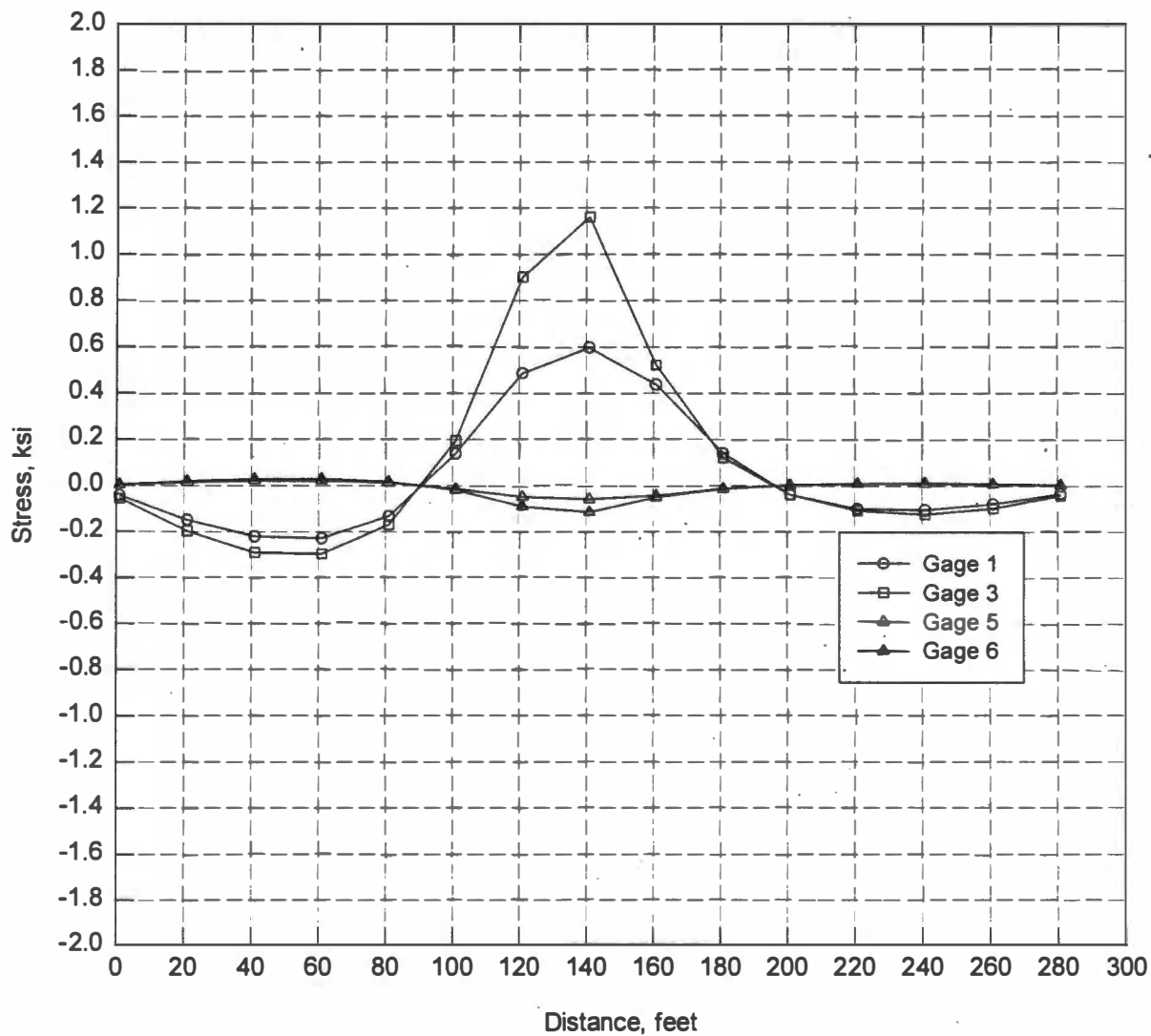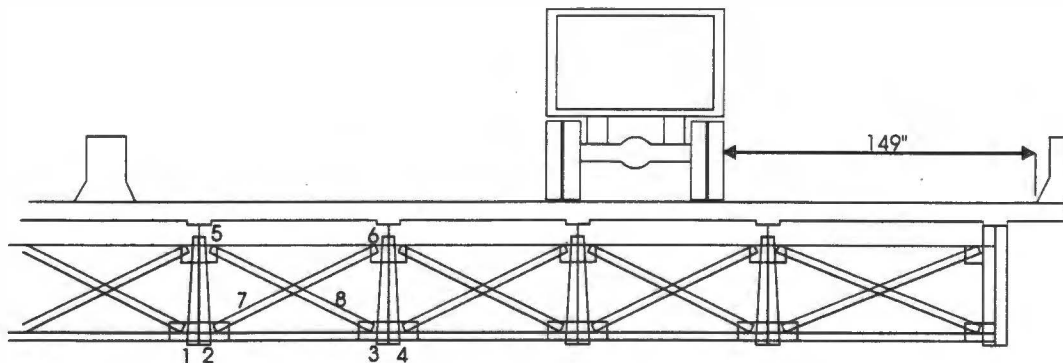
80

Figure 43. Truck Moving in Shoulder, Finite Element Analysis at Group 1 Location
(Compare to Figure 21)

81
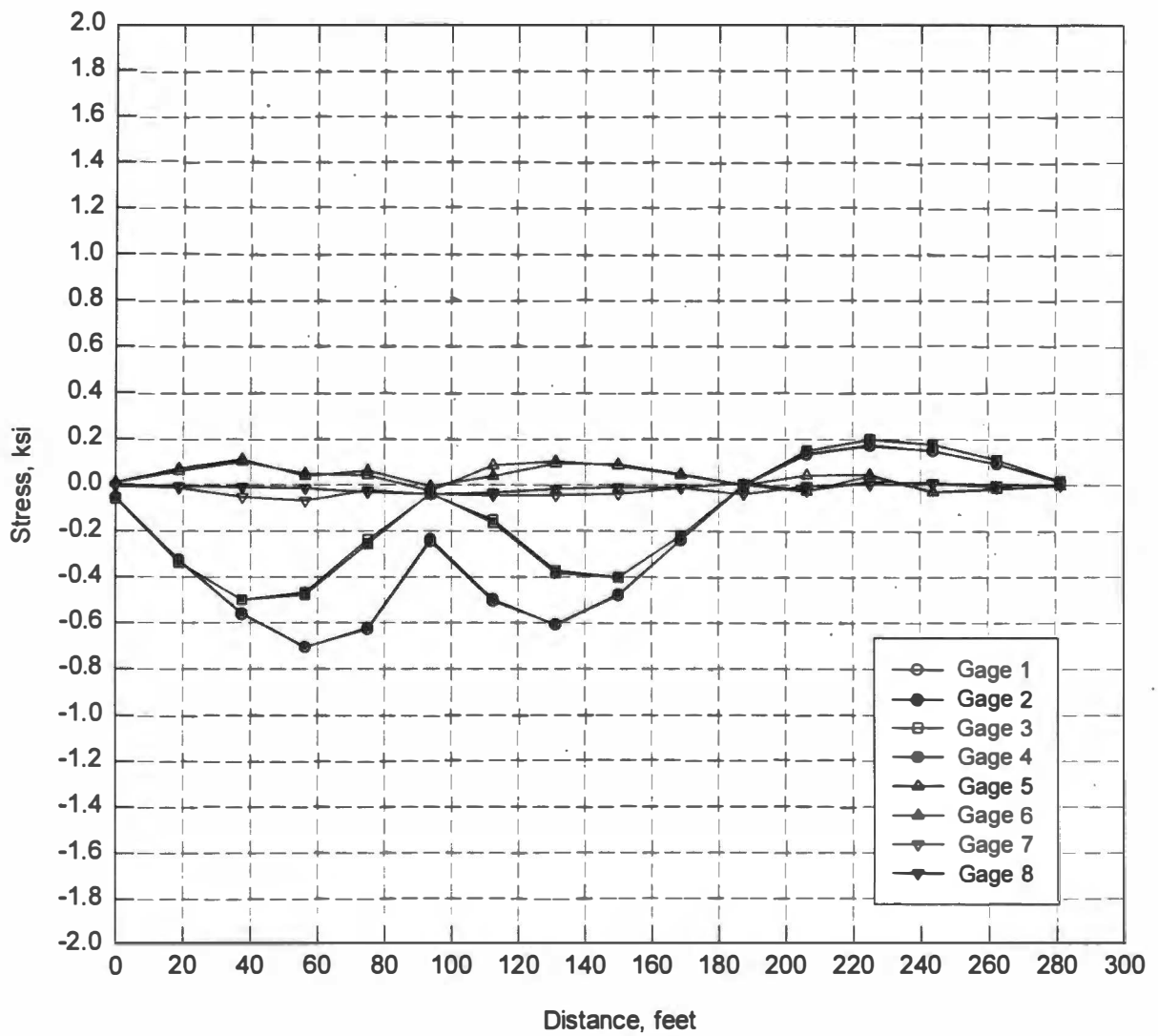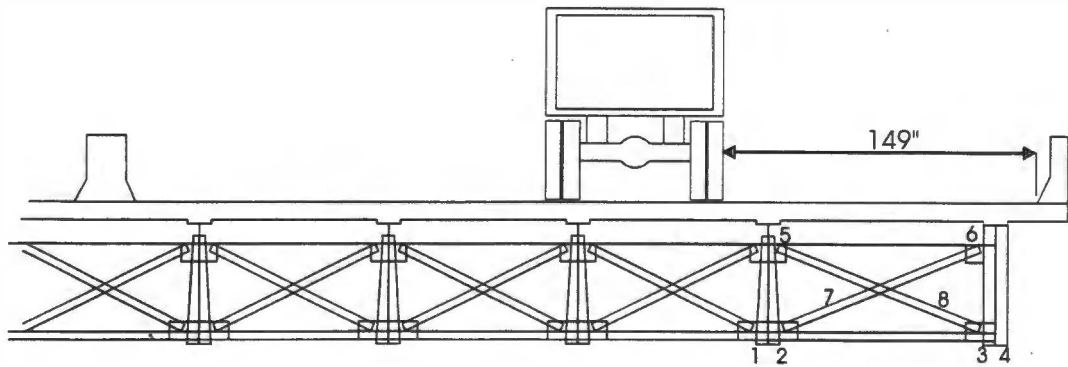
Figure 44. Truck Moving in Right Lane, Finite Element Analysis at Group 1 Location
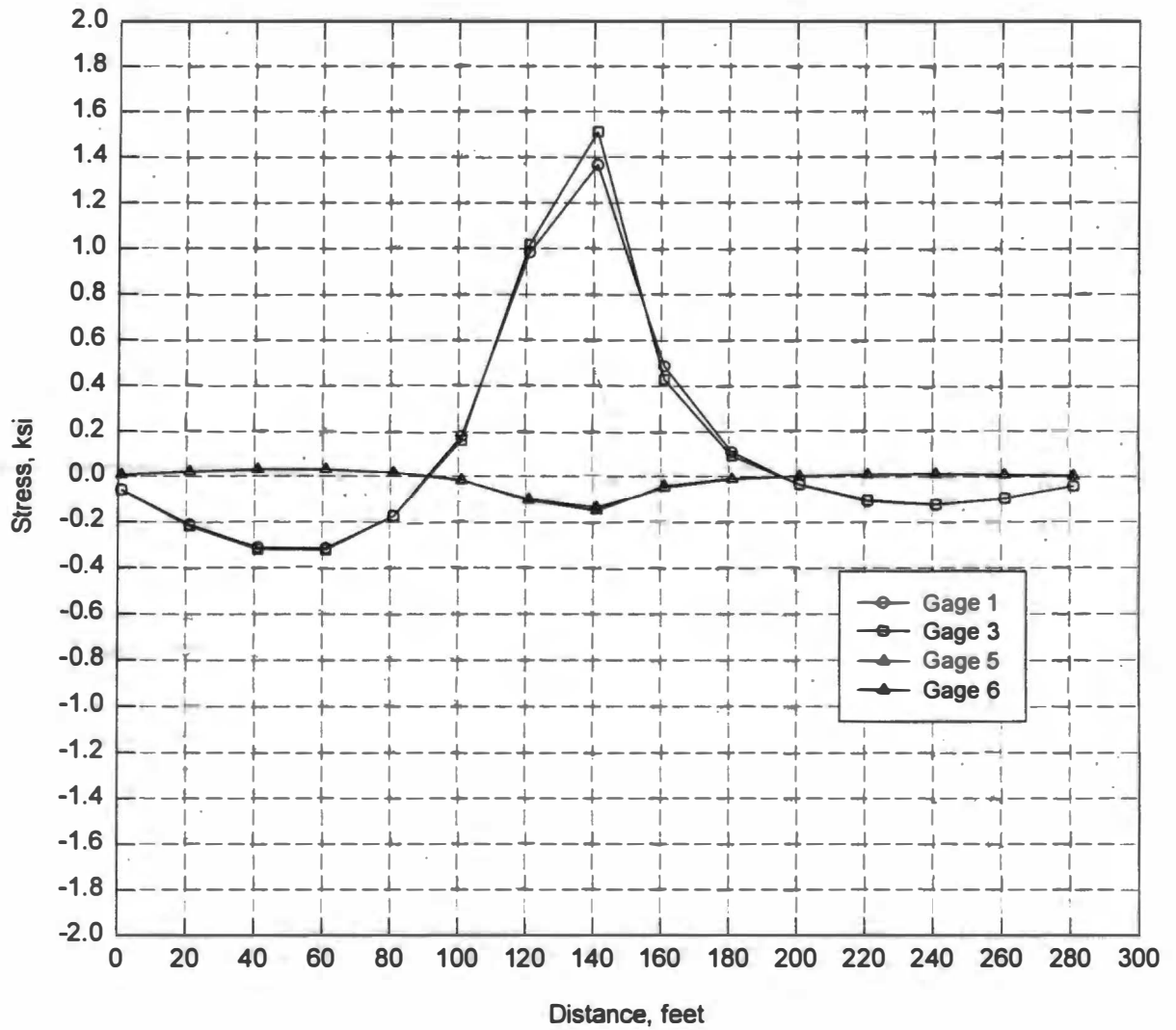(Compare to Figures 20 and 22)

82
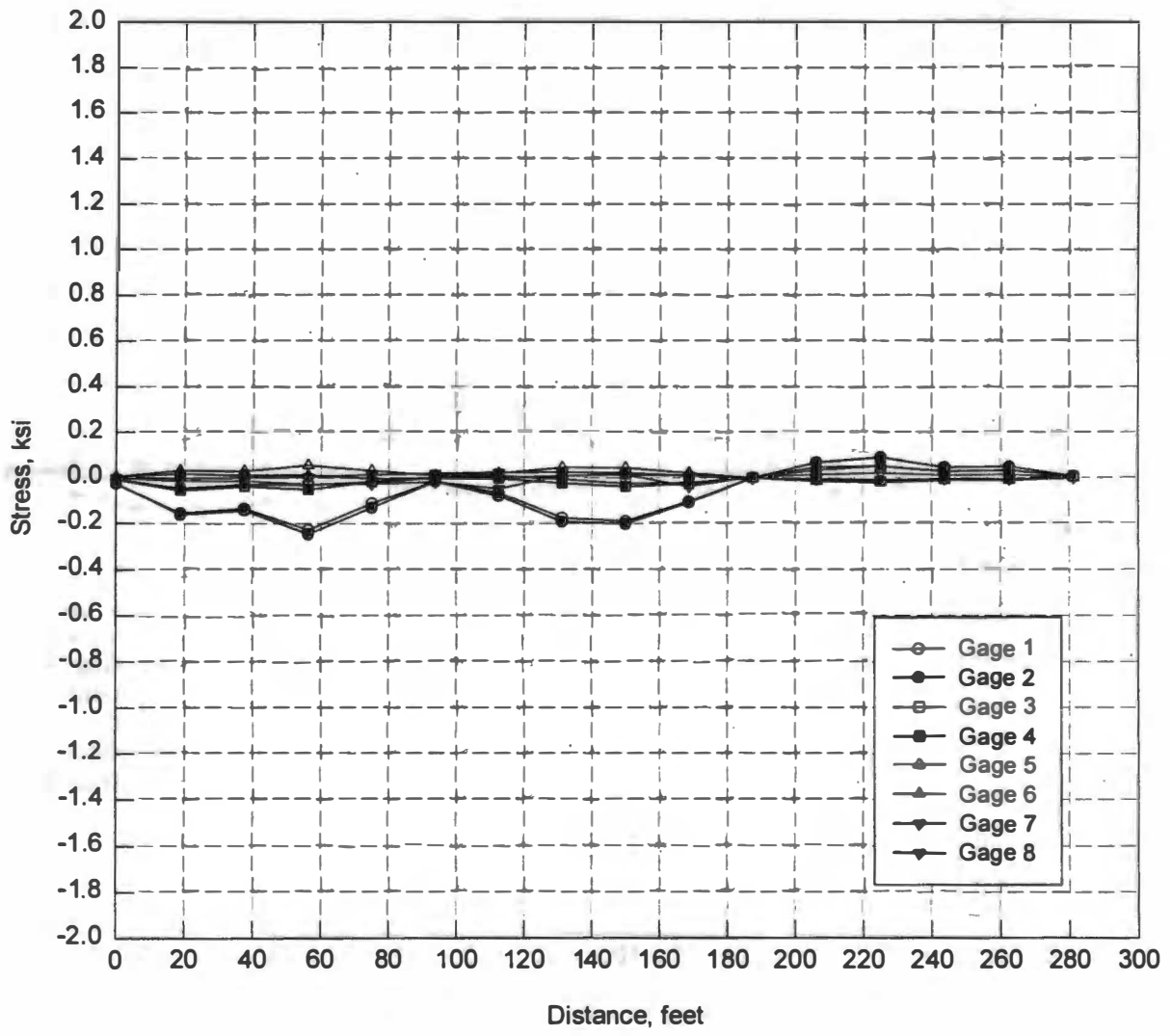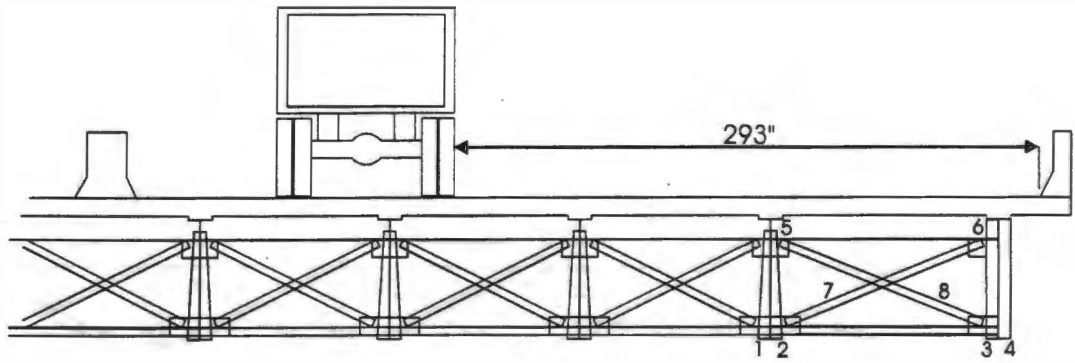
Figure 45. Truck Moving in Left Lane, Finite Element Analysis at Group 1 Location
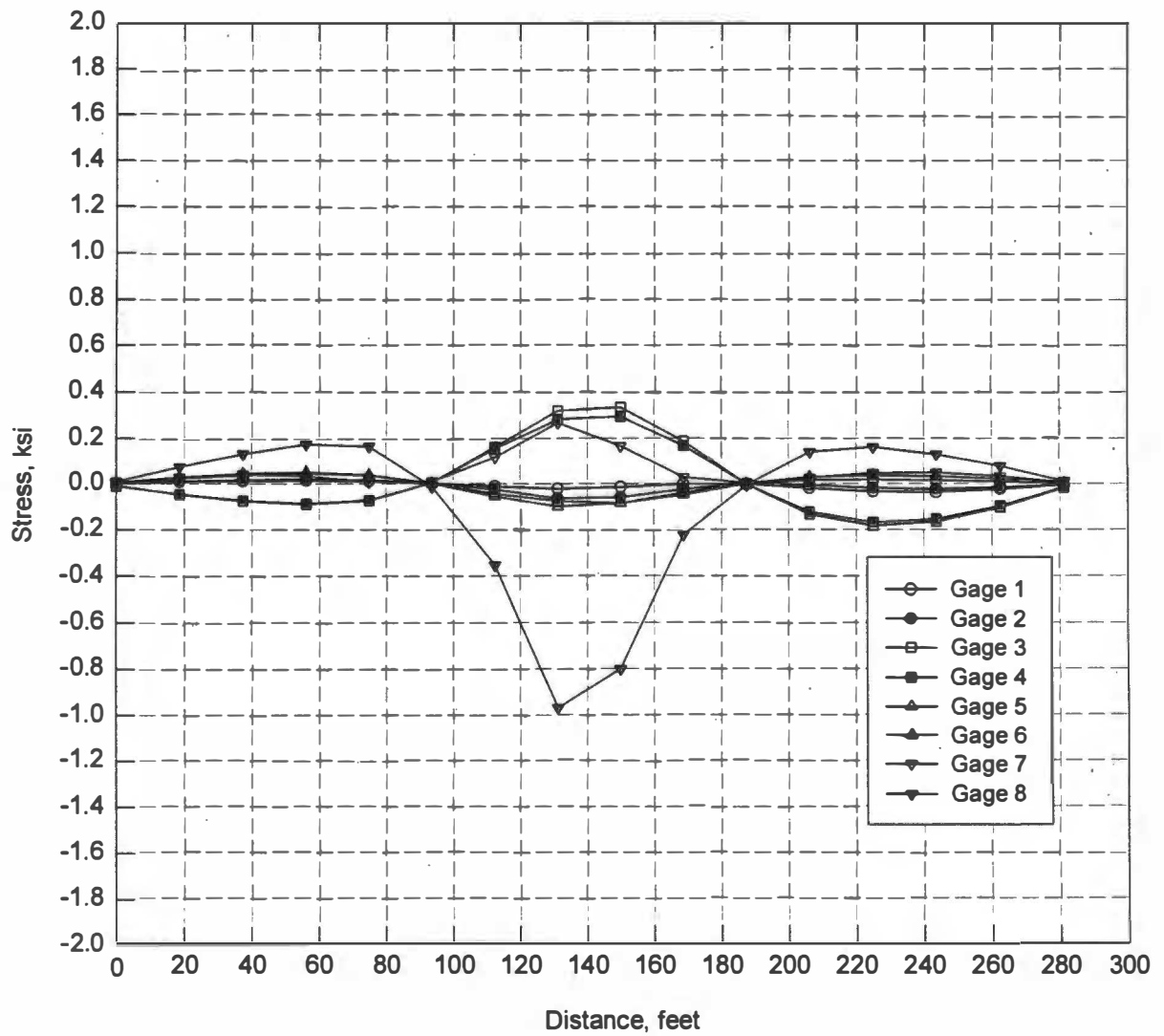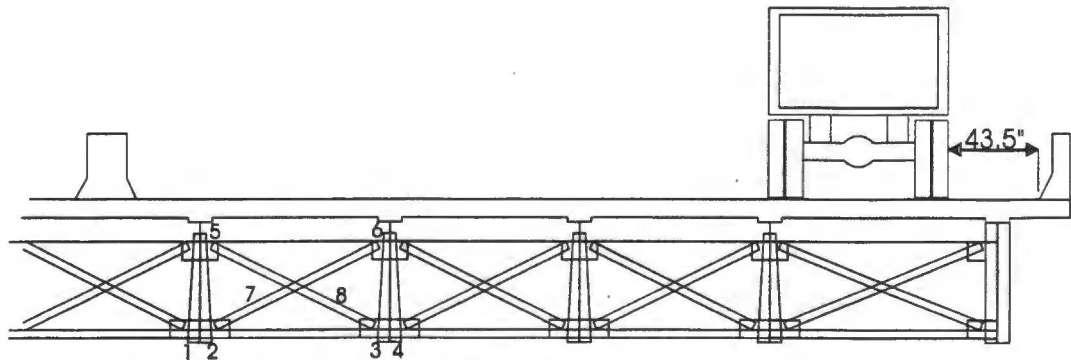
Figure 46. Truck Moving in Shoulder, Finite Element Analysis at Group 2 Location
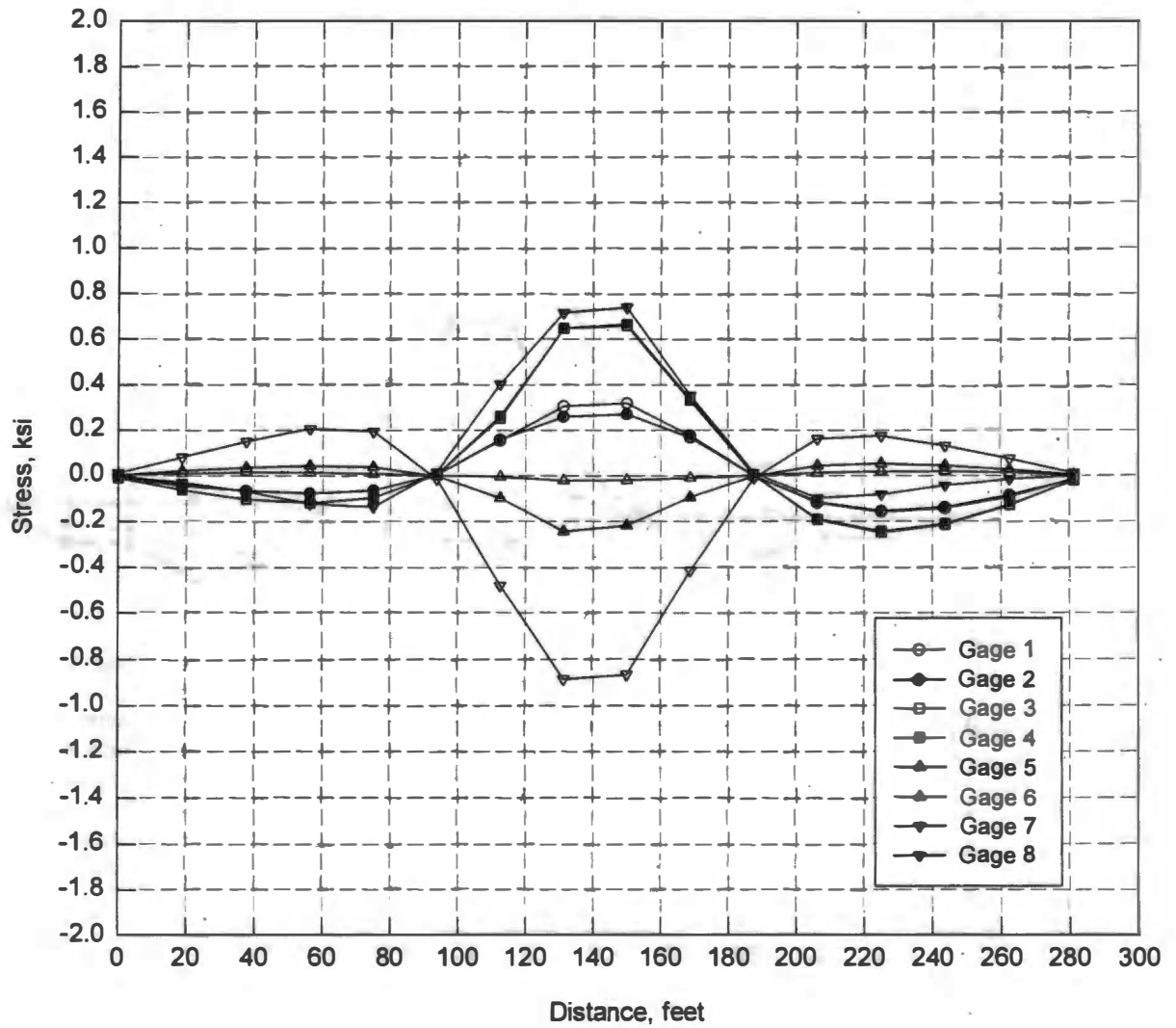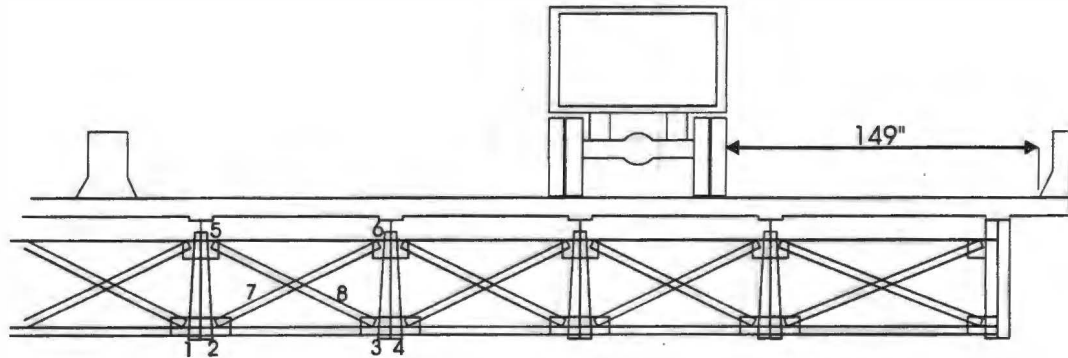
Figure 47. Truck Moving in Right Lane, Finite Element Analysis at Group 2 Location
(Compare to Figures 25 and 26)
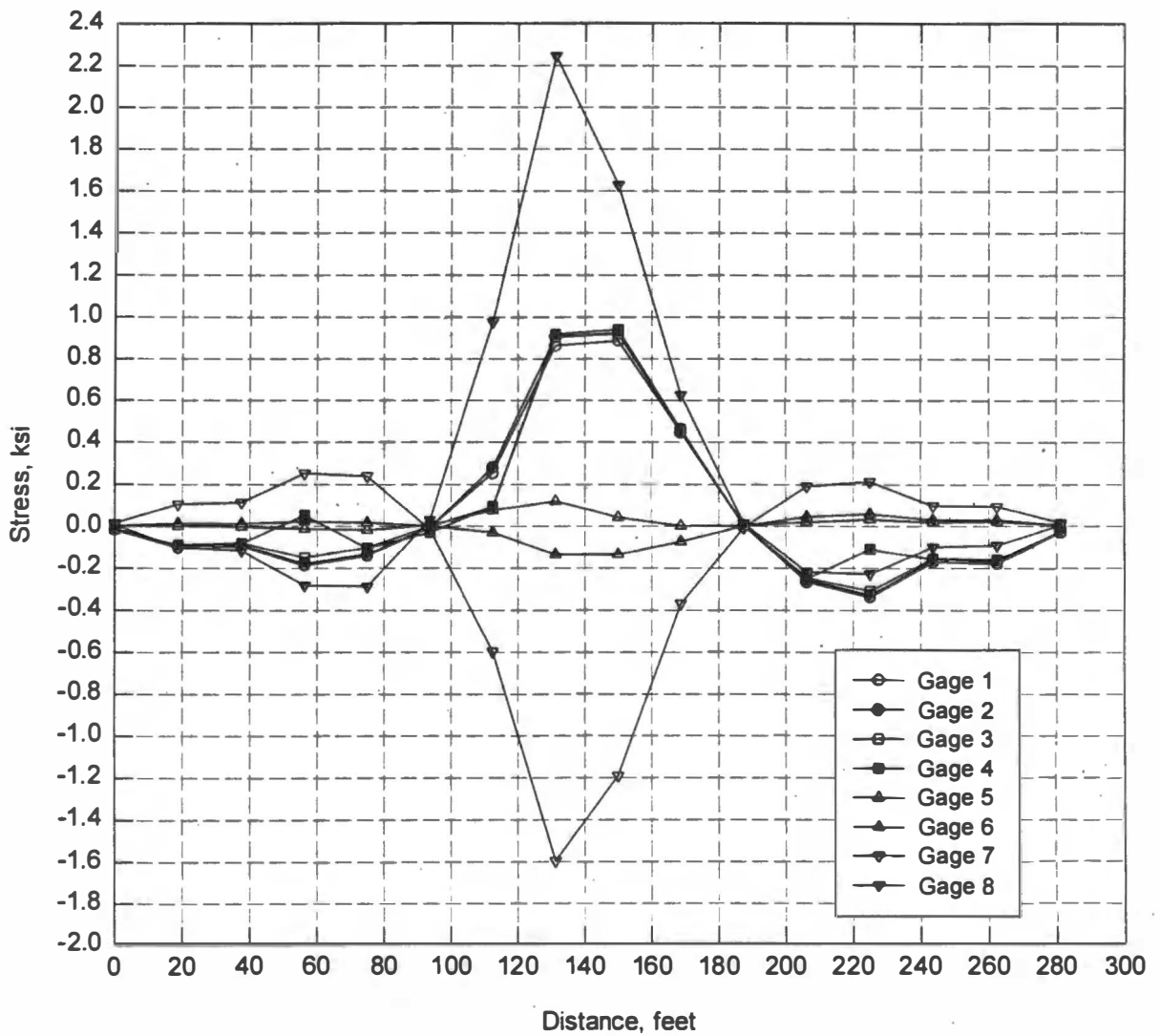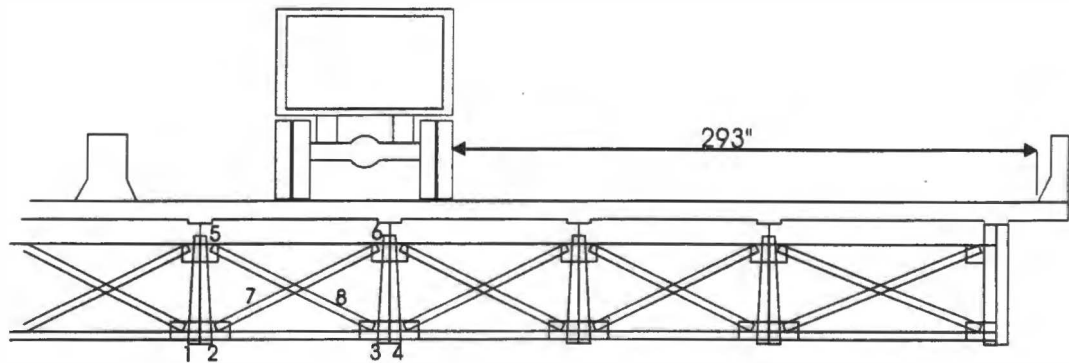
Figure 48. Truck Moving in Left Lane, Finite Element Analysis at Group 2 Location
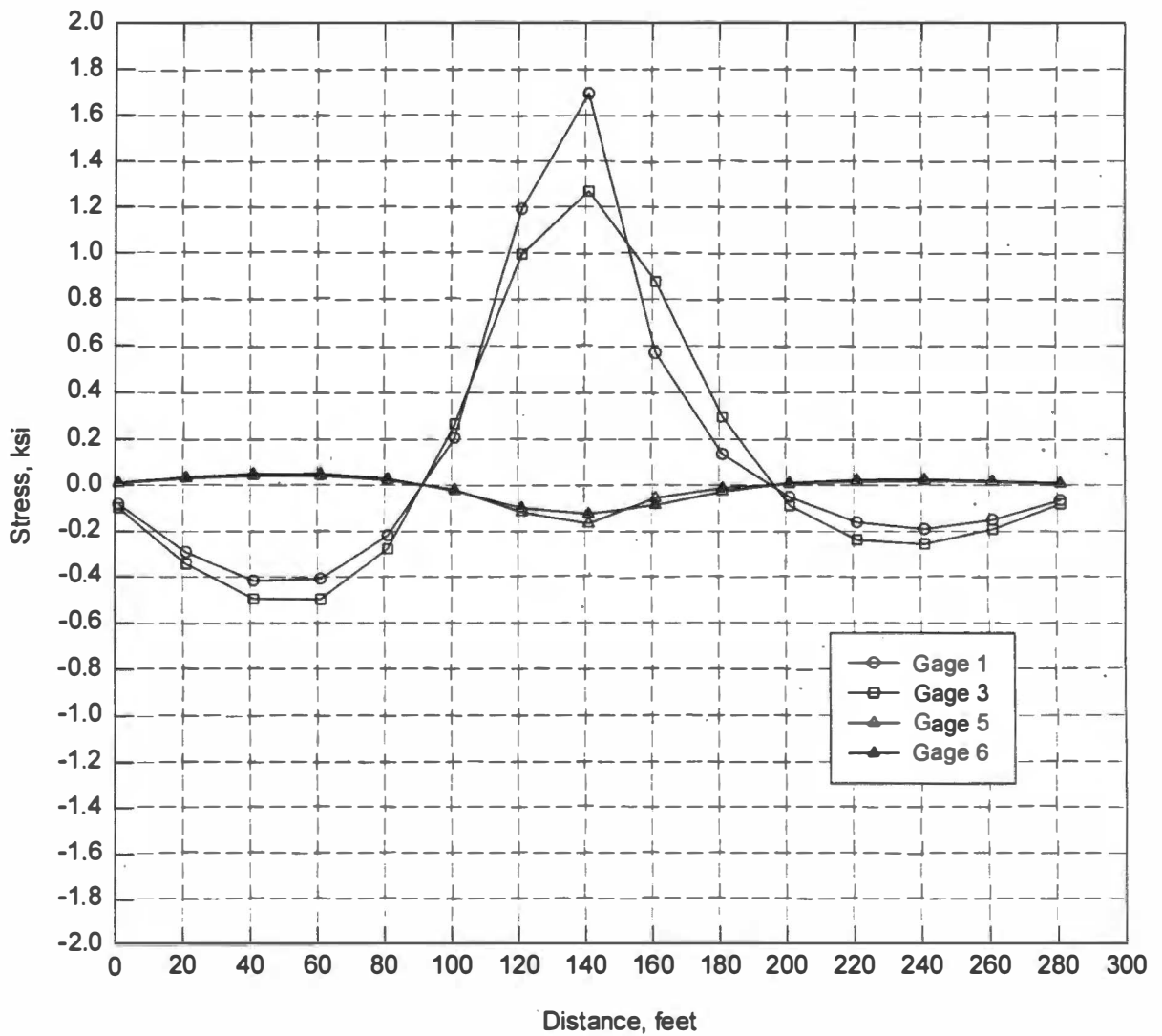(Compare to Figures 27 and 28)
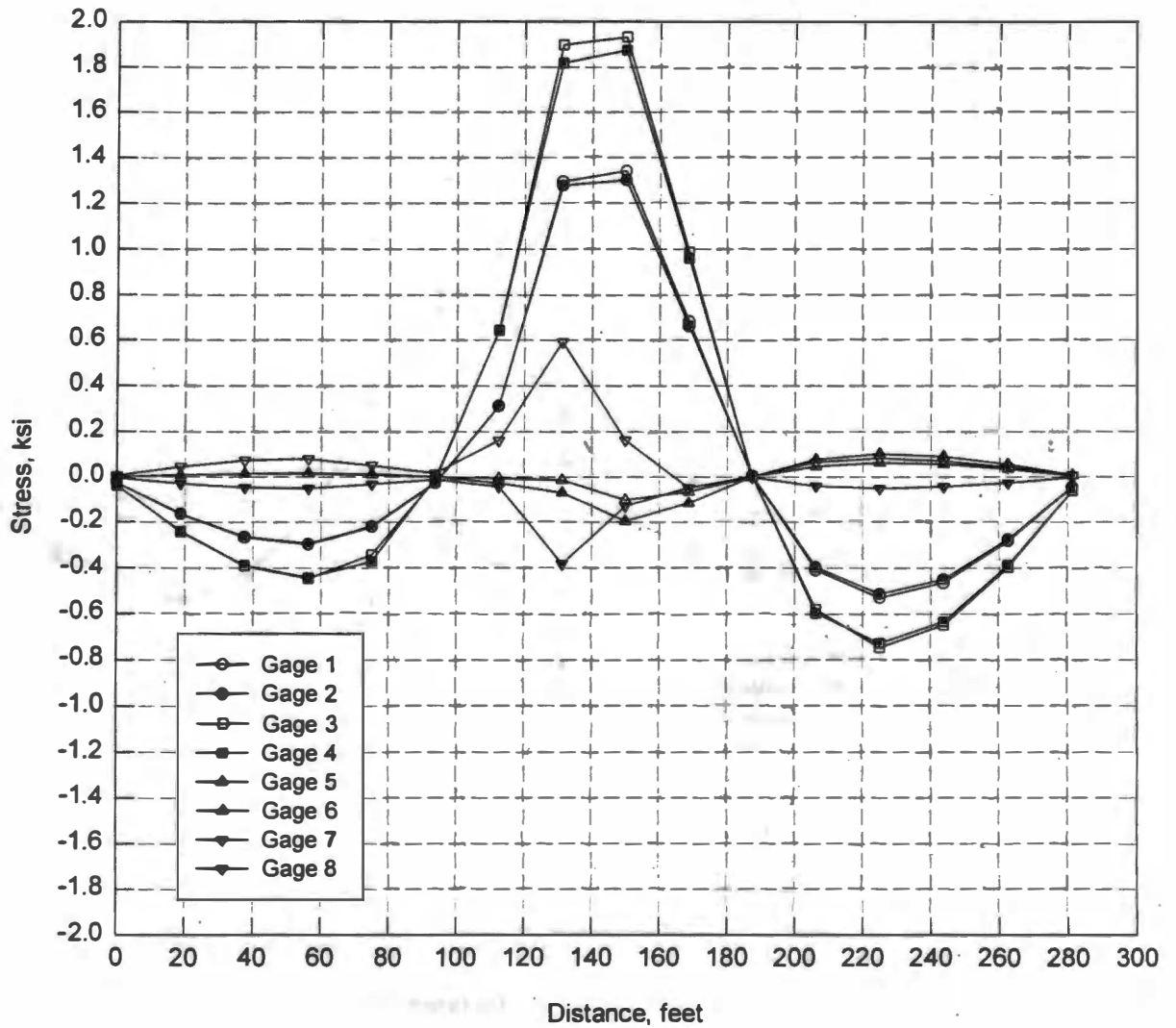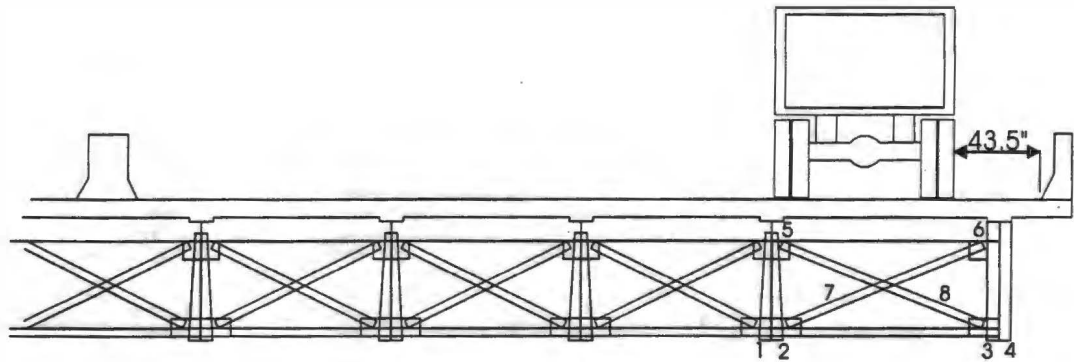
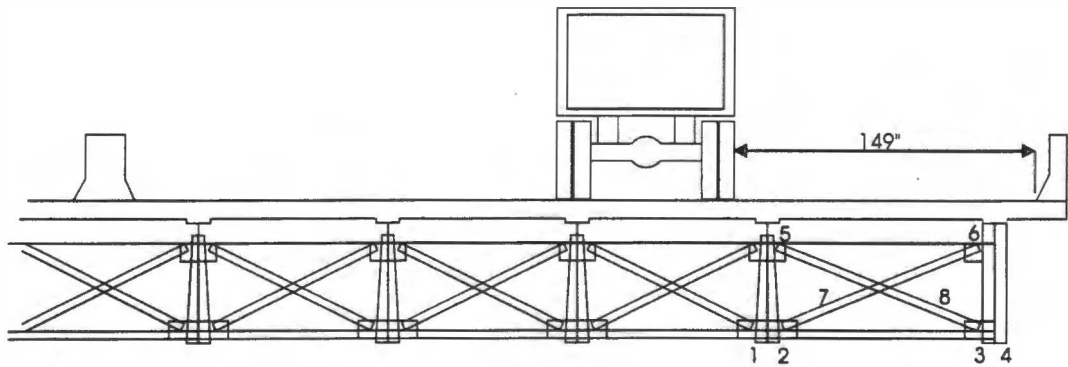Figure 49. Truck Moving in Shoulder, Finite Element Analysis at Group 3 Location
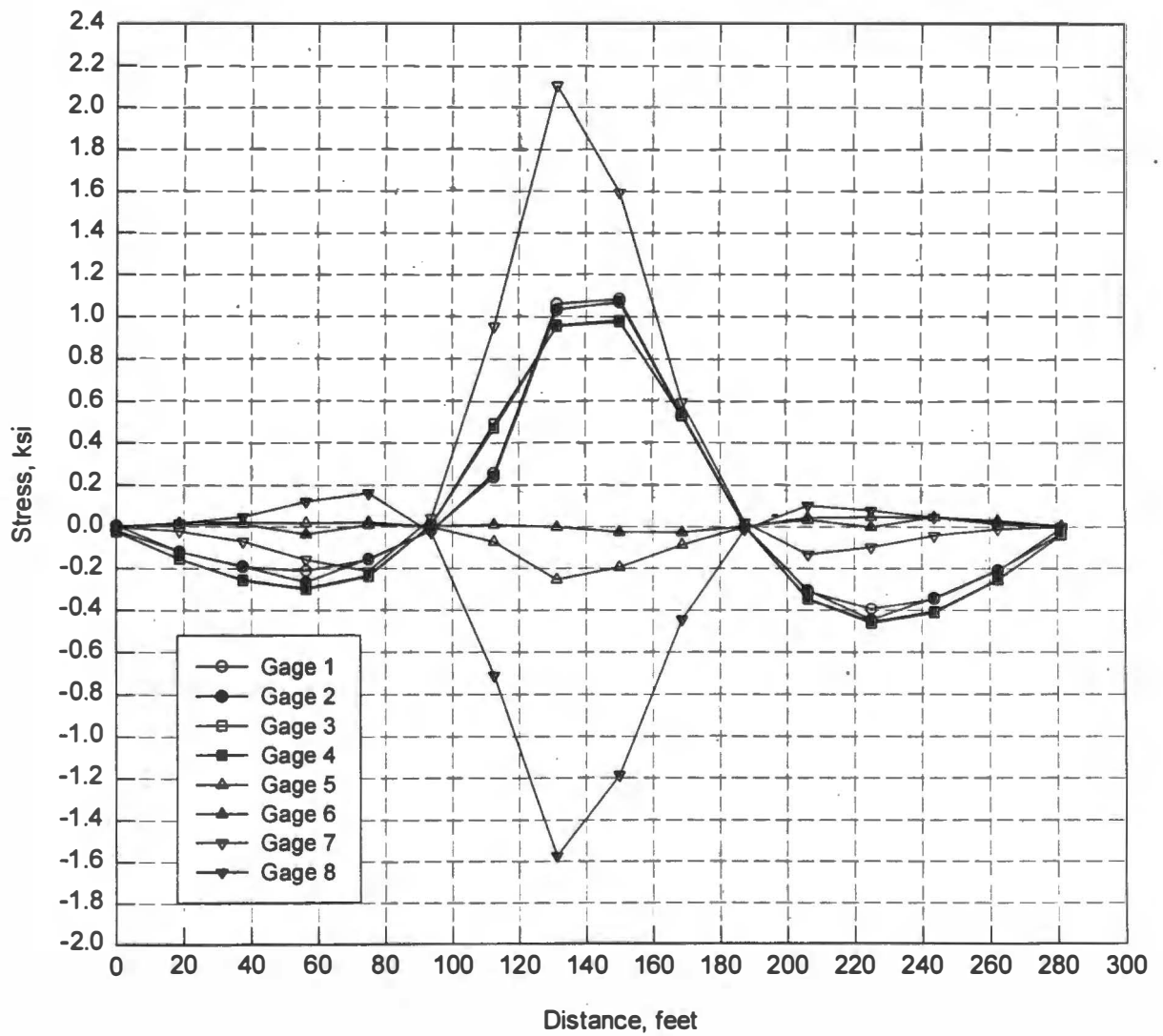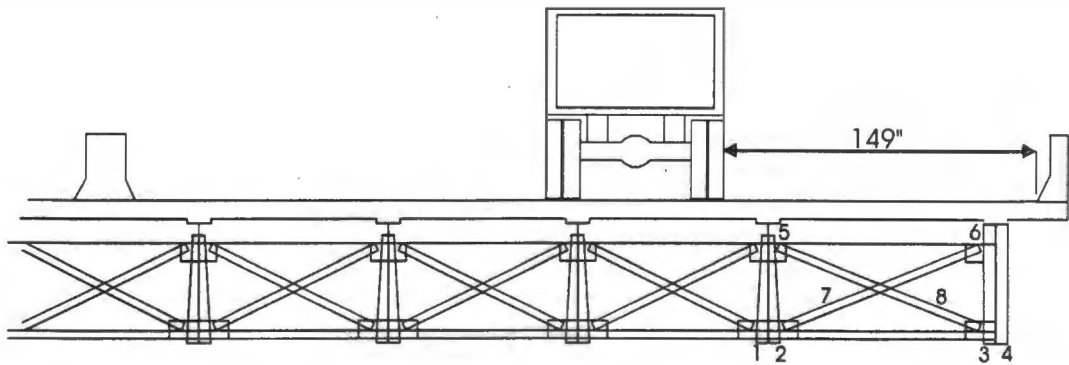
Figure 50. Truck Moving in Right Lane, Finite Element Analysis at Group 3 Location
(Compare to Figures 31 and 32)
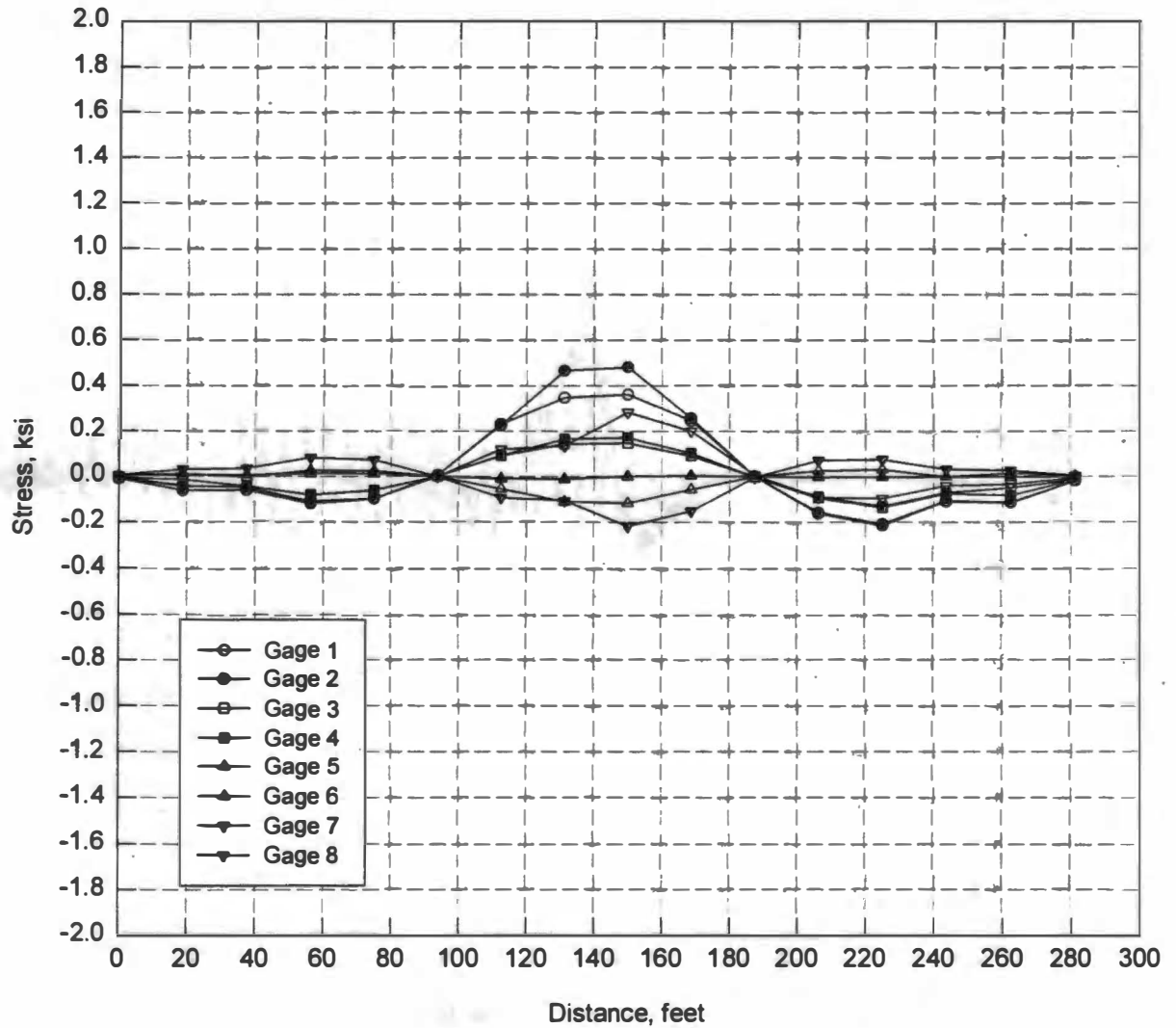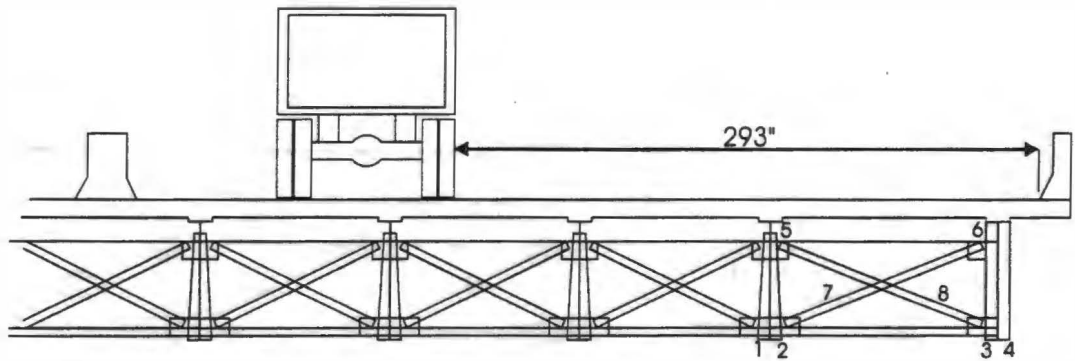
Figure 51. Truck Moving in Left Lane, Finite Element Analysis at Group 3 Location
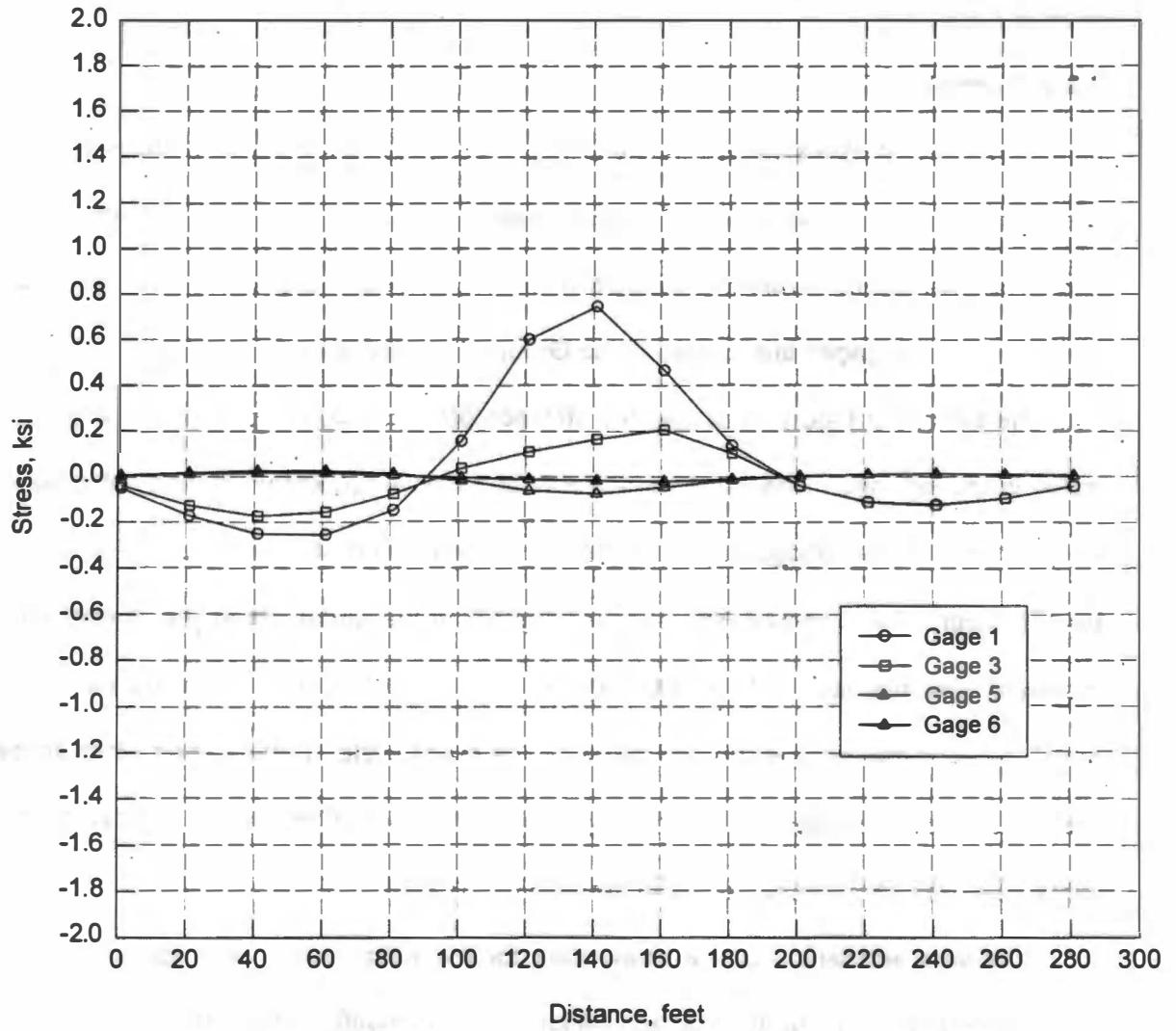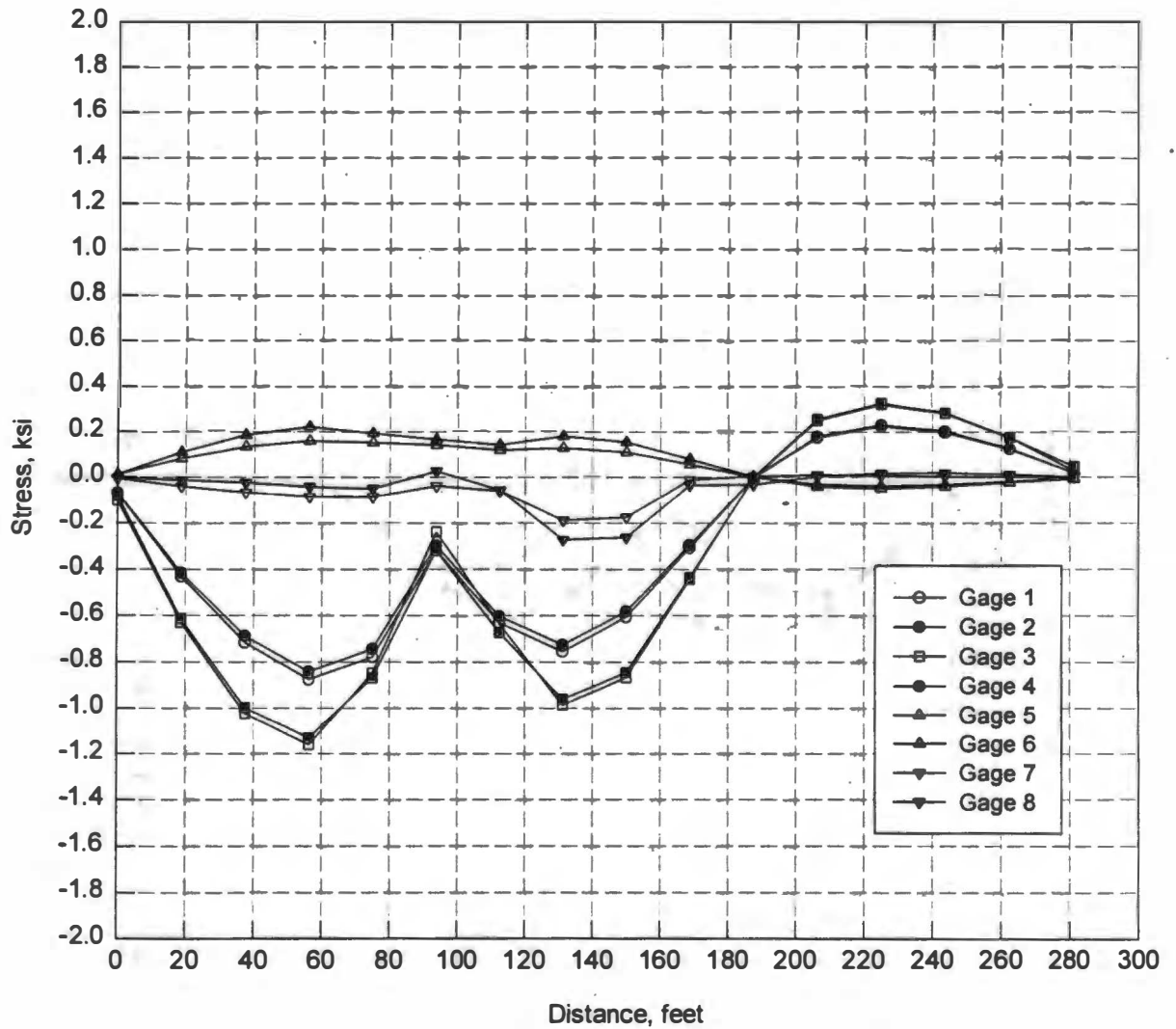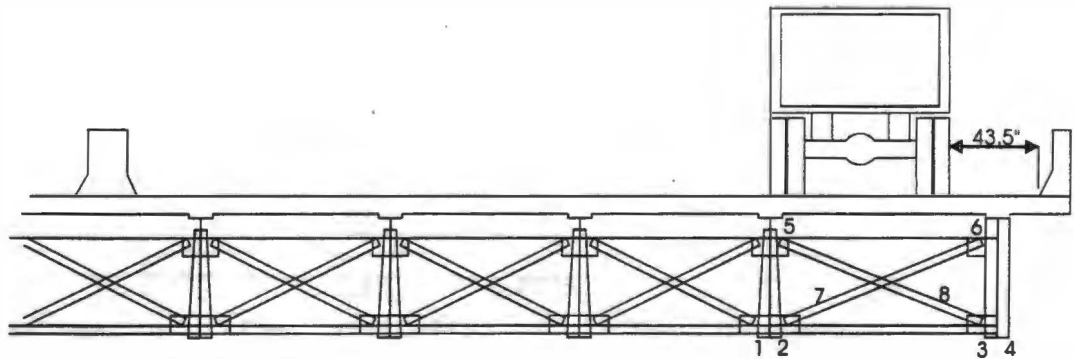(Compare to Figures 33 and 35)
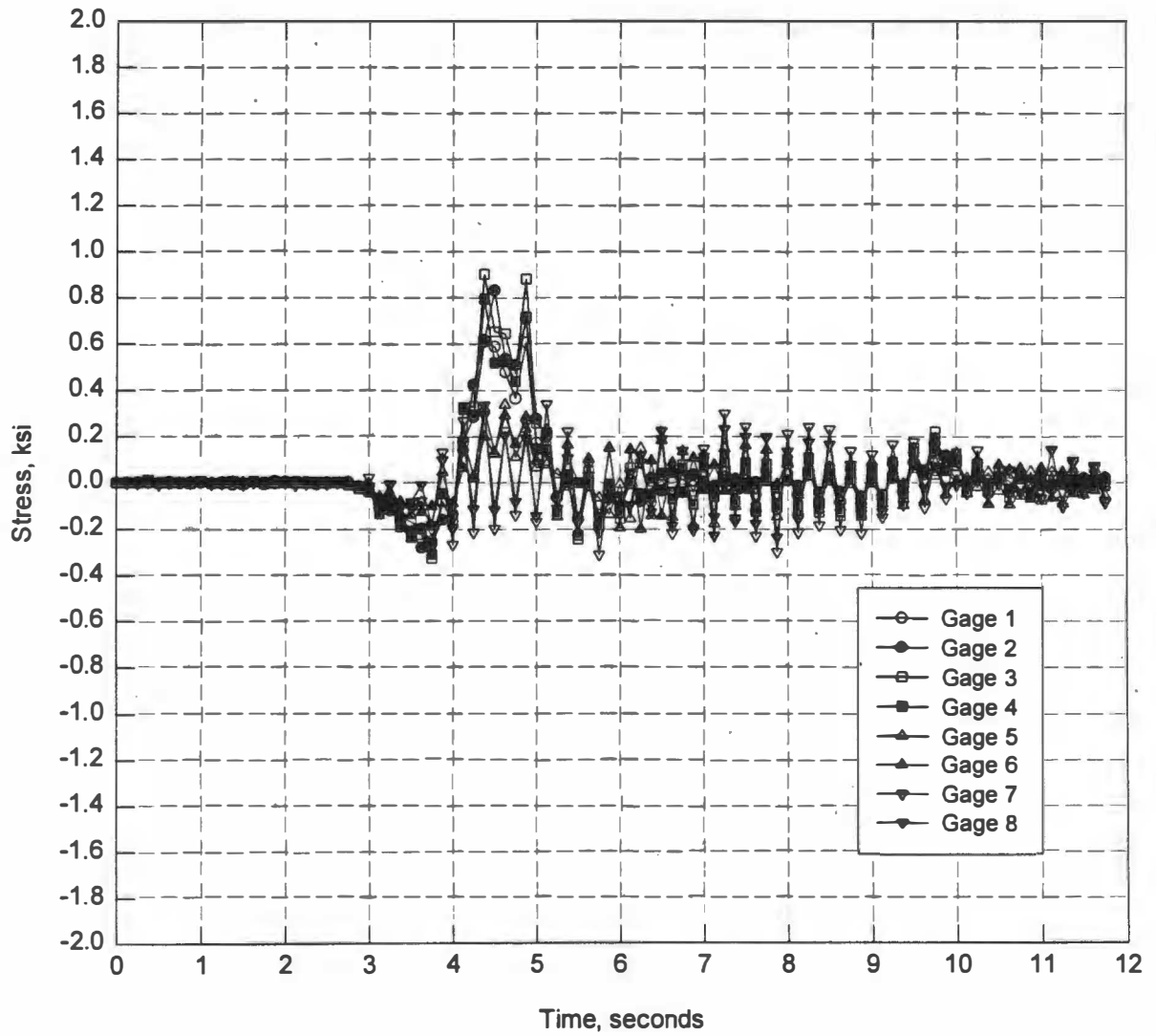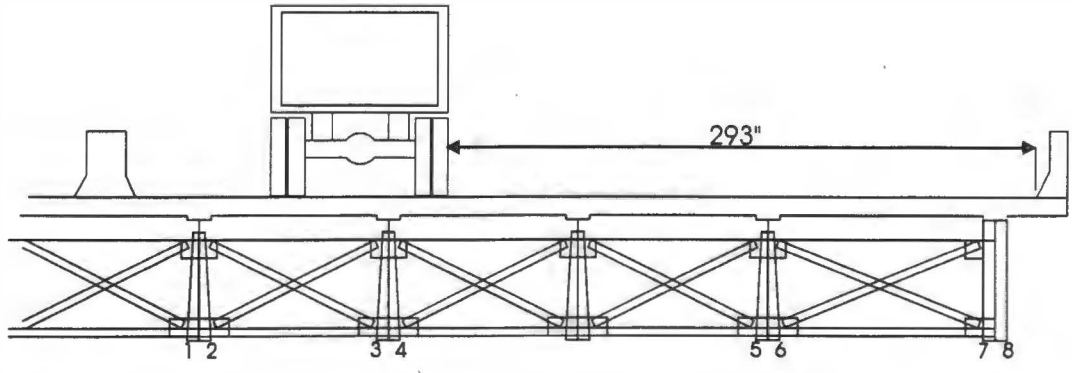
Figure 52. Tractor-Trailer in Left Lane, from Measurements at Gages Shown

rainflow counting algorithm is used to decompose the variable amplitude stress-time history into constant amplitude cycles [Downing et al, 1982]. All equipment and wiring is clamped to the plate girders under the bridge so that it cannot be seen from the roadway. After two weeks, the datalogger is reconnected to a microcomputer on the bridge deck and information is downloaded for analysis.

The datalogger stores histograms for each gage for each twenty-four hour period beginning on the first midnight after the system is activated. In this particular case, the first histogram stored was for Tuesday, February 1, 1994; the last was for Monday, February 14, 1994. A typical stress range histogram is shown in Figure 53. Gage numbering corresponds to that shown in Figure 52.

In addition to generating a histogram from the collected data, the datalogger is programmed to compute and store the maximum stress range, the effective stress range, and the average number of cycles per hour for each 24-hour period. This information is shown with the histogram in Figure 53. The effective stress range is based on the root mean cube version of Miner's Rule [Miner, 1945; Paris et al, 1963], with all cycles included in the Miner's sum.

Figure 54 shows the variation of effective stress range for each gage over the two-week period of data acquisition. Gage 7 is obviously out of line with the other gages and goes completely off scale for a large portion of the record. The effective stress range data is replotted in Figure 55 with gage 7 omitted. Close study of the individual gage lines shows that gage 8 is also behaving erratically. The erratic behavior of gage 8 is more obvious in Figures 56 and 57. In Figure 56, gage 3 also behaves erratically for a short time, but falls back in line over most of the record. Gages 7 and 8 are on the exterior girder and may have been damaged by the rain which occurred during the test period. It is very unlikely that the exterior girder would have experienced stresses so

91
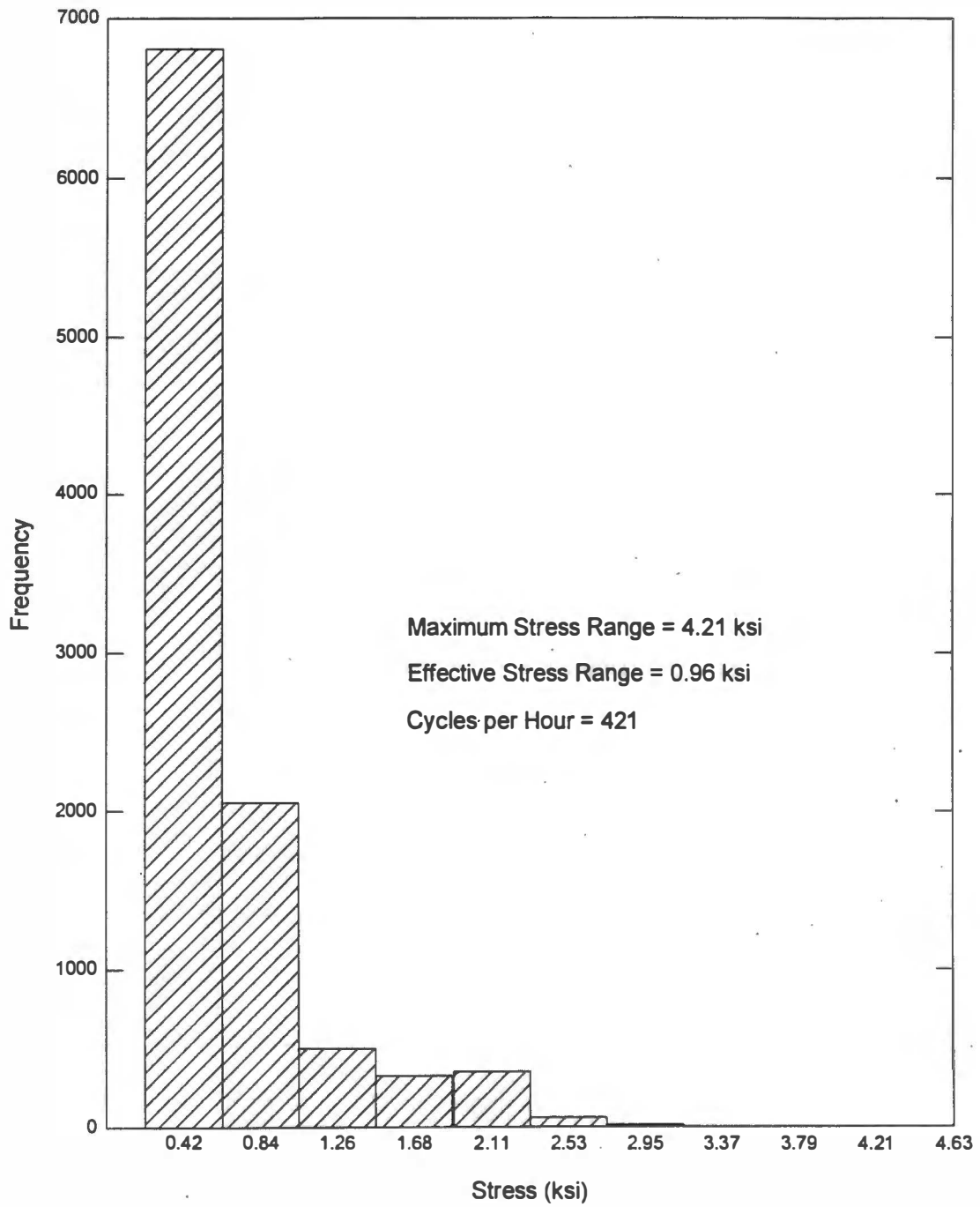
Figure 53. Stress Range Histogram for Gage 4 on the Second Friday of the Two Week Test Period

Maximum Stress Range = 4.21 ksi

Effective Stress Range = 0.96 ksi
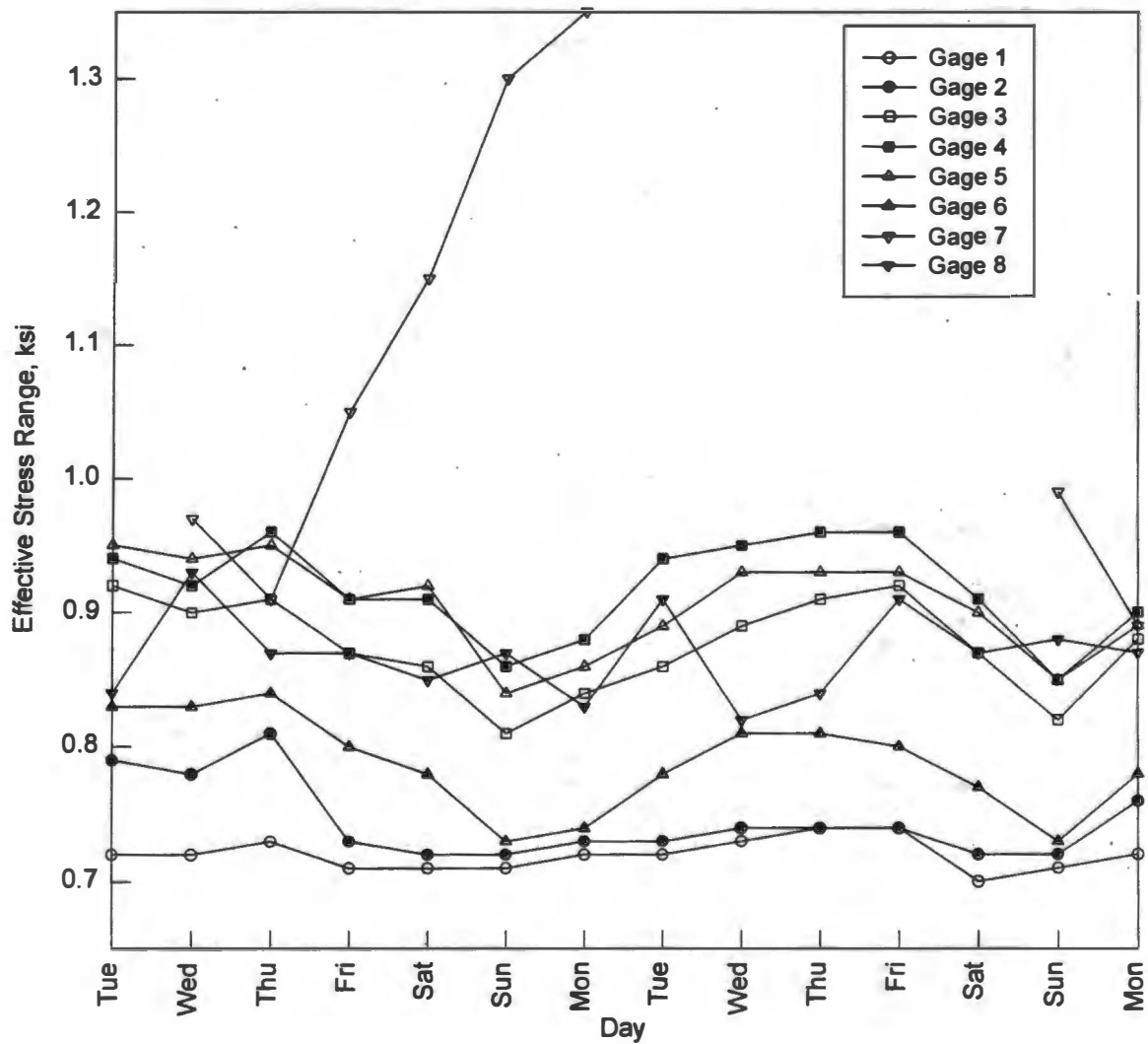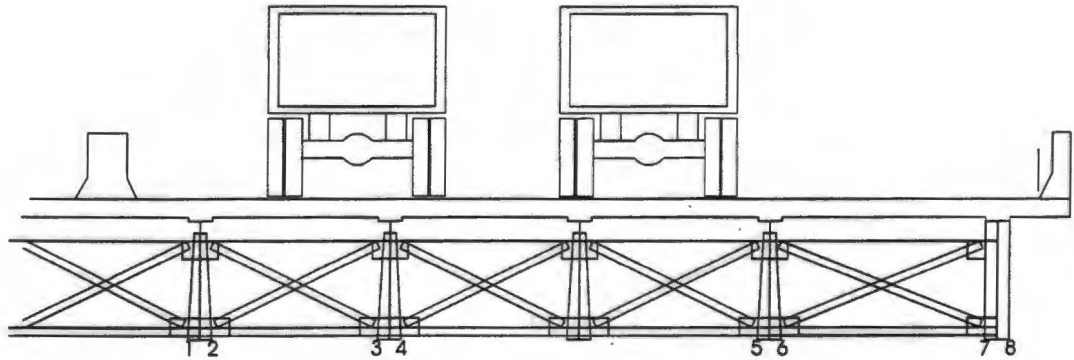
Cycles per Hour = 421

Figure 54. Effective Stress Ranges Over a Two Week Period
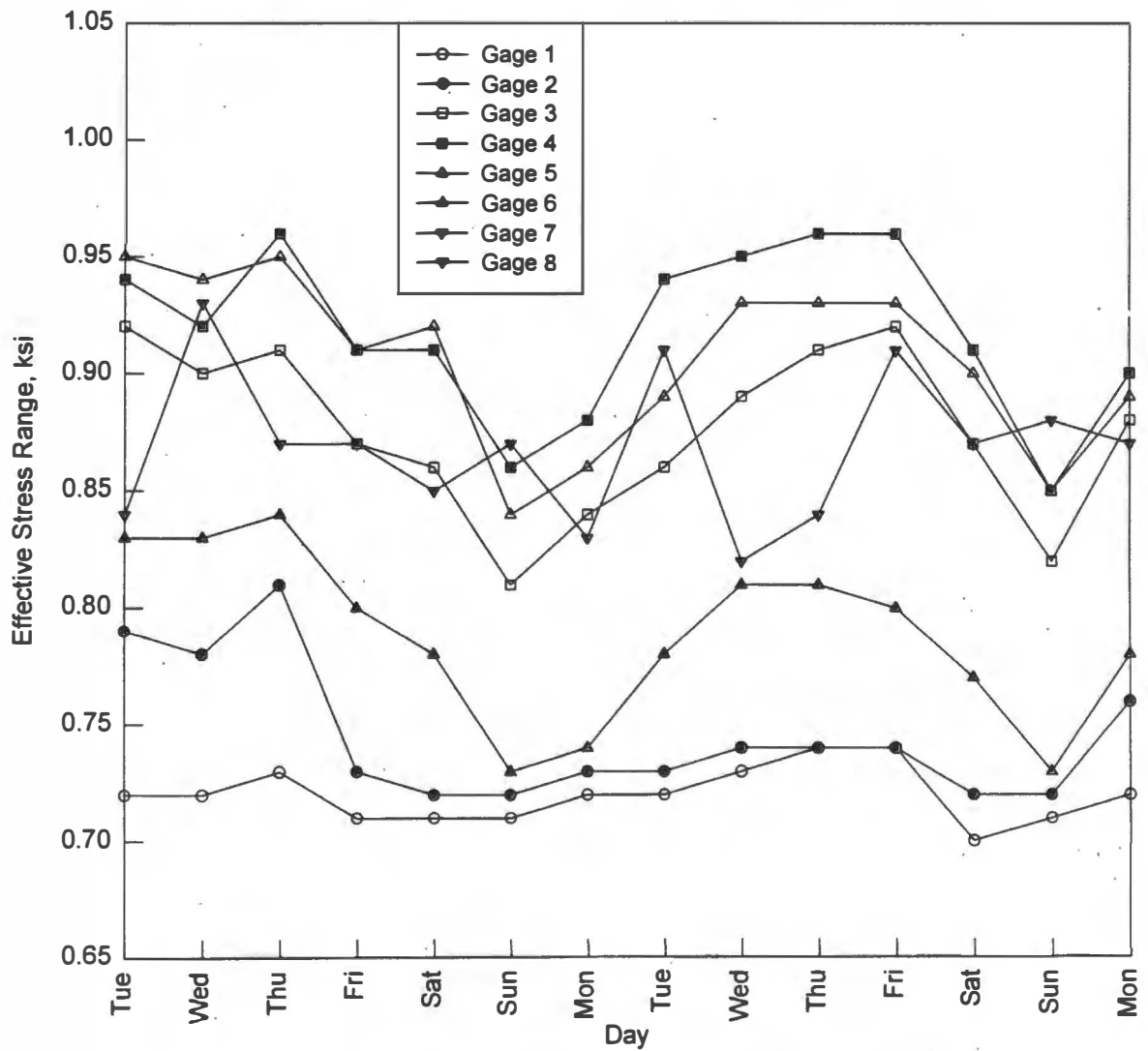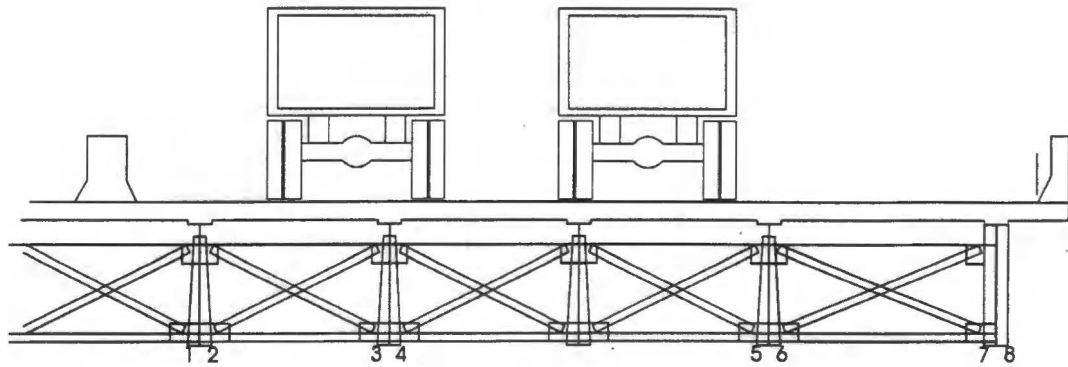
Figure 55. Effective Stress Ranges Over a Two Week Period, Channel 7 Omitted
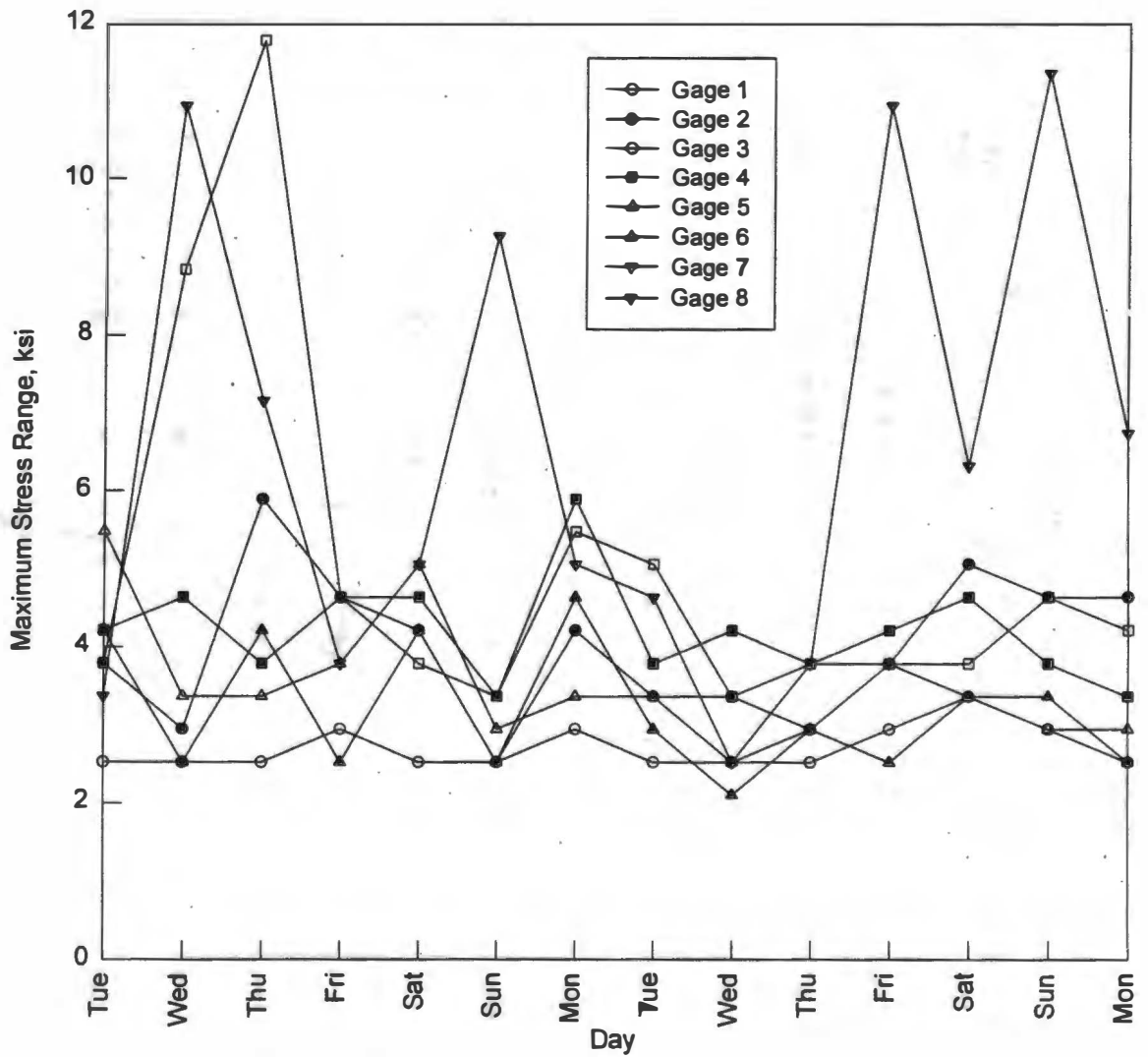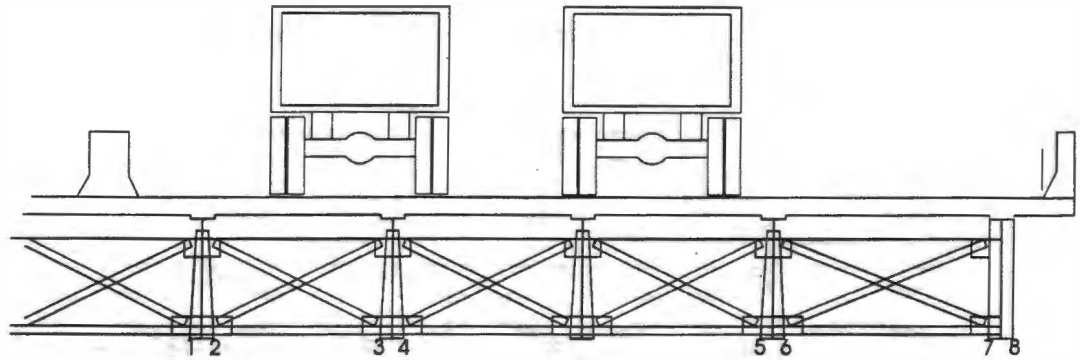
Figure 56. Maximum Stress Range Each Day Over a Two Week Period,
Channel 7 Omitted
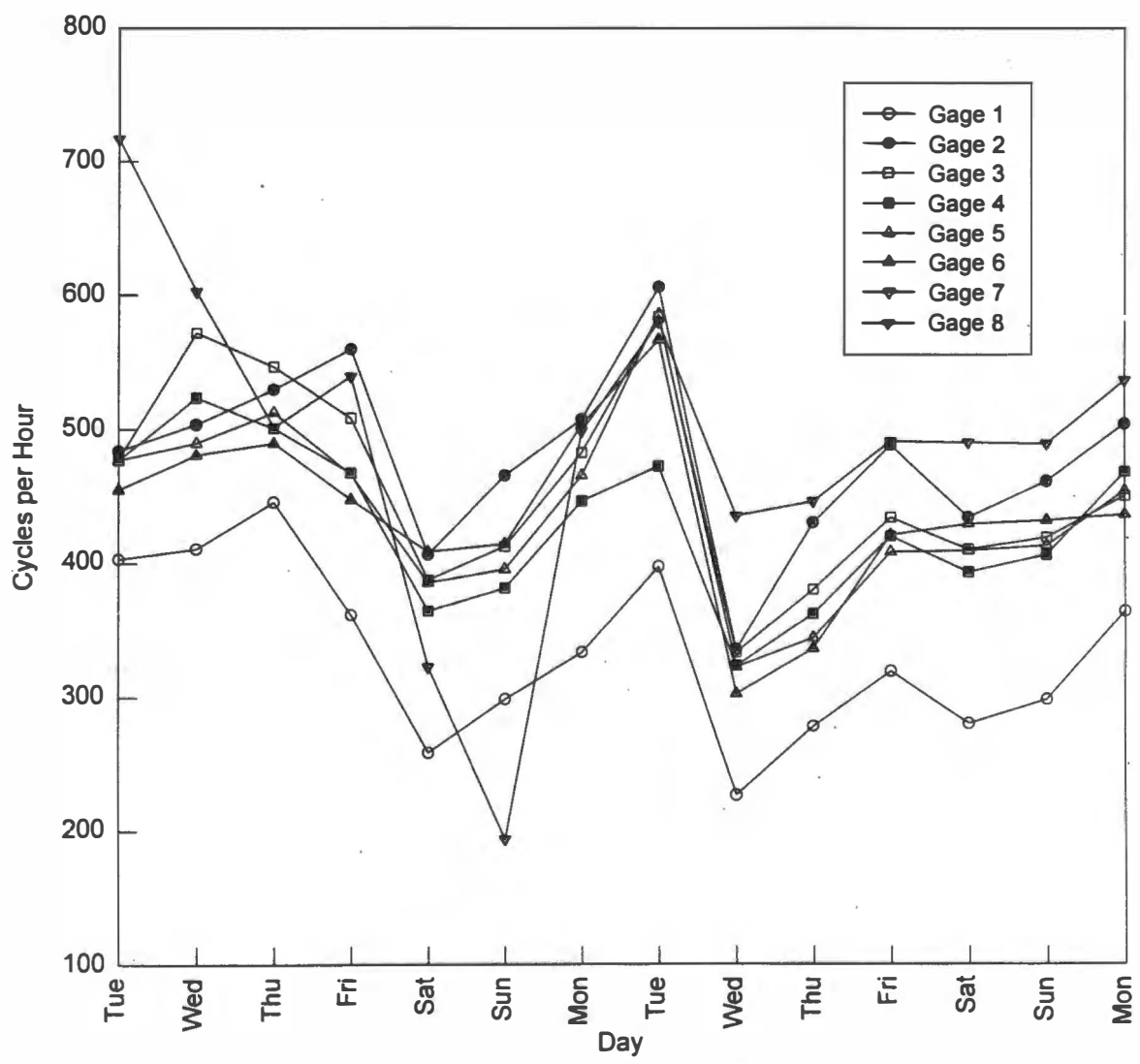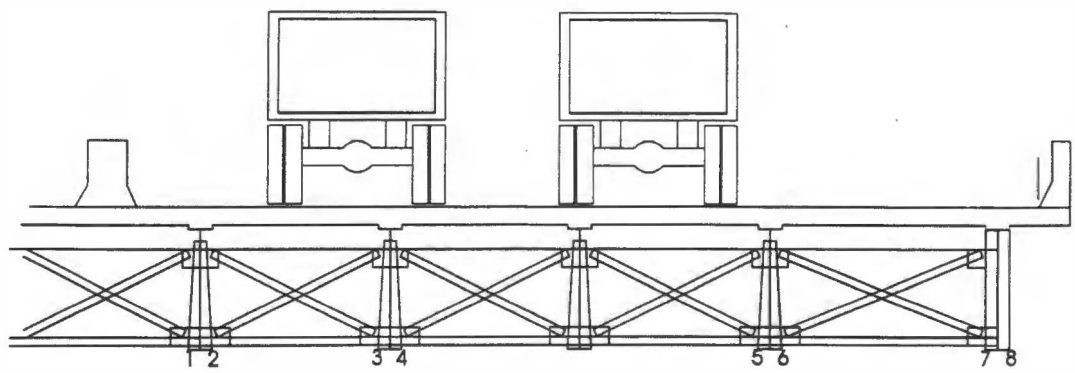
Figure 57. Cycles per Hour Each Day Over a Two Week Period, Channel 7 Omitted

much greater that the first interior girder. Data from gages 7 and 8 are not considered in the assessment of the bridge.

Data for gages 1 through 6 are replotted in Figures 58, 59, and 60. It can be seen that the pattern of variation is similar for all gages. Also notice that the magnitude of the stresses is very low. The highest stress range is 5.9 ksi (excluding two data points for gage 3 which appear to be an aberration) and the highest effective stress range is 0.96 ksi. Although these values are much lower than typical design values, they are comparable to measurements made elsewhere [Moses et al., 1987]. A collection of 215 individual histograms from 41 bridges in 11 states yielded a maximum stress range of 10.5 ksi and a maximum effective stress range of 4.9 ksi; effective stress ranges usually fell between 1 and 3 ksi. Low effective stress ranges are caused by the high number of small stress range cycles per truck passage, as can be seen in Figure 52. The maximum number of cycles per hour is 606.

3.4 Laboratory Testing

3.4.1 Fabrication of Test Specimens

Three specimens were prepared for fatigue testing. All three test specimens were W14x43 rolled beams with one-sided transverse stiffeners attached to the web and both flanges. The beam and stiffener material used for fabricating the test specimens was ASTM A36 structural steel. For all specimens, six one-sided transverse stiffeners were attached symmetrically about the midpoint of each beam length, where the length of each beam was 20 ft. Attaching the stiffeners in this fashion allowed the fatigue testing of one beam to result in two data points at three different stress ranges for a total of six possible data points per beam. A diagram showing longitudinal dimensions and stiffener locations for a typical test specimen is given in Figure 61. The stiffeners used on the test specimens were steel plates with a width of 3 in. and a thickness of 3/8 in. The
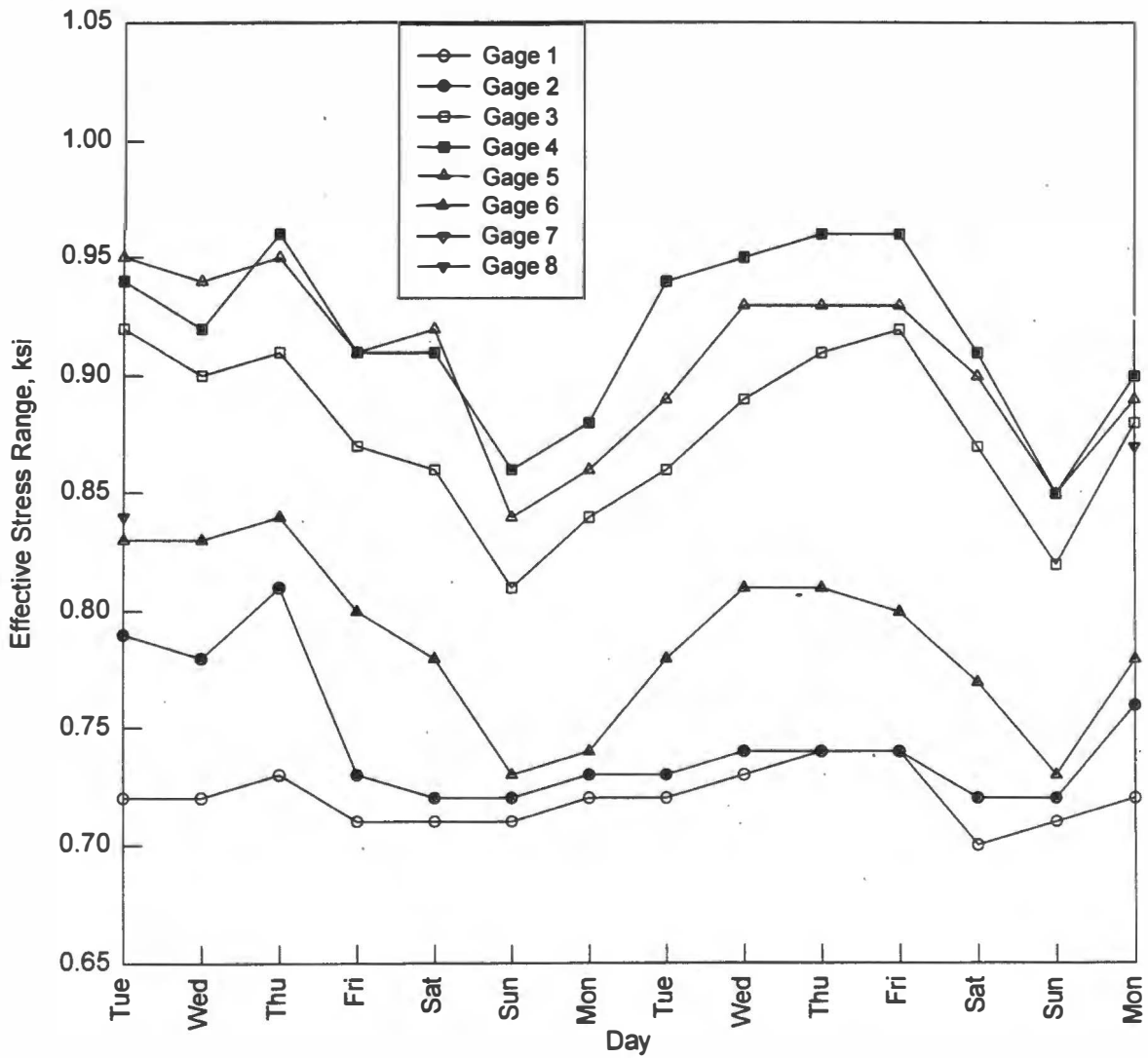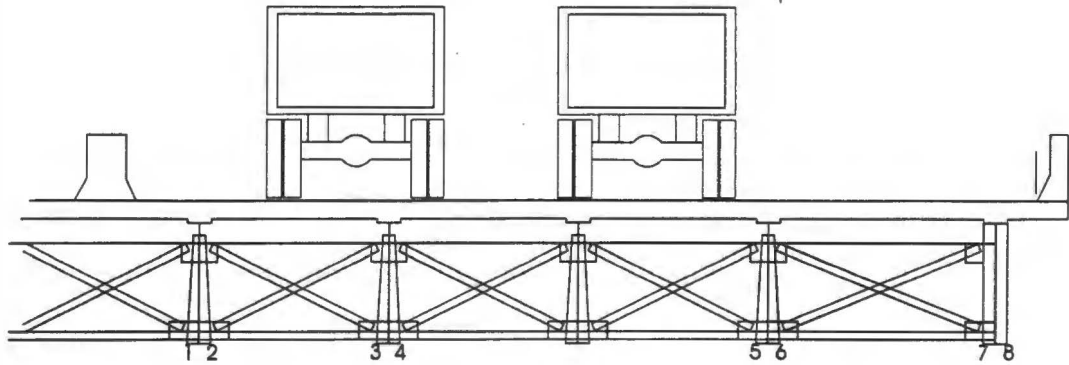
Figure 58. Effective Stress Ranges Over a Two Week Period,
Channels 7 and 8 Omitted
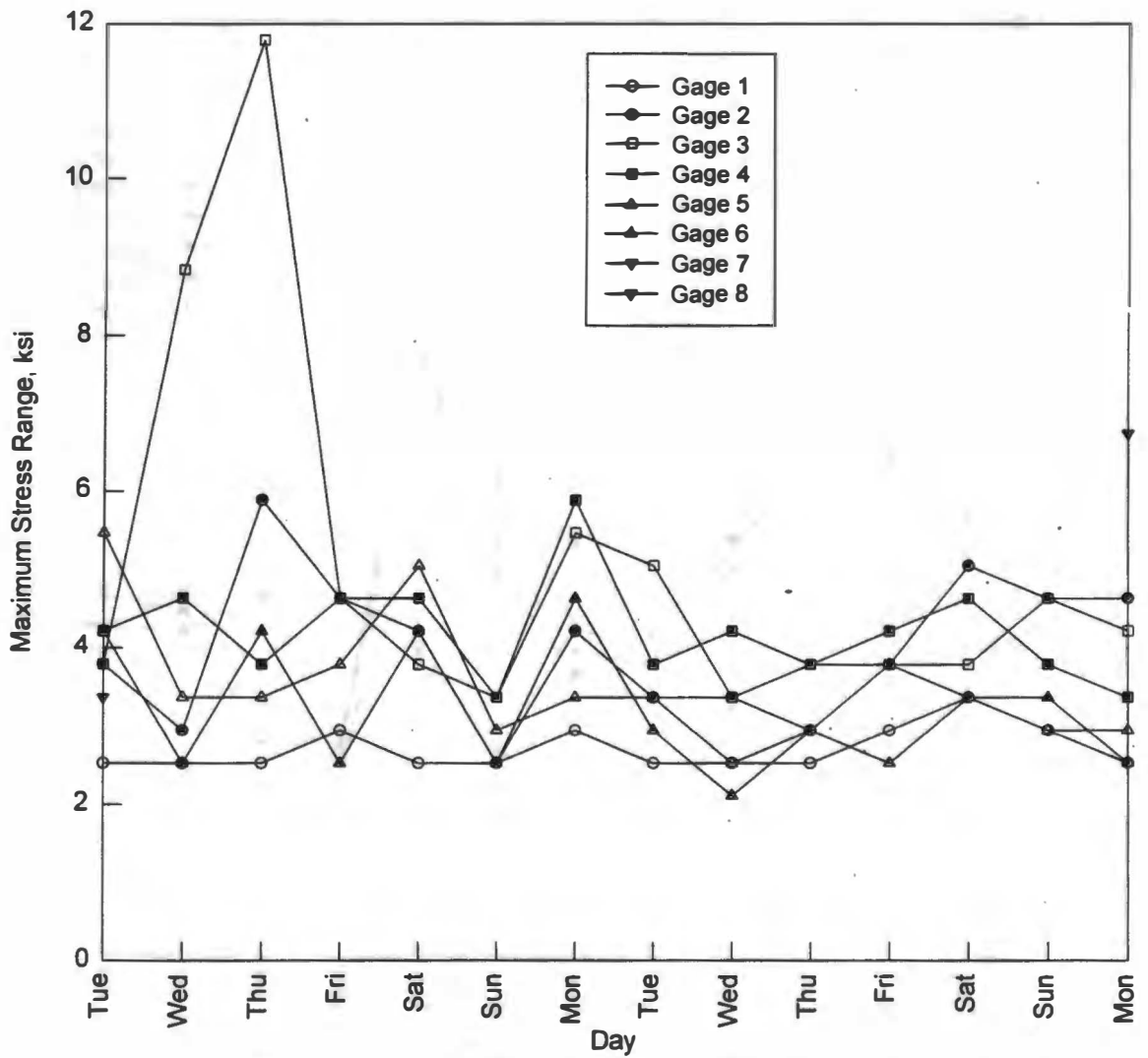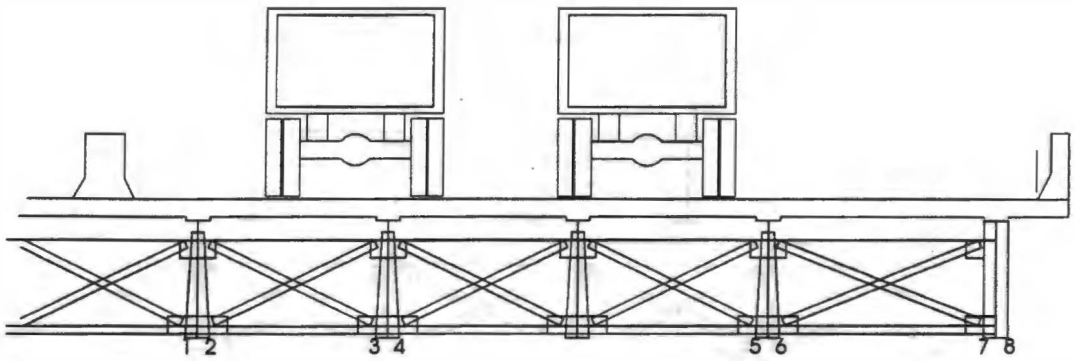
Figure 59. Maximum Stress Range Each Day Over a Two Week Period,
Channels 7 and 8 Omitted
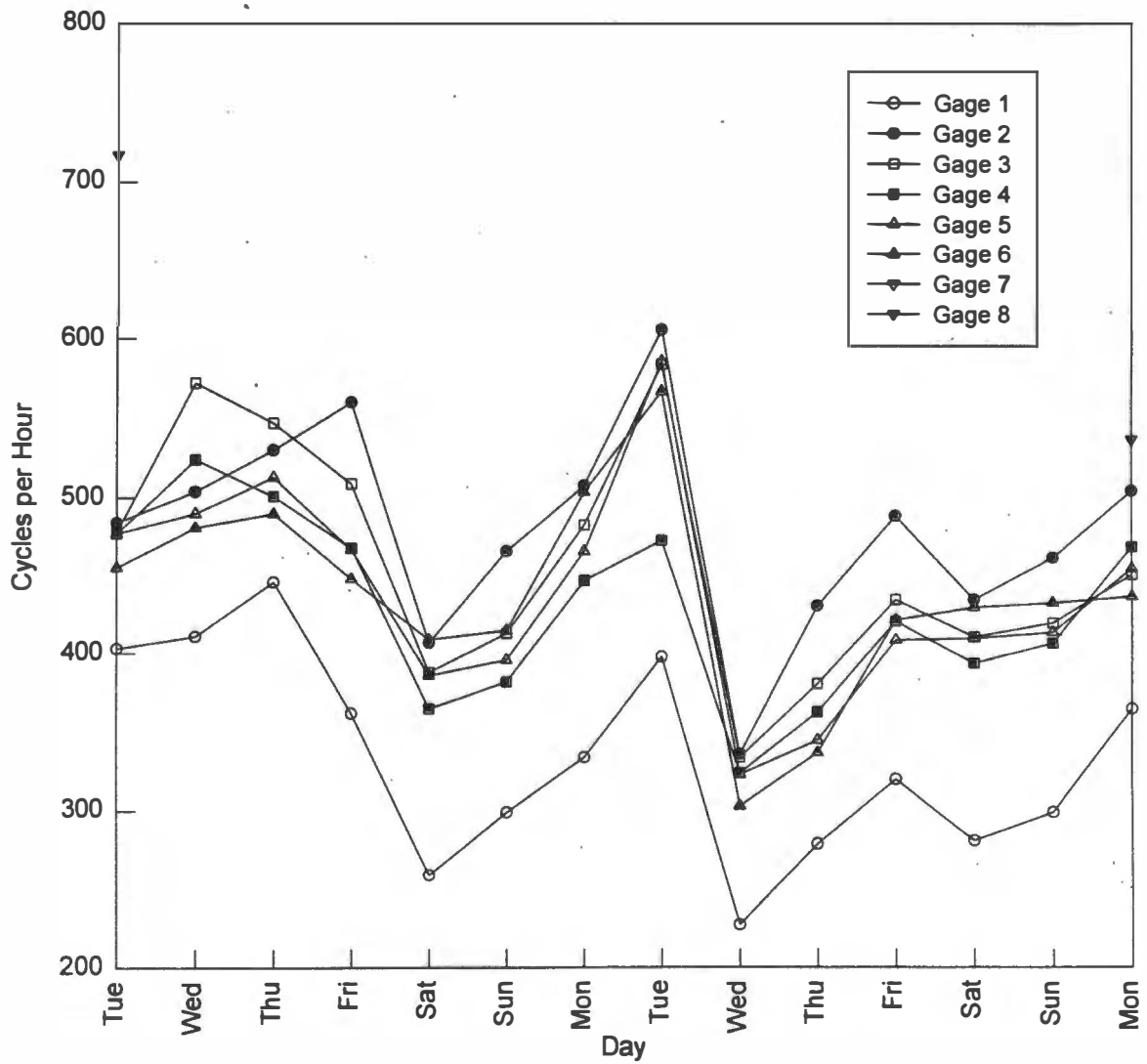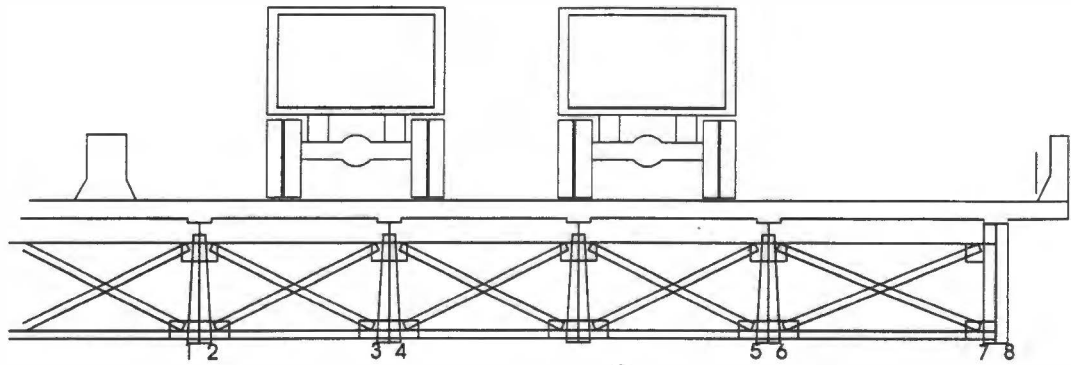
Figure 60. Cycles per Hour Each Day Over a Two Week Period, Channels 7 and 8 Omitted
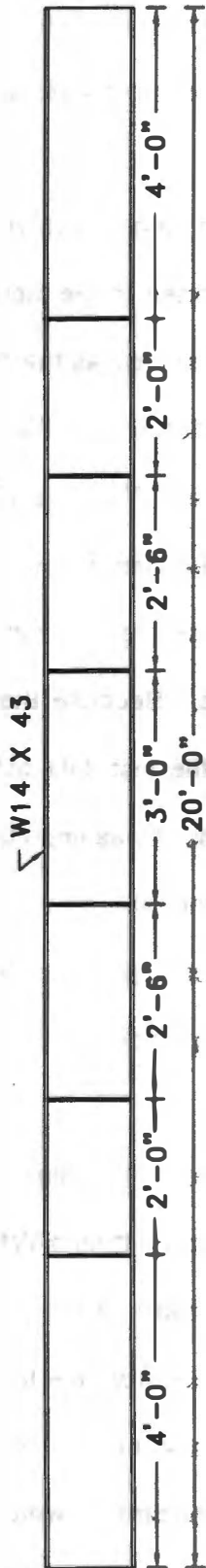
Figure 61. Longitudinal View of a Typical Test Specimen

stiffeners were attached to the web and flanges of each beam with 1/4 in. fillet welds. A diagram showing cross-sectional dimensions and weld specifications for a typical test specimen is given in Figure 62.

To provide a basis for comparing test data and to ensure that the test procedures yielded results comparable to results reported in the literature, a control was needed. One of the three test specimens prepared served as the control. The control specimen was prepared by a reputable steel fabrication shop. The fabricator was sent the plans and specifications for a typical test specimen. Taking a 20 ft length of a W14x43 rolled steel beam, the fabricator attached the one-sided transverse stiffeners by welding to the web and both flanges. The fabricator attached the stiffeners with 1/4 in. fillet welds using the flux cored arc welding process. Because the test data obtained from the control specimen would be compared to the test data obtained from previous tests on stiffener details fabricated with quality welds, it was important for the control specimen to be fabricated with quality welds. Hence, the fabricator was instructed to use fabrication techniques and workmanship conforming to the requirements of the ANSI/AASHTO/AWS D1.5 Bridge Welding Code. A typical welded joint made on the control specimen is shown in Figure 63.

The two remaining test specimens were fabricated in the testing laboratory. The completed control specimen along with two 20-ft long W14x43 plain rolled steel beams without stiffeners were transported on a trailer from the steel fabrication shop to the testing laboratory. The steel beams obtained from the fabricator were used to make the two remaining test specimens. Additionally, several feet of 3-in. by 3/8-in. flat plate stock needed for fabricating the test specimens were obtained from a local steel supplier, and the welding materials needed for fabricating the test specimens were obtained from a local materials distributor.
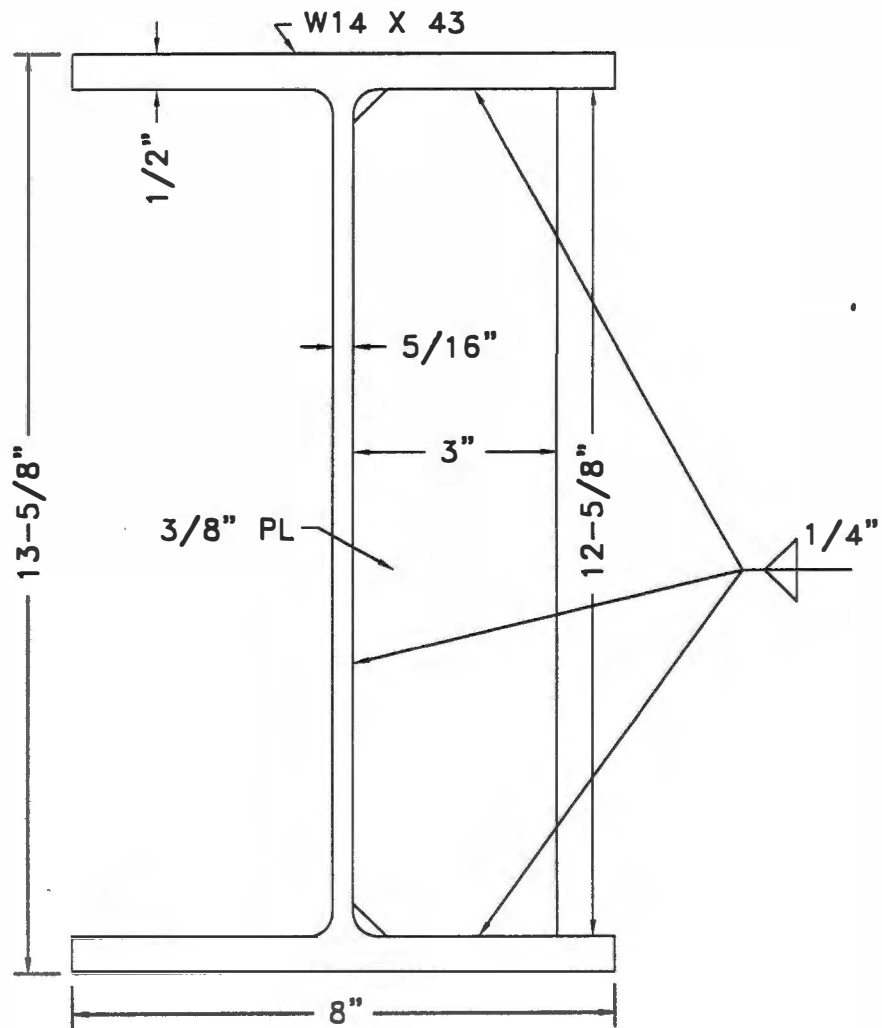
Figure 62. Cross Section of a Typical Test Specimen
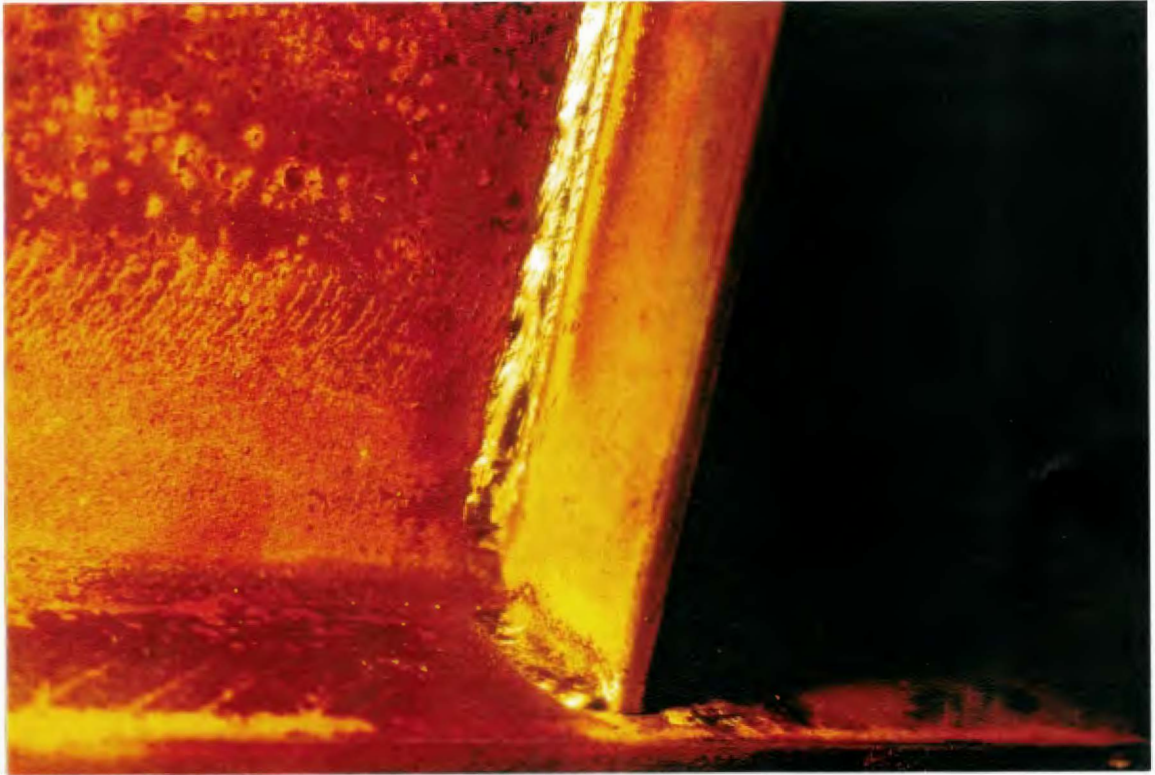
Figure 63. A Typical Welded Joint on the Control Specimen

104

Stiffeners for the two remaining test specimens were fabricated from the 3-in. by 3/8-in. flat plate stock. A bandsaw was used to cut the plate into stiffeners that would fit between the top and bottom flanges of each beam. In addition, the corners on the stiffener plates adjacent to the web of each beam were cut at a 3/4-in. by 3/4-in. diagonal. This allowed the stiffeners to be placed against the web of each beam without interference from the rounded fillets occurring at the intersections of the web and flanges. Using a bench grinder, the top and bottom edges of the stiffener plates were ground slightly, allowing them to fit firmly against the web and flanges of each beam.

After fabricating the stiffener plates, they were located along the two 20-ft long plain rolled beams. The stiffener locations were measured from the midpoint of each beam outward. The locations were identified along the bottom flange of each beam using a punch and a colored marker. The stiffener plates were made square with the web and flanges of each beam using a framing square and a carpenter's level.

When the stiffener plates were in place, they were secured by welding both sides of the plates to the web and flanges of each beam. The welds were manually produced using the shielded metal arc welding (SMAW) process. Figure 64 shows the welding equipment used alongside one of the test specimens being welded. As shown in Figure 64, welding was performed while the webs of the beams were in an upright position. Welding was performed with the beams in this position to simulate field welding a girder detail on an existing steel bridge. The power source used for welding was operated at 200 amps of alternating current, and the electrodes used for welding were 1/8-in. diameter E6011 rods. The electrodes were left exposed to the laboratory environment for several days prior to welding.

To properly represent the field welds being evaluated, the welding performed on the two specimens fabricated in the laboratory was to be sufficiently poor as to produce

Figure 64. Welding a Test Specimen

substandard welds. Poor quality welds containing excessive discontinuities were obtained by simply using substandard welding techniques. Electrodes were left exposed to the laboratory environment for several days prior to welding to allow the flux to absorb moisture from the atmosphere. Welding with excessive arc current and with electrodes high in hydrogen content aided in producing substandard welds. The failure to preheat also encouraged welds with poor quality. Furthermore, the laboratory technician responsible for welding the details was instructed to produce poor quality welds by moving the electrode in and out at several locations. Manipulating the electrode in this manner was intended to simulate the movement that would occur while welding to a bridge with traffic present. The combination of poor welding techniques employed resulted in welds with excessive discontinuities. A typical welded joint made on one of the test specimens fabricated in the laboratory is shown in Figure 65.

On one of the test specimens fabricated with poor quality welds, an attempt was made to repair a welded joint at one of the stiffener details. The stiffener detail selected was located closest to the midpoint of the beam where stress range would be the highest. Furthermore, the welded joint selected was located at the intersection of the stiffener plate and the tension flange of the beam, where obvious undercut was present in the flange. Repair was accomplished by grinding along the fillet welds joining both sides of the stiffener plate to the tension flange. Both weld material and flange material were reduced by grinding until undercut was removed and a smooth transition was obtained. This helped to minimize stress concentrations and reduce weld discontinuities. By grinding, the flange thickness was reduced by a maximum of 0.044 in. The ground joint is shown in Figure 66. Grinding was performed using both a rotary burr grinder and a small disc grinder. The pneumatically powered rotary burr grinder was used to quickly remove the majority of unwanted material. The electrically powered
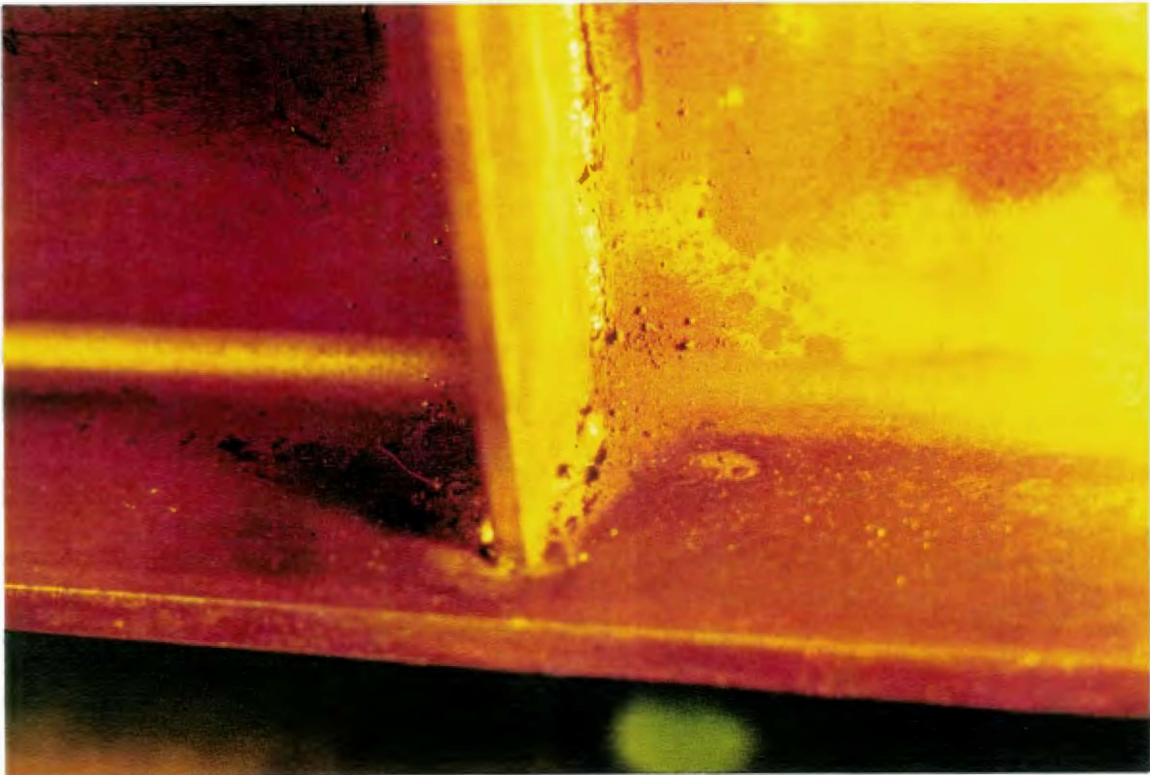
Figure 65. A Typical Welded Joint with Substandard Welds

Figure 66. Repaired Joint

disc grinder was used to smooth out scratches left by the rotary burr grinder. Completely grinding the welded joint took approximately 15 minutes.

Before testing, the three specimens were fitted with strain gages so that actual stress ranges could be determined. Strain gages were placed along the inside of the tension flange of each beam. More specifically, strain gages were placed approximately 4 in. away from the stiffener details and approximately 1 in. from the edges of the tension flange. The strain gages were placed on each side of the tension flange. The diagram in Figure 67 shows the strain gage configuration at a stiffener detail.

3.4.2 Fatigue Test Apparatus

All specimens were tested on simple supports. The rotational freedom of the simple supports was provided by a cylindrical roller trapped between two thick plates. The plates were rounded to accommodate the cylindrical roller. The rounded plates and the cylindrical roller were thoroughly coated with grease to reduce friction. To prevent unwanted movement of the test specimen, threaded fasteners held the specimen firmly against the simple supports. Figure 68 shows a side view of the simple supports. All specimens were tested on an 18 ft span with two-point loading where the distance between the load points was 5 ft. The load configuration is shown in Figure 69. At the load points, rotational freedom was allowed by a rotational mechanism similar to that used on the simple supports.

Loads were applied by a hydraulic actuator and were distributed to the two locations on the test specimens through a spreader beam. The servo-controlled hydraulic actuator operated between 0.6 and 2.7 cycles of load application per second with a maximum capacity of 50 kips. The servos were commanded by an electronic control unit near the test site, and the actuator was activated by a hydraulic pump located beyond the test site. The hydraulic actuator was supported above by a steel

110
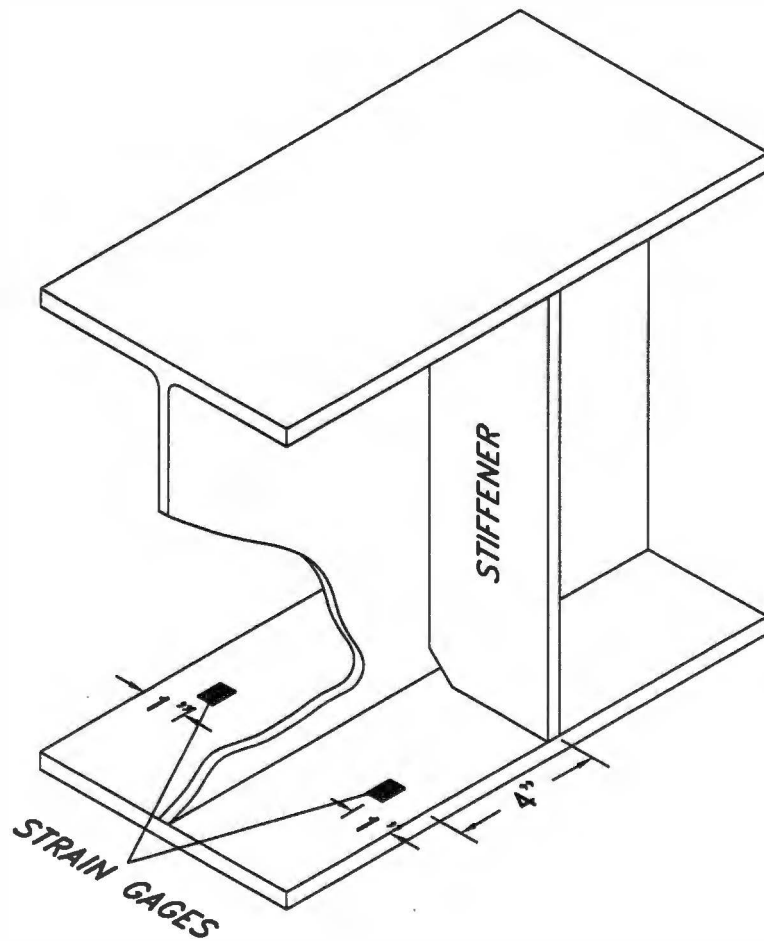
Figure 67. Strain Gage Configuration on Test Specimen
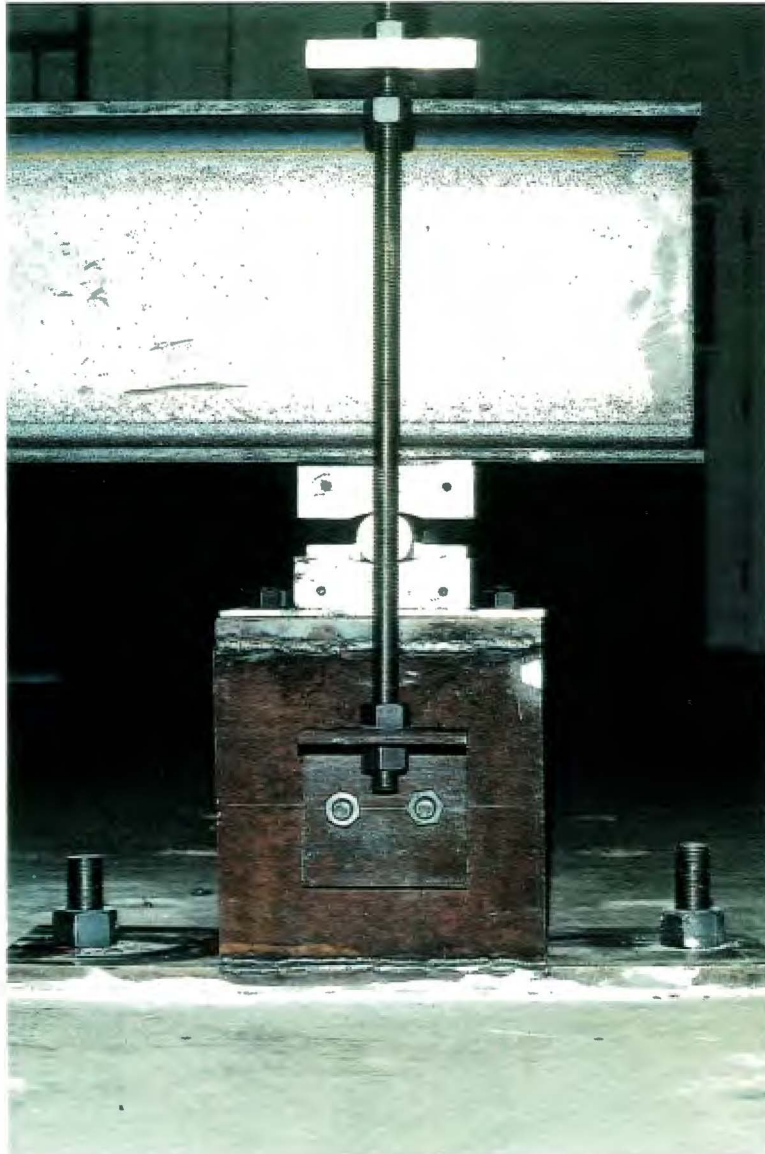
Figure 68. Simple Support
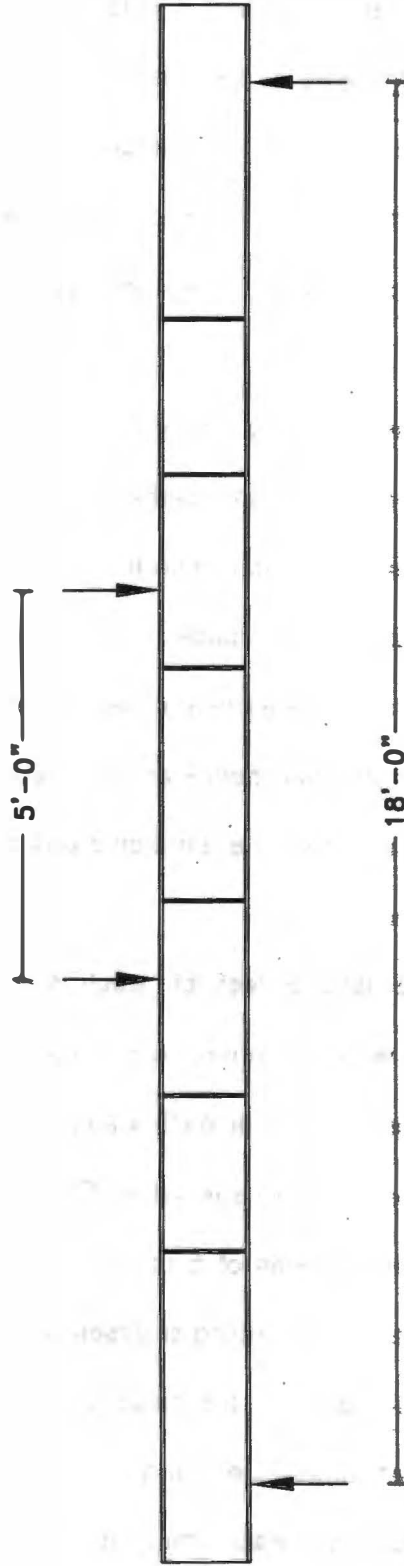
Figure 69. Load Configuration on Test Specimen

5'-0"

18'-0"

frame. The frame and the simple supports were securely fastened to a reinforced concrete reaction floor. For safety, side rollers attached to the columns of the frame were positioned against the web of the spreader beam to prevent possible buckling. The test setup is shown in Figure 70. All components of the test setup such as the test frame, the simple supports, and the spreader beam were designed to withstand the numerous load cycles required to fatigue test the three specimens.

3.4.3 Test Procedures

Each test specimen was carried from the fabrication site to the test site and manipulated at the test site with an overhead crane. The manual controls on the overhead crane allowed each test specimen to be carefully placed into position without harming the stiffener details or strain gages. With a test specimen positioned between the simple supports and the spreader beam, the web of the test specimen was carefully aligned with the center of the load points and all restraining fasteners were tightened. Once the specimen was secured, the electronic unit commanding the servos and the hydraulic pump was powered.

Before beginning the fatigue test on each specimen, a static load test was performed. These tests were performed while monitoring the strain gages along the tension flange of each specimen. For each static load test, the load was increased by increments of 5 to 10 kips up to a peak value. Once the peak value was reached, the load was decreased by increments of 5 to 10 kips. Strains were recorded for each increment of load and the corresponding stresses were calculated. To determine if the test specimen was properly aligned, the actual stresses occurring in the test specimen were compared to theoretical stresses, and the strains occurring on each side of the tension flange were compared to each other. If improper alignment was suspected, the test specimen was simply adjusted until favorable strains were measured.

Figure 70. Test Setup

On occasion, the fatigue test was stopped, and the static load test was performed while monitoring the strain gages. This was done to determine if the test specimen needed readjusting. After adjustment, the fatigue test was continued.

Fatigue testing was performed on the three test specimens starting with the control specimen. For all test specimens, the load applied was constant amplitude cyclic loading without stress reversal. The load applied through the hydraulic actuator was compressive, causing the bottom flange of the test specimens to experience tension at all times. The stress range at the stiffener-to-tension flange weld was the controlling variable for all fatigue tests. A counter on the electronic control unit recorded the total number of load cycles each test specimen experienced. Fatigue testing on each specimen continued until a crack occurring at stiffener detail reduced beam stiffness and allowed for relatively large deflections. The electronic control unit stopped the hydraulic pump when internal circuitry sensed the large displacements of the hydraulic actuator. After each crack, the stress range at the stiffener-to-tension flange weld and the total number of load cycles to failure were recorded.

After failure, the cracked flange was repaired so that fatigue testing could be continued to obtain cracks at other stiffener locations. The repairs were accomplished by splicing across the cracked region. Splice plates with a thickness of 3/8-in. were bolted above and below the tension flange with 3/4-in. diameter A325 bolts. The bolts were accommodated by drilling holes through the tension flange and splice plates. Because of the nature of the fatigue loading, the splice plate details were designed as slip-critical connections requiring several bolts on each side of a crack. A typical splice plate detail is shown in Figure 71.

Figure 71. Splice Plate Detail

3.4.4 Laboratory Test Results

The data acquired from fatigue testing the three specimens included the total number of load cycles, N, each stiffener detail sustained until failure and the corresponding stress range, S_r, occurring at each of the failed stiffener details. The stress range was calculated at the fillet weld joining the stiffener to the tension flange. The simple bending stress formula from strength of materials was used to calculate stress ranges.

$$\sigma = \frac{My}{I}$$

where σ = stress; M = moment; y = distance from neutral axis to stressed fiber; and I = moment of inertia.

Stress range values calculated from the bending stress formula were validated by comparing them to stress range values calculated from strain gage readings. As previously discussed, strain gages were monitored while performing static load tests. For all test specimens, the stress range values calculated from strain gage readings varied less than 3.8 percent from the stress range values calculated from the bending stress formula. It is therefore reasonable to assume that the stress range values calculated from the bending stress formula are reliable. In addition, strains recorded near opposite edges of the tension flange at the same locations along the span varied less than 3.7 percent for all test specimens. Hence, twisting of the test specimens was minor and torsion need not be considered. These results were observed throughout the fatigue tests.

All failures occurring in the fatigue tests were the result of a crack initiating and growing adjacent to the fillet weld joining the stiffener to the tension flange. A typical failure is shown in Figure 72. Beams reached the end of their fatigue life when the crack had destroyed most of the tension flange and deflections had become large. Some of
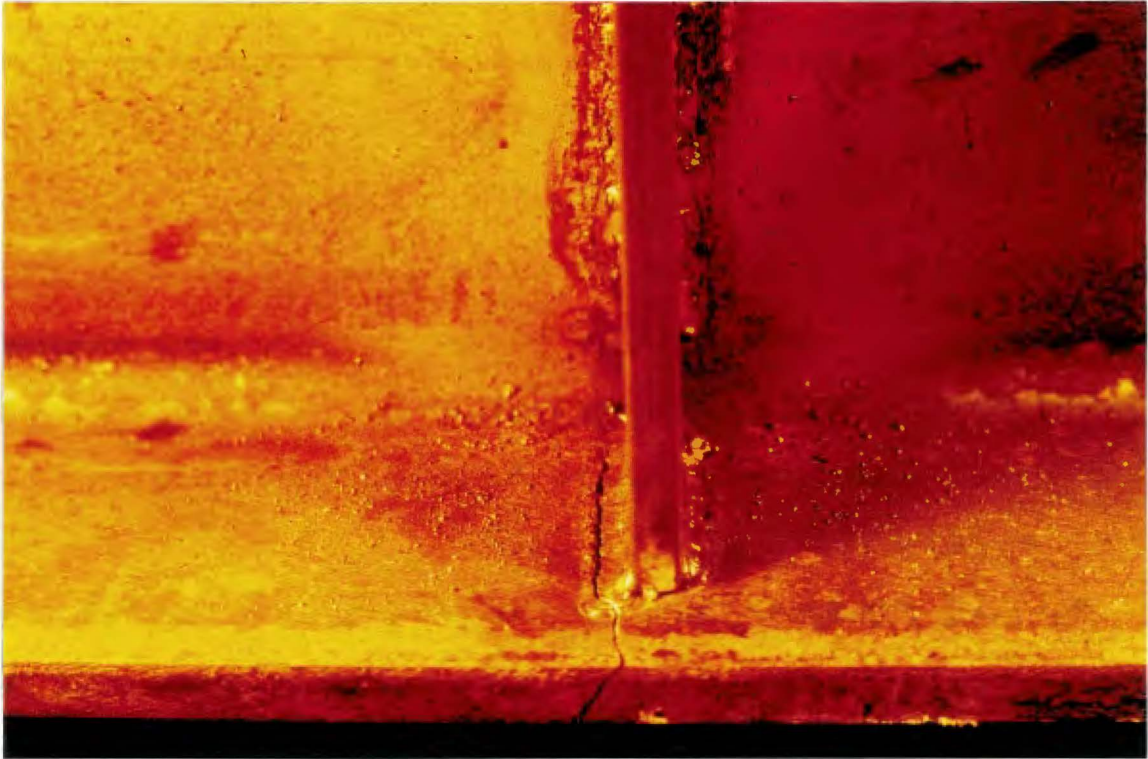
Figure 72. A Typical Crack at a Stiffener Detail

the cracks propagated up into the web of the test specimens. A typical crack starting from a surface discontinuity at the toe of the fillet weld is shown in Figure 73. The cross-sectional view presented in Figure 73 is for a typical stiffener detail on a test specimen fabricated with substandard welds. The region where slow growth prevailed over a large portion of the life is apparent from the smooth fracture appearance [Fisher et al., 1974].

The load cycles to failure and the stress range data obtained from each test specimen are shown in Table 4. The results for the control specimen are in close agreement with those presented by Fisher et al. [1974]. Recalling from an earlier discussion, data were accumulated by Fisher et al. in numerous tests examining the fatigue strength of stiffener details. In Figure 74, the data obtained from fatigue testing the control specimen is compared to the curve generated from a linear regression analysis of Fisher's data. The close agreement between the results for the control specimen and Fisher's results indicates the reliability of the test setup and the test procedures followed in this study.

The results obtained from fatigue testing the stiffener details fabricated with poor quality welds are presented in Figure 75. Included in Figure 75 are the data points, the curve generated from a linear regression analysis of the data, and the lower bound curve derived from the approximate 95 percent confidence limit for the data. The fatigue limit for the stiffener details with substandard welds was not clearly defined; however, one stiffener detail sustained over 4.9 million load cycles at a stress range of 13.2 ksi without failure or visible crack growth. Fatigue testing of the specimen containing this stiffener detail was stopped as a result of fatigue cracks occurring elsewhere along the span.

In Figure 76, the data for the stiffener details having poor weld quality are plotted along with the AASHTO fatigue curves for Category C and D details. Also shown in

120
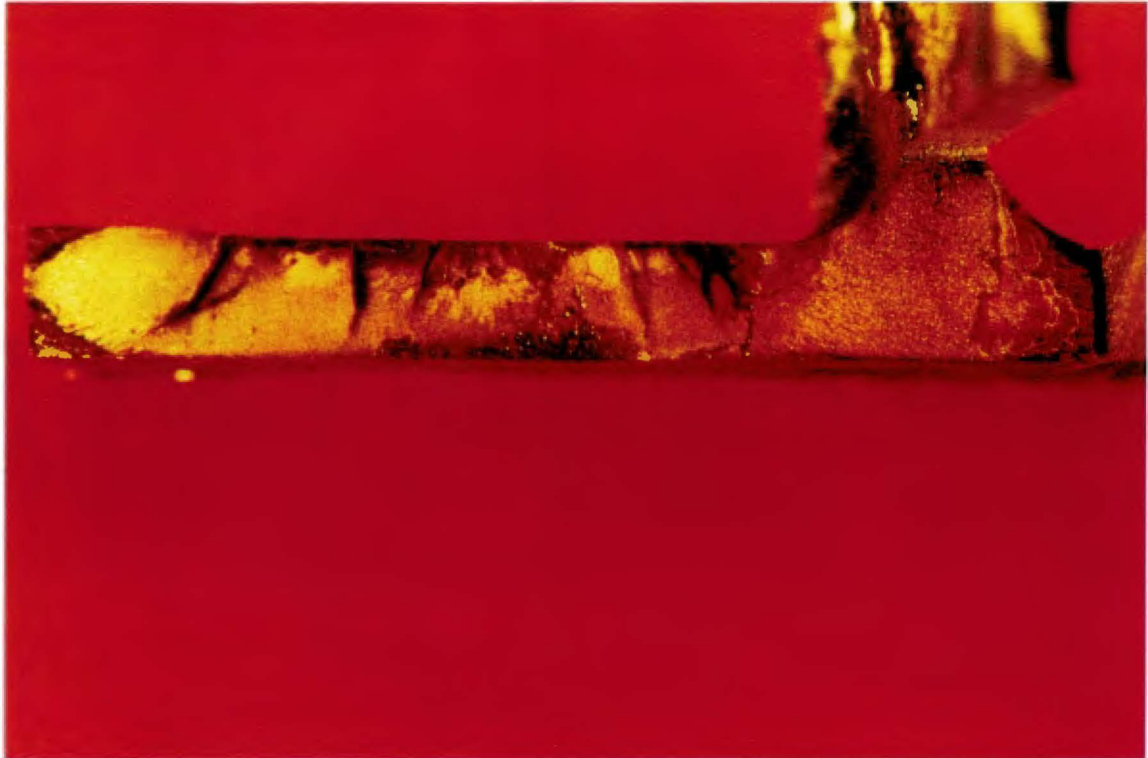
Figure 73. Crack Surface at a Stiffener Detail

Table 4. Fatigue Test Data

Specimen No.	Stress Range, S_r (ksi)	Cycles to Failure, N
1-control	27.6	322,510
	27.6	332,410
	21.2	828,170
	21.2	842,630
2	27.6	59,260
	27.6	80,320
	21.2	104,650
	21.2	549,150
	12.7	2,105,650
3	17.2	625,700
	17.2	625,700
	13.2	2,201,510
	13.2	4,964,770*

*No failure.

The graph shows axes labeled "Stress Range, S_r (ksi)" on the vertical axis (ranging from 10 to 40) and "Cycles to Failure, N" on the horizontal axis (ranging from 10^4 to 10^7).

$$\log N = 10.595 - 3.505 \cdot \log S_r$$
(regression line from Fisher et al.)
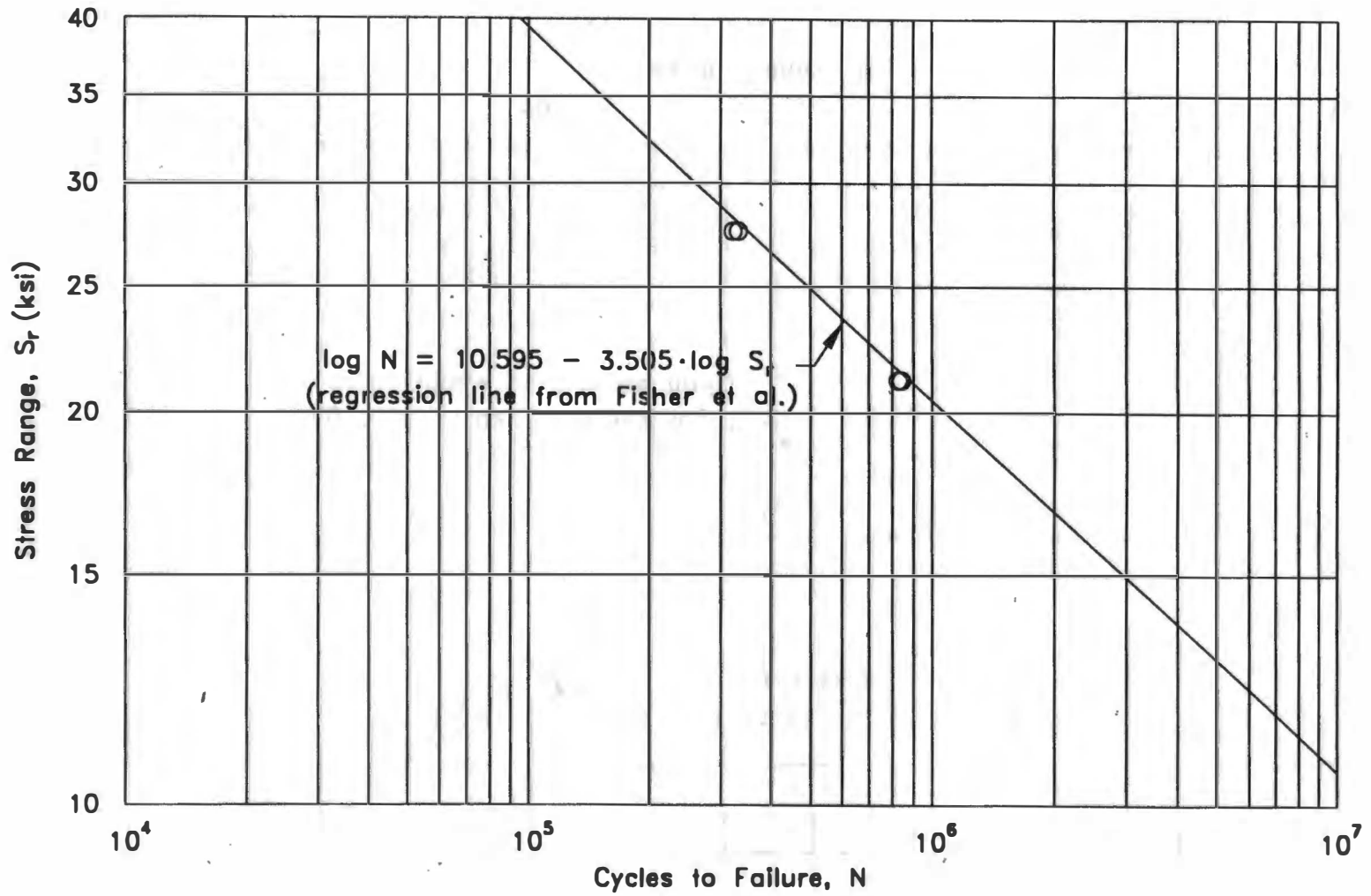
Figure 74. Comparison of Control Specimen Test Data and Fatigue Curve
Generated by Fisher et al.
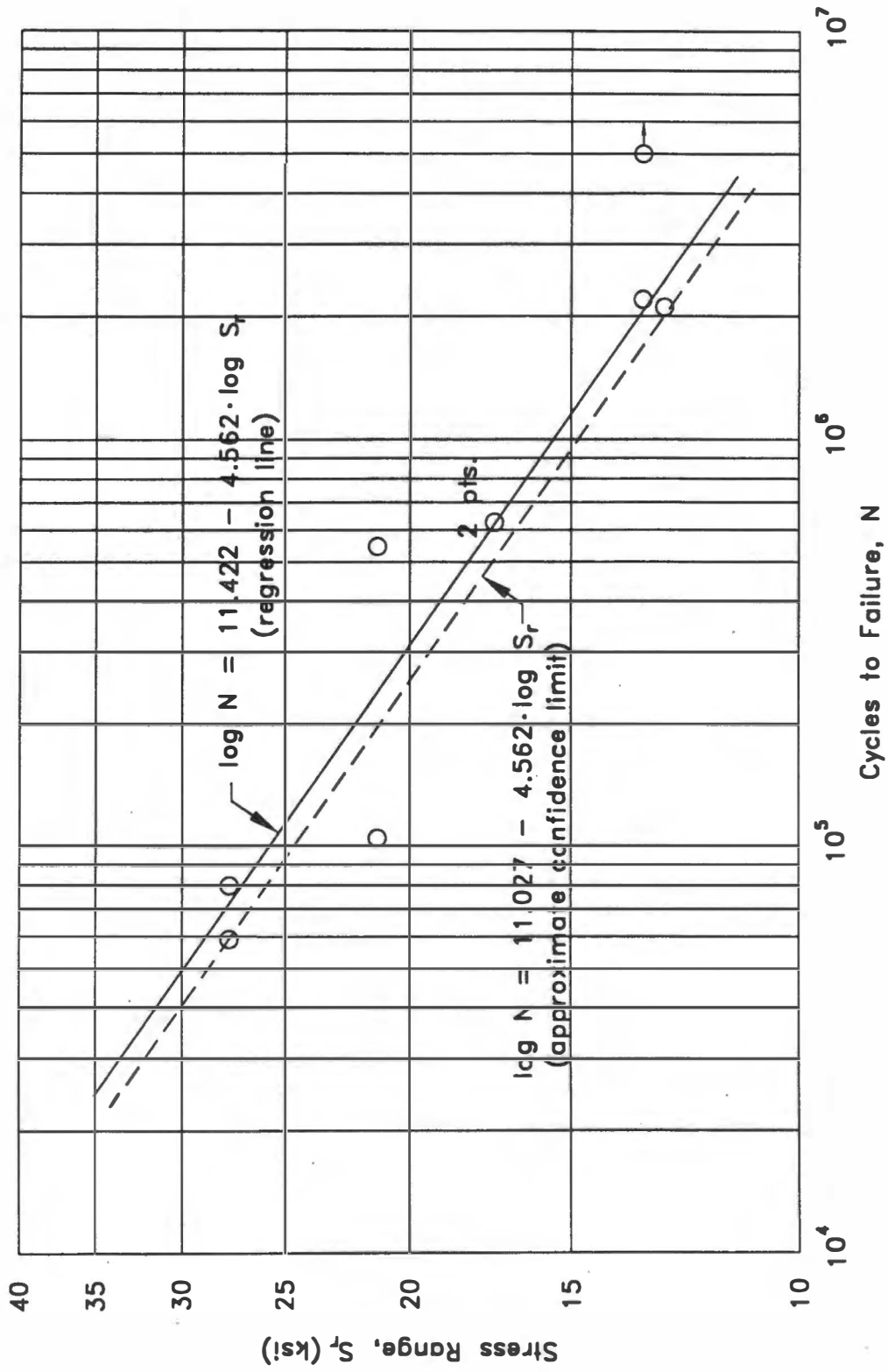
Figure 75. Test Data for Stiffener Details With Substandard Welds

124
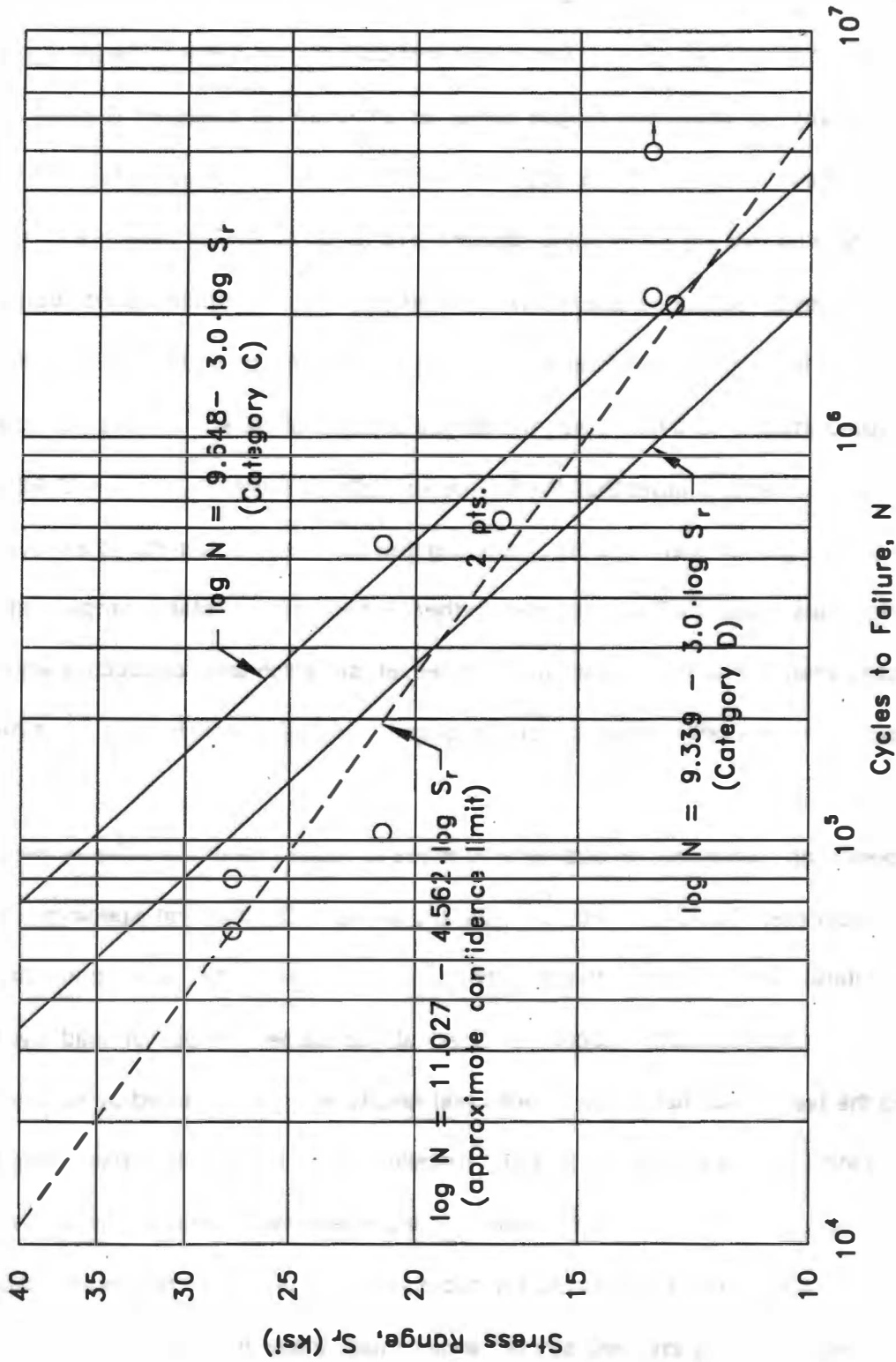
Figure 76. Comparison of Test Data to AASHTO Fatigue Curves

125

Figure 76 is the lower bound fatigue curve derived from the approximate 95 percent confidence limit for the test data. Most of the test data for the stiffener details having poor weld quality fall below the fatigue curve for an AASHTO Category C detail. In further comparison, the slope of the fatigue curve for the stiffener details with poor weld quality is 4.56 whereas the slope of the fatigue curve for an AASHTO Category C detail is 3.0. The lower bound fatigue curve derived from the approximate 95 percent confidence limit for the test data intersects the fatigue curve for an AASHTO Category C detail at approximately 12.0 ksi. Thus, the fatigue strength of stiffener details fabricated with substandard welds is lower than the fatigue strength of AASHTO Category C details at stress ranges greater than 12.0 ksi. Recalling that the lowest stress range examined in the fatigue tests was 12.7 ksi indicates further testing at lower stress ranges would help to completely define the fatigue curve. However, since the tests conducted appear to be approaching the fatigue limit, the time required to completely define the curve may be excessive.

As previously discussed, an attempt was made to repair one of the stiffener details on a test specimen fabricated with substandard welds. On this test specimen, the repaired stiffener detail and one other stiffener detail experienced the same stress range of 17.2 ksi. Ironically, both specimens failed at the same number of load cycles indicating the repair was ineffective. These test results may be explained by relying on an investigation by Gregory et al. [1989]. Recalling from earlier discussion, Gregory conducted fatigue tests on stiffener details that were repaired by rotary burr and disc grinding. Although Gregory obtained favorable results showing increases in fatigue strength, Gregory's tests involved stress ranges much lower than 17.2 ksi. Thus, it seems reasonable to assume the repairs on the test specimen would have been more effective on a stiffener detail subjected to a lower stress range.

3.5 Fatigue Life Estimation

In this section two different approaches are used to estimate the remaining fatigue life of the U.S. 69 bridge. In the first approach, applied stress range and number of cycles are based on field measurements made under normal traffic. In the second approach, the stress range is obtained by analyzing the bridge under the AASHTO fatigue truck and the number of cycles is based on the estimated traffic volume.

In both approaches, the computed fatigue life is based on the results of the fatigue tests on stiffener details fabricated with substandard welds. In Figure 75, the curve generated from a linear regression analysis of the fatigue test data, and the lower bound curve derived from the approximate 95 percent confidence limit for the fatigue test data are presented. The logarithmic equations defining these curves are also presented in Figure 75. The slope and intercept values shown in these equations are used below to calculate the remaining fatigue life of the U.S. 69 bridge.

3.5.1 Effective Stress Range From Normal Traffic

The remaining fatigue life calculation for the U.S. 69 bridge follows from the fatigue evaluation procedures presented in Section 2.5. The procedures in Section 2.5 may be used to calculate either remaining mean life or remaining safe life. The remaining mean life calculation for the U.S. 69 bridge uses the mean curve which is equivalent to the fatigue curve generated from the linear regression analysis of the test data shown in Figure 75. The remaining safe life calculation for the U.S. 69 bridge uses the allowable curve which is equivalent to the lower bound fatigue curve derived from the approximate 95 percent confidence limit for the test data shown in Figure 75. As given in Section 2.5, remaining mean life and remaining safe life are calculated from Equation 2.1.

127

$$Y_f = \frac{f\,K \times 10^6}{T_a C (R_s S_r)^b} - a$$

The effective stress range, S_n, at specific locations along the bridge is calculated from stress range histograms. Stress range histograms were obtained from field measurements on the bridge under normal traffic. The highest effective stress range measured on the U.S. 69 bridge was 0.96 ksi. This effective stress range occurred in girder 7 (Figure 1), which was not a girder involved in the bridge widening. The next highest effective stress range of 0.95 ksi occurred in girder 9, which was subjected to substandard field welds.

The grid analysis indicates that, of the girders subjected to substandard welds, girder 9 is expected to support the greatest positive moment range for the truck position limited to the driving lanes. Girder 10 supports a greater moment if the truck is allowed on the outer shoulder, but it is reasonable to assume that the number of cycles involved in this type of loading will be low. The maximum moment in girder 9 occurs in the first span of the three span unit; but since the section modulus is higher in the first span, the maximum stress occurs in the middle span. As a result, the critical stress range for estimating the fatigue life of the bridge is the measured 0.95 ksi stress range.

The effective stress range is computed from all of the stress cycles applied at a point on the bridge, including the minor vibration cycles. Therefore, the number of cycles used in the fatigue life estimate should be based on this total cycle count rather than the average daily truck traffic. The number of cycles per hour associated with the 0.95 ksi effective stress range is 513. The resulting number of cycles per day is 12,312.

Although the fatigue limit is not defined in this research, it is expected that 0.95 ksi is below the limit for the detail of concern. However, it will not be automatically assumed that the detail has infinite life. Research has shown [Fisher et al., 1983; Zwerneman et

al., 1988] that if any stress cycles applied to the bridge are above the threshold, all of the cycles will be damaging. Since the substandard welding has reduced the threshold and it is possible that a future stress range will exceed the 5.9 ksi stress range measured, all cycles must be assumed damaging.

The number of cycles counted above is based on the present average daily truck volume. It is expected that truck traffic will increase with time, causing the number of cycles per day to increase. In Section 2.5.5 of this report a procedure [Moses et al., 1987] is presented for computing the lifetime average daily truck volume from the present average daily truck volume. The same procedure will be used here to compute the lifetime average cycles per day from the present cycles per day.

The annual growth rate is determined from Table 3. For a rural U.S. route such as U.S. 69, the growth rate value is 2.87 percent. This value is rounded up making the annual growth rate, $g = 3.0$. The U.S. 69 bridge was originally constructed in 1963 making the present age of the bridge, $a = 32$ years. Applying the values determined for T, g, and a to Figure 6 gives a truck volume ratio (T_a/T) of approximately 1.2 and a lifetime average cycle count of approximately 14,774 cycles per day.

To determine the remaining safe life, the reliability factor, R_s, is calculated from Equation 2.3,

$$R_s = R_{so} (F_{s1})(F_{s2})(F_{s3})$$

Because the effective stress range, S_r, was determined from stress-range histograms, $F_{s1} = 0.85$ and $F_{s2} = F_{s3} = 1.0$. Since the most critical stiffener detail is attached to a redundant member, $R_{so} = 1.35$. Substituting these values into Equation 2.3,

$$R_s = 1.35 (0.85)(1.0)(1.0) = 1.15$$

To determine the remaining mean life, the reliability factor, $R_s = 1.0$

The fatigue curve constants (K, b, and f) are obtained from the fatigue curves presented in Figure 75. From Figure 75, the equation defining the lower bound curve derived from the approximate 95 percent confidence limit for the test data is given in the form of Equation 2.5:

$$\log N = \log A - b \cdot \log S_r$$

where log A has a value of 11.027, and A has a value of 1.064 X 10^{11}. Using the intercept, A, the fatigue curve constant K is calculated from Equation 2.6:

$$K = \frac{A}{365 \times 10^6} = \frac{1.064 \times 10^{11}}{365 \times 10^6} = 292$$

Also from Figure 75, the slope b has a value of 4.562.

To compute the remaining safe life, $f = 1.0$. To compute the remaining mean life, $f =$ the ratio of the mean curve intercept, A', and the allowable curve intercept, A. As discussed above, the mean curve and the allowable curve are the curves shown in Figure 75. The intercept A' for the mean curve has a value of 2.642 X 10^{11}. Thus, the ratio, f, used to compute the remaining mean life is determined as

$$f = \frac{2.642 \times 10^{11}}{1.064 \times 10^{11}} = 2.48$$

The final step in the fatigue evaluation procedures is to calculate the remaining mean life and the remaining safe life. The variables determined above for the U.S. 69 bridge are substituted into Equation 2.1:

$$Y_f = \frac{f K \times 10^6}{T_a C (R_s S_r)^b} - a$$

The remaining safe life is

$$Y_f = \frac{1.0 \cdot 292 \times 10^6}{14{,}774 \cdot 1.0 (1.15 \cdot 0.96)^{4.562}} - 32 = 12{,}553 \text{ years}$$

The remaining mean life is

$$Y_f = \frac{2.48 \cdot 292 \times 10^6}{14,774 \cdot 1.0(1.0 \cdot 0.96)^{4.562}} - 32 = 59,017 \text{ years}$$

From the calculations above, it is clear that the remaining fatigue life of the U.S. 69 bridge crossing the South Canadian River far exceeds the design life. For comparison, when the remaining safe life of the U.S. 69 bridge is calculated using the allowable stress range curves for AASHTO Category C, D, and E details, the results are 581 years, 269 years, and 116 years, respectively. Furthermore, if the remaining safe life desired is 100 years, the stress range allowed on the U.S. 69 bridge at the most critical detail is 2.61 ksi based on the laboratory curve and 1.26 ksi based on the AASHTO Category D fatigue curve. Fatigue lives based on AASHTO curves are less than the fatigue life based on the laboratory curve because the AASHTO curves fall below the laboratory curve at low stress ranges.

3.5.2 Stress Range From Fatigue Truck

Remaining fatigue life can also be estimated using the stress range computed for the AASHTO fatigue truck loading and the number of cycles based on an estimate of the average daily truck volume for the life of the bridge. Since the analysis is static and the small vibrational cycles are not present, the computed stress range (based on the one major cycle produced by the fatigue truck) will be greater than the measured effective stress range (based on a weighted average of all cycles). However, the higher computed stress range will be countered by a lower number of cycles.

The grid model used for comparisons to field measurements can again be used to compute stresses, with the fatigue truck replacing the dump truck. The results of the analyses are shown in Figure 77. From previous calculations, it is known that the critical location is girder 9 at the crossframe 40 ft north of pier 1. The stress at this point varies
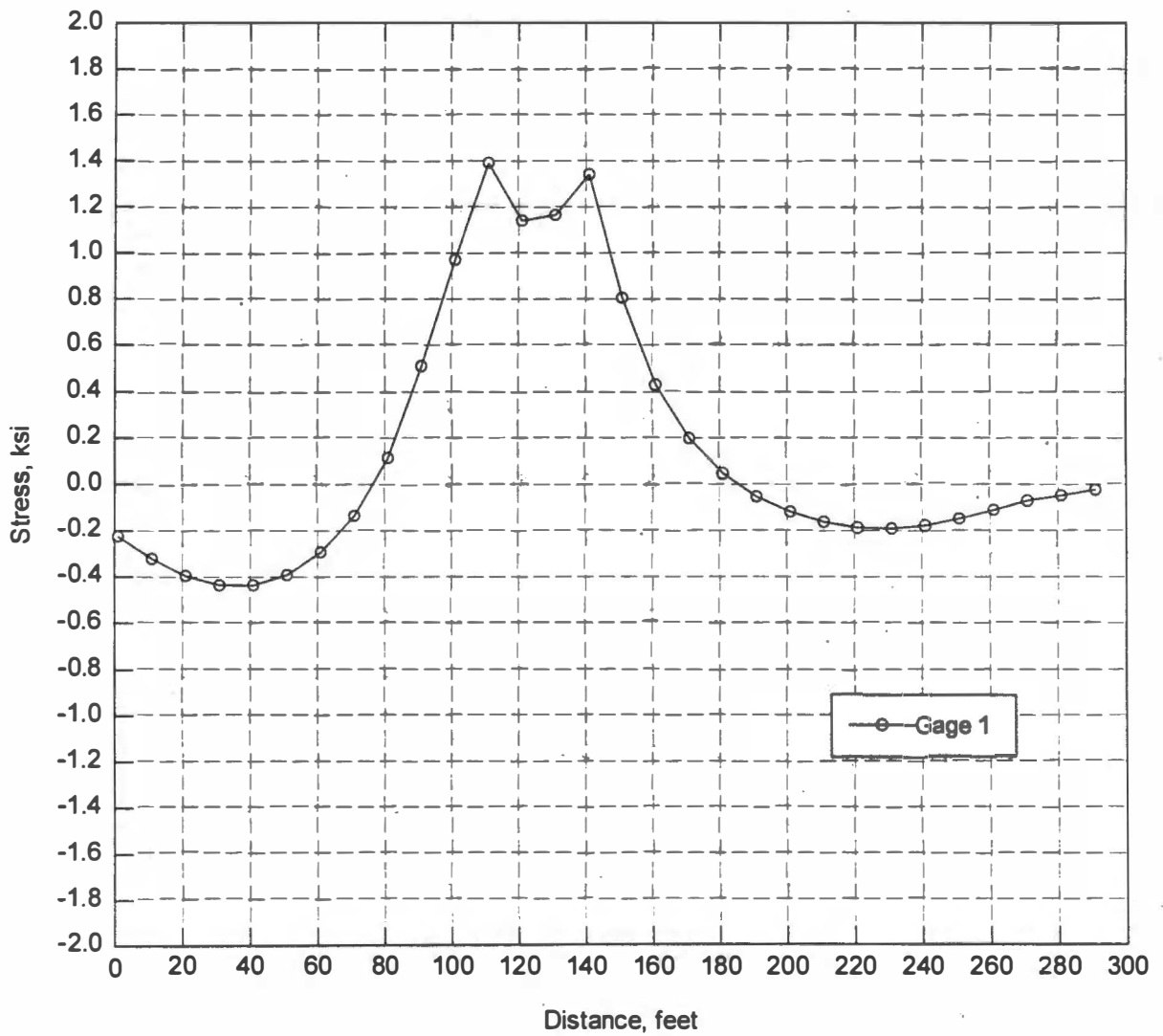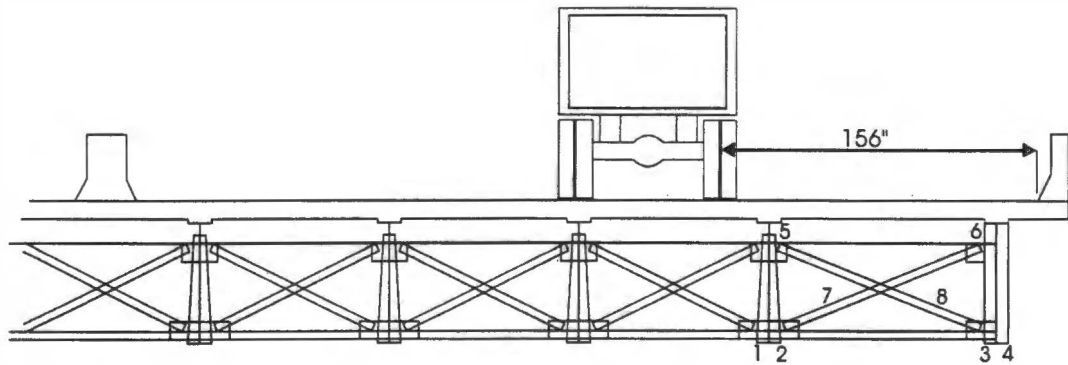
Figure 77. Fatigue Truck Moving in Right Lane, Grid Analysis at Group 3 Location

from 0.44 ksi compressive to 1.39 ksi tensile, resulting in a total stress range of 1.83 ksi. In the fatigue life computation, this stress range is increased by 10 percent to account for impact [Moses et al., 1987].

As discussed in Section 2.5.5, the lifetime average daily truck volume, T_a, is determined from the present average daily truck volume in the outer lane, T, the annual growth rate, g, and the present age of the bridge, a. The present average daily truck volume in the outer lane, T, is calculated from Equation 2.7,

$$T = (ADT) \, F_T F_L$$

According to bridge design data provided by ODOT, the present average daily traffic volume on the bridge is 9700 vehicles per day. Since U.S. 69 is a rural highway supporting 2-way traffic in 4 lanes, the fraction of trucks in the traffic, F_T, has a value of 0.15, and the fraction of trucks in the outer lane, F_L, has a value of 0.45. These values are substituted into Equation 2.7:

$$T = (ADT) \, F_T F_L = (9700)(0.15)(0.45) = 655 \text{ trucks per day}$$

As shown in the preceding section, the truck volume ratio (T_a/T) is approximately 1.2, making the lifetime average truck volume, T_a, equal to approximately 786 trucks per day.

The number of stress cycles per truck passage, C, is determined as shown in Section 2.5.3. The U.S. 69 bridge consists of continuous girders with spans greater than 40 ft. Thus, the stress cycles per truck passage, C, has a value of 1.0. Based on one cycle per truck passage and a lifetime average truck volume of 786 trucks per day, it is expected that the bridge will see 21,520,000 cycles in a 75-year life. This compares favorably with a typical 10,000,000 to 150,000,000 cycles in a bridge lifetime [Moses et al., 1987].

The reliability factor for computing remaining safe life will be different from that used in the preceding section because, in this section, stresses are computed rather than

measured. Since the AASHTO fatigue truck is used for loading and stresses are computed, $F_{s1} = F_{s2} = 1.0$; $F_{s3} = 0.96$ because lateral load distribution is based on a grid analysis rather than approximate tabular values or parametric equations. $R_{so} = 1.35$ as before since the member under investigation remains a redundant member. Substituting the above values into Equation 2.3:

$$R_s = (1.35)(1.0)(1.0)(0.96) = 1.30$$

To compute remaining mean life, $R_s = 1.0$.

Fatigue curve constants are the same as in the preceding section. That is $K = 292$, $b = 4.562$, $f = 1.0$ for remaining safe life, and $f = 2.48$ for remaining mean life. Substituting into Equation 2.1, the remaining safe life is $Y_f = 4,613$ years and the remaining mean life is $Y_f = 37,868$ years. This result reinforces the results presented in the preceding section. The remaining fatigue life of the U.S. 69 bridge crossing the South Canadian River far exceeds the design life.

CHAPTER 4

SUMMARY AND CONCLUSIONS

Field tests and computer-aided analyses were conducted on the U.S. 69 bridge crossing the South Canadian River on the western side of Lake Eufaula. Field tests were conducted in two parts. The first part involved measuring strains in girders and crossframes as a truck of known weight traveled along the bridge. The second part involved measuring strains and counting strain cycles under normal traffic for a two-week period. Results of the first part of the field tests were used primarily to calibrate the analytical model. Results of the second part were used to compute an effective stress range for estimating bridge life.

Based on measured strains, the known truck produced a maximum stress range of 1.9 ksi at the critical location on the bridge. This value is low, but is comparable to results reported by other researchers conducting measurements on highway bridges. The maximum effective stress range at the critical location was found to be 0.95 ksi at a current average cycle volume of 12,312 per day.

The bridge was modeled analytically using both a grid and three-dimensional finite elements. Results of both the grid analyses and the finite element analyses closely match field measurements. The grid analyses indicate a maximum stress range of 2.1 ksi at the critical location on the bridge while the finite element analyses indicated a maximum stress range of 1.4 ksi at the same location.

In addition to the field tests and analytical modeling, laboratory fatigue tests were conducted to determine the fatigue life of the critical detail. The tests showed that the

135

details performed at below the AASHTO Category D level for stress ranges above 20 ksi, but above an extension of the Category D curve for stress ranges below 20 ksi. It should be noted, however, that previous research has shown the fatigue limit to be approximately 14 ksi for details similar to the one tested here. As a result of the poor welding procedures employed in fabricating the current specimens, failures did occur at stress ranges below 14 ksi. Repairing the weld by smoothing the transition between the stiffener and the flange did not improve the performance, but the repair was only tested at a relatively high stress range.

Two different techniques, employing combinations of field measurements, analytical results, and laboratory data, were used to estimate the fatigue life of the U.S. 69 bridge. Based on these estimates, it is concluded that, for all practical purposes, the fatigue life of the bridge is infinite.

This conclusion is not intended to promote or excuse the poor welding practice employed on the subject bridge. It should be recalled that approximately two years and tens of thousands of dollars were spent in arriving at this conclusion. It would have been much simpler and cheaper to employ proper welding procedures as specified on the project drawings. It should also be understood that the same conclusion does not extend to all bridges. If the lateral load distribution system had been less effective, it may have been necessary to undertake extensive repairs.

Metal fatigue is not an imagined problem; numerous bridge failures and closings have occurred as a result of fatigue, and the fatigue problem is always the result of poor detailing or fabrication practice. Poor detailing and fabrication can be excused in bridges erected more than 30 years ago, before the fatigue problem was well documented, but there can be no good reason for such poor welding practice to occur on new construction.

REFERENCES

American Association of State Highway and Transportation Officials. *Standard Specifications for Highway Bridges.* 15th Ed. Washington, DC, 1992.

American Welding Society. *Welding Technology*, Welding Handbook Vol. 1, 8th Ed. Miami, FL. 1987.

American Welding Society. *Structural Welding Code - Steel*, ANSI/AWS D1.1-90. Miami, FL. 1990.

American Welding Society. *Welding Processes*, Welding Handbook, Vol. 2, 8th Ed. Miami, FL. 1991.

Barton, F. W. and W. T. McKeel. "Development of an Improved Capability for Predicting the Response of Highway Bridges." Final Report, Virginia Highway and Transportation Research Council, VHTRC 86-R45, June 1986. (From Annotated Bibliography in Burdette, E. G. and D. W. Goodpasture. "Correlation of Bridge Load Capacity Estimates With Test Data." National Cooperative Highway Research Program Report 306. Transportation Research Board. Washington, DC. 1988)

Buckle, I. G., A. R. Dickson, and M. H. Phillips, "Ultimate Strength of Three Reinforced Concrete Bridges." International Conference on Short and Medium Span Bridges, Toronto, 1982. (From Annotated Bibliography in Burdette, E. G. and D. W. Goodpasture. "Correlation of Bridge Load Capacity Estimates With Test Data." National Cooperative Highway Research Program Report 306. Transportation Research Board. Washington, DC. 1988)

Burdette, E. G. and D. W. Goodpasture. "Full Scale Bridge Testing: An Evaluation of Bridge Design Criteria." University of Tennessee, December 1971. (From Annotated Bibliography in Burdette, E. G. and D. W. Goodpasture. "Correlation of Bridge Load Capacity Estimates With Test Data." National Cooperative Highway Research Program Report 306. Transportation Research Board. Washington, DC. 1988)

Burdette, E. G. and D. W. Goodpasture. "Correlation of Bridge Load Capacity Estimates With Test Data." National Cooperative Highway Research Program Report 306. Transportation Research Board. Washington, DC. 1988.

Downing, S. D. and D. F. Socie. "Simple Rainflow Counting Algorithms." *International Journal of Fatigue*, Jan. 1983. pp. 31-40.

Fisher, J. W., K. H. Frank, M. A. Hirt, and B. M. McNamee. "Effect of Weldments on the Fatigue Strength of Steel Beams." National Cooperative Highway Research Program Report 102. Highway Research Board. Washington, DC. 1970.

Fisher, J. W., P. A. Albrecht, B. T. Yen, D. J. Klingerman, and B. M. McNamee, "Fatigue Strength of Steel Beams With Welded Stiffeners and Attachments." National Cooperative Highway Research Program Report 147. Transportation Research Board. Washington, DC. 1974.

Fisher J. W., A. W. Pense, H. Hausammann, and M. D. Sullivan. "Detection and Repair of Fatigue Damage in Welded Highway Bridges." National Cooperative Highway Research Program Report 206. Transportation Research Board. Washington, DC. 1979.

Fisher, J. W., D. R. Mertz, and A. Zhong. "Steel Bridge Members Under Variable Amplitude Long Life Fatigue Loading." National Cooperative Highway Research Program Report 267. Transportation Research Board. Washington, DC. 1983.

Gregory, N., S. Graham, and C. Woodley. "Welded Repair of Cracks in Steel Bridge Members." National Cooperative Highway Research Program Report 321. Transportation Research Board. Washington, DC. 1989.

Gurney, T. R. "Fatigue Strength of Beams With Stiffeners Welded to the Tension Flange." *British Welding Journal*. Sep. 1960. pp. 569-576.

Gurney, T. R. *Fatigue of Welded Structures,* 2nd Ed. Cambridge: University Press. 1979. pp. 156-173.

Highway Research Board. "The AASHO Road Test: Report 4 - Bridge Research." *Special Report 61D*. Highway Research Board. 1962. (From Annotated Bibliography in Burdette, E. G. and D. W. Goodpasture. "Correlation of Bridge Load Capacity Estimates With Test Data." National Cooperative Highway Research Program Report 306. Transportation Research Board. Washington, DC. 1988)

Keating, P. B., and J. W. Fisher. "Evaluation of Fatigue Tests and Design Criteria on Welded Details." National Cooperative Highway Research Program Report 286. Transportation Research Board. Washington, DC. 1986.

Miner, M. A. "Cumulative Damage in Fatigue." *Journal of Applied Mechanics Transactions*, ASME Vol. 67, Sep. 1945. pp. A149-A164.

Minner, H. H. and T. Seeger. "Improvement of Fatigue Life of Welded Beams by TIG-Dressing." *Fatigue of Steel and Concrete Structures*. Proceedings of the International Association of Bridge Structural Engineers Colloquium. Lausanne. 1982. pp. 385-392.

Moses, F., C. G. Schilling, and K. S. Raju. "Fatigue Evaluation Procedures for Steel Bridges." National Cooperative Highway Research Program Report 299. Transportation Research Board. Washington, DC. 1987.

Nowak, A. S. *Bridge Evaluation, Repair and Rehabilitation*. Kluwer Academic Press. 1990. p. 371.

Paris, P. C. and F. E. Erdogan. "A Critical Analysis of Crack Propagation Laws." *Journal of Basic Engineering*, Series D of the Transactions of ASME, Vol. 85, 1963. pp. 528-534.

Post, G. J., K. H. Frank, and B. Tahmassebi. "Estimating Residual Fatigue Life of Bridges." Research Report 464-1F, Project 3-5-86-464, Center for Transportation Research, Bureau of Engineering Research, The University of Texas at Austin. Mar. 1988.

Rodgerson J. H. *Quality Assurance of Welded Construction*. New York: Elsevier Science Publisher. 1983. pp. 115-131.

Tsai, C. L., and M. J. Tsai. "Significance of Weld Undercut in Design of Fillet Welded T-Joints." *Welding Journal*, Vol. 63, No. 2. Feb. 1984. pp. 64s-70s.

Viest, I. M. "Review of Research on Composite Steel-Concrete Beams." *Journal of the Structural Division*, ASCE, Vol. 86, No. ST6. June 1960. pp. 1-21.

Zwerneman, F. J., and K. H. Frank. "Fatigue Damage Under Variable Amplitude Loads." *Journal of the Structural Division*, ASCE, Vol. 114, No. 1, Jan 1988. pp. 67-83.